Supplementary Information (SI) for Inorganic Chemistry Frontiers.

Supporting Information

When Ligands Promote, Inhibit, or Disappear: Reaction-Dependent Roles in Au and Cu Catalysis

Mariya V. Grudova, Alexey S. Galushko, Vladimir A. Skuratovich, Anastasiya O. Nakhatova, Valentiva V. Ilyushenkova, Victor M. Chernyshev*, Valentine P. Ananikov*

Zelinsky Institute of Organic Chemistry, Russian Academy of Sciences, Leninsky Pr. 47, Moscow, 119991, Russia; E-mail: val@ioc.ac.ru; https://AnanikovLab.ru

Department of Chemistry, Lomonosov Moscow State University, 1 Leninskie Gory, Moscow 119991, Russian Federation Center for Energy Science and Technology

Skolkovo Institute of Science and Technology, Bolshoy Boulevard 30, bld. 1, Moscow, 121205 Russia. E-mail: chern13@yandex.ru

Table of contents

S1. General experimental information

Chemicals and Solvents

The solvents were dried according to standard methods and stored over activated 3 Å molecular sieves prior to use. Column chromatography was performed on silica gel 60 (230−400 mesh, Merck). The glassware was dried at 120 °C in an oven for at least 3 h before use. NHC proligands IMes·HCl,[1] $IMes^{SPh}$·HCl,[2] IMes(Me)py·HCl,[2] and complexes DMS-AuCl,[3] Ph_3PCuCl,[4] IMesCuCl,[5] and $[IMesH][CuCl_2]$[6] were synthesized as described in the literature. The X-Ray structures of these complexes Ph_3PAuCl,[7] Ph_3PCuCl,[8,9] IMesAuCl,[10] IMesCuCl[11]and the complex salt $[IMesH][CuCl_2]$[6] were described in literature. All other chemicals were obtained from commercial sources.

Physical measurements and instrumentation

NMR study. NMR spectra were recorded on Bruker Avance-NEO 300, Bruker Fourier 300HD. The spectrometers operated at the following frequencies: 300.1 MHz for 1H, 76 MHz for 13C, and 282.4 MHz for 19F. ^{1}H and ^{13}C NMR chemical shifts were reported relative to the residual signals as internal standards: 7.26 ppm/77.2 ppm for $CDCl_3$, and 5.32 ppm/54.0 ppm for CD_2Cl_2. ^{19}F NMR chemical shifts were reported relative to C_6F_6 used as internal standard ($\delta^{19}F$ = −162.9 ppm with respect to $CFCl_3$). All the measurements were performed at room temperature.

ESI-HRMS study. High-resolution mass spectra (HRMS) were recorded using a Bruker maXis QTOF (tandem quadrupole/time-of-flight) mass analyzer equipped with an electrospray ionization (ESI) source. The m/z scanning range was 50–3000. Measurements were carried out in both positive (+) and negative (-) ion modes. In positive ion mode, the grounded spray needle was set to -4500 V, the high-voltage capillary was set to 500 V, and the HV End Plate was set to 0 V. In negative ion mode, the grounded spray needle was set to +4000 V, the high-voltage capillary was set to -500 V, and the HV End Plate Offset was set to 0 V. The mass scale was externally calibrated using a low-concentration calibration solution, "Tuning Mix" (Agilent Technologies). The samples were injected using a 500-µL Hamilton RN 1750 syringe (Switzerland). The flow rate during injection was controlled with a syringe pump at 3 µL/min. Nitrogen was used as the nebulizer gas at 1.0 bar, and dry gas was used at 4.0 L/min and 200 °C. The data were processed via Bruker Data Analysis 4.0 software. The samples used for the ESI-TOF-HRMS experiments were prepared in 1.8-mL glass vials with screw-top caps fitted with Teflon-lined septa (Agilent Technologies).

GC−MS measurements were carried out with an Agilent 7890A GC system equipped with an Agilent 5977A mass-selective detector (electron ionization, 70 eV) and an HP-5MS column (30 m/0.25 mm/0.25 µm film) using helium as the carrier gas at a flow rate of 1.0 ml min^{-1}. All the samples were dissolved in HPLC-grade MeCN or HPLC-grade DCM. The yields of the model reaction products were determined from the imine peak intensity via an appropriate calibration plot.

TEM analysis. The sample morphology was studied via a Hitachi SU8000 (Hitachi High-Technologies Corporation, Hitachinaka-shi, Japan) scanning electron microscope and a Regulus8230 (Hitachi High-Technologies Corporation, Hitachinaka-shi, Japan) scanning electron microscope at a 2–10 kV accelerating voltage. DFSTEM images were acquired in annular dark-field mode at a 30 kV accelerating voltage using a Regulus 8230 (Hitachi) scanning electron microscope. Energy-dispersive X-ray spectroscopy (EDX) studies were carried out using an Oxford Instruments X-max EDX system (Oxford Instruments plc, Abingdon, UK).

X-ray crystallographic data and refinement details. X-ray diffraction data were collected at 100K on a four-circle Rigaku Synergy S diffractometer equipped with a HyPix6000HE area-detector (kappa geometry, shutterless ω-scan technique), using monochromatized Cu K_a-radiation. The intensity data were integrated and corrected for absorption and decay by the CrysAlisPro program (Version 1.171.41. *Rigaku Oxford Diffraction*, **2021**). The structure was solved by direct methods using SHELXT[12] and refined on F^2 using SHELXL-2018[13] in the OLEX2 program.[14] All non-hydrogen atoms were refined with individual anisotropic displacement parameters. All hydrogen atoms were placed in ideal calculated positions and refined as riding atoms with relative isotropic displacement parameters. A rotating group model was applied for methyl groups.
Crystal data, data collection and structure refinement details for **[IMesH][AuCl$_2$]**, **6e**, **6f**, and **6k** are presented in Section S6. The structures have been deposited at the Cambridge Crystallographic Data Center with the reference CCDC numbers 2530447 (**6l**) 2530448 (**6f**) 2530449 (**6e**) 2530450 (**[IMesH][AuCl$_2$]**); they also contain the supplementary crystallographic data. These data can be obtained free of charge from the CCDC *via* https://www.ccdc.cam.ac.uk/structures/

S2. Synthetic procedures and characterization of synthesized compounds

Chloro(triphenylphosphine)gold(I) (Ph_3PAuCl). The synthesis was conducted according to a slightly modified procedure described in the literature.[15] Triphenylphosphine (1.54 g, 5.87 mmol) was added slowly over 30 min to a magnetically stirred solution of $HAuCl_4 \cdot 3H_2O$ (1.02 g, 2.59 mmol) in ethanol (30 mL) at room temperature. The resulting mixture was stirred for an additional 15 min. The white precipitate that formed was collected by filtration, washed successively with cold ethanol (15 mL) and diethyl ether (10 mL), and dried under vacuum overnight at room temperature to afford Ph_3PAuCl (1.35 g, 99% yield) as a white powder.
^{1}H NMR (300 MHz, $CDCl_3$) δ 7.57 – 7.44 (m, 15H).

1,3-Bis(2,4,6-trimethylphenyl)-1,3-dihydro-2*H*-imidazol-2-ylidene](chloro)gold(I) (IMesAuCl). The synthesis was conducted according to a previously described procedure.[16]
^{1}H NMR (CD_2Cl_2, 300 MHz) δ 7.15 (s, 2H), 7.08 – 7.07 (m, 4H), 2.38 (s, 6H), 2.13 (s, 12H), 1.54 (s, 6H).

1,3-Bis[2,4,6-trimethylphenyl]-1H-imidazolium dichloroaurate ([IMesH][$AuCl_2$]). The synthesis was conducted according to a slightly modified procedure described in the literature.[17] IMes·HCl (0.140 g, 0.41 mmol) and DMS-AuCl (0.120 g, 0.41 mmol) were dissolved in acetone (4 mL). Then acetone was rotary evaporated under reduced pressure. The resulting residue was dissolved in dichloromethane (4 mL) and filtered through a syringe filter. *n*-Hexane (15 mL) was then added to the filtrate, and the resulting precipitate was collected by filtration and dried under vacuum to give [IMesH][$AuCl_2$] (0,206 g, 90% yield) as a pale beige powder.
^{1}H NMR ($CDCl_3$, 300 MHz) δ 9.33 (s, 1H), 7.60 (d, J = 1.4 Hz, 2H), 7.10 (s, 4H), 2.39 (s, 6H), 2.19 (s, 12H).

Investigation of Copper and Gold Precatalysts in the Chan–Evans–Lam Reaction (General Procedure)

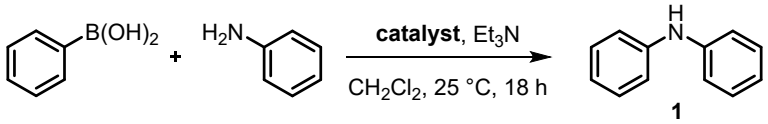

All experiments were conducted under an air atmosphere in 4 mL screw-capped glass vials equipped with a magnetic stir bar. A solution of the corresponding precatalyst (0.025 mmol, Table 1) in dichloromethane (0.5 mL) was mixed with aniline (23 mg, 0.25 mmol), phenylboronic acid (30 mg, 0.25 mmol), triethylamine (51 mg, 0.5 mmol), CS_2 (if used for poisoning experiments, 0.2 mg, 0.0025 mmol). The resulting mixture was stirred at 25 °C for 18 h. An aliquot (100 µL) of the reaction mixture was then diluted with $CDCl_3$ (600 µL) containing CH_2Br_2 (4 mg/mL) as an internal standard. The solution was analyzed by ^{1}H NMR spectroscopy. The yield of compound **1** (Table 1) was determined by integrating the characteristic signal of the aromatic CH group (δ = 7.24 ppm) relative to the integral intensity of the internal standard (CH_2Br_2, δ 4.93 ppm).

Investigation of Copper and Gold Precatalysts in the Azide–Alkyne Cycloaddition Reaction (General Procedure)

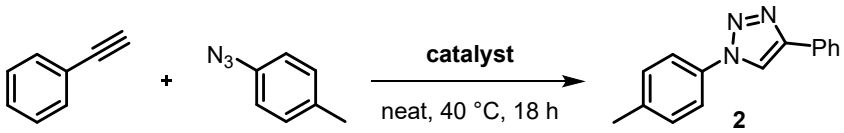

2

All experiments were conducted under an air atmosphere in 1.5 mL screw-capped glass vials equipped with a magnetic stir bar. The corresponding precatalyst (0.012 mmol, Table 1) was placed in a vial, followed by the addition of phenylacetylene (25 mg, 0.25 mmol), 4-azidotoluene (25 mg, 0.25 mmol) and CS_2 (if used for poisoning experiments, 0.1 mg, 0.0012 mmol). The resulting mixture was stirred at 40 °C for 18 h, then cooled to room temperature. The resulting mixture was dissolved in $CDCl_3$ (600 µL) containing CH_2Br_2 (4 mg/mL) as an internal standard. The solution was analyzed by ^{1}H NMR spectroscopy. The yield of compound **2** (Table 1) was determined by integrating the characteristic signal of the CH group (δ = 8.20 ppm) relative to the internal standard (CH_2Br_2, δ 4.93 ppm).

Investigation of Copper and Gold Precatalysts in the Ullmann-type coupling (General Procedure)

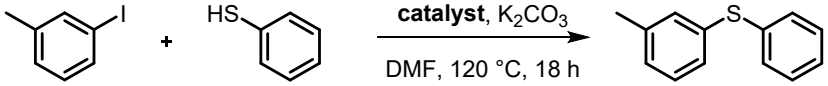

3

All experiments were conducted under an argon atmosphere in 1.5 mL screw-capped glass vials equipped with a magnetic stir bar. A mixture of 3-iodotoluene (66 mg, 0.3 mmol), thiophenol (33 mg, 0.3 mmol), potassium carbonate (52 mg, 0.375 mmol), the corresponding precatalyst (0.015 mmol, Table 1), and CS_2 (if used for poisoning experiments, 0.1 mg, 0.0015 mmol) in dry DMF (1.0 mL) was heated at 120 °C while stirring for 18 h, then cooled to room temperature. An aliquot (1 µL) of the reaction mixture was taken with a syringe and diluted with methanol (1.5 mL), followed by the addition of 100 µL of an internal standard solution (diphenylamine, 0.1 mg/mL in methanol) and analyzed by GC–MS. The yield of compound **3** (Table 1) was determined relative to the internal standard (diphenylamine).

Investigation of Copper and Gold Precatalysts in the A³ (Aldehyde–Amine–Alkyne) Coupling Reaction (General Procedure)

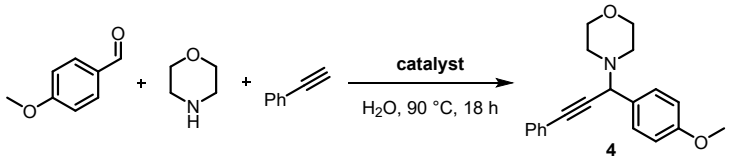

4

All experiments were conducted under an argon atmosphere in 1.5 mL screw-capped glass vials equipped with a magnetic stir bar. A mixture of 4-methoxybenzaldehyde (68 mg, 0.5 mmol), morpholine (48 mg 0.55 mmol), and phenylacetylene (76 mg, 0.75 mmol), the corresponding precatalyst (0.01 mmol, Table 1), and CS_2 (if used for poisoning experiments, 0.1 mg, 0.001 mmol) in water (0.5 mL) was heated at 90 °C or 18 h while vigorous stirring. The reaction mixture was then cooled to room temperature and extracted with $CHCl_3$ (3×2 mL). The combined organic extracts were dried over anhydrous Na_2SO_4 and evaporated to dryness under reduced pressure.

The residue was dissolved in of $CDCl_3$ (600 µL) containing CH_2Br_2 (4 mg/mL) as an internal standard and analyzed by ^1H NMR spectroscopy. The yield of compound **4** was determined by integrating the characteristic signal of the tertiary CH group (δ = 4.85 ppm) relative to the internal standard (CH_2Br_2, δ 4.93 ppm).

Investigation of Copper and Gold Precatalysts in the Hydration of Phenylacetylene (General Procedure)

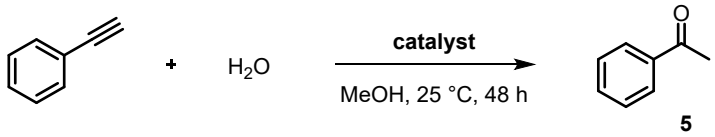

5

All experiments were conducted under an air atmosphere in 1.5 mL screw-capped glass vials equipped with a magnetic stir bar. Water (18 mg, 1 mmol) was added to a solution of phenylacetylene (25.5 mg, 0.25 mmol), the corresponding precatalyst (0.012 mmol, Table 1), and CS_2 (if used for poisoning experiments, 0.1 mg, 0.0012 mmol) in methanol (0.5 mL). The resulting mixture was stirred at 25 °C for 48 h. An aliquot (100 µL) of the reaction mixture was taken, dissolved in 600 µL of $CDCl_3$ containing CH_2Br_2 (4 mg/mL) and analyzed by ^1H NMR. The yield of compound **5** was determined by integrating the characteristic signal of the CH_3 group (δ = 2.61 ppm) relative to the internal standard (CH_2Br_2, δ 4.93 ppm).

Investigation of Copper and Gold Precatalysts in the Hydroamination of Phenyl Acetylene with Aniline (General Procedure)

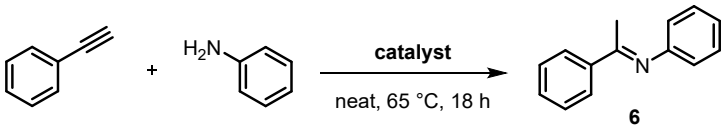

6

All experiments were conducted under an argon atmosphere in 1.5 mL screw-capped glass vials equipped with a magnetic stir bar. A mixture of aniline (224 mg, 2.4 mmol), phenylacetylene (24.5 mg, 0.24 mmol), the corresponding precatalyst (0.0048 mmol, Table 1), and CS_2 (if used for poisoning experiments, 0.04 mg, 0.00048 mmol) was stirred at 65 °C for 18 h, then cooled to room temperature. An aliquot (25 µL) of the reaction mixture was taken, dissolved in $CDCl_3$ (600 µL) containing CH_2Br_2 (4 mg/mL) as an internal standard and analyzed by ^1H NMR spectroscopy. The yield of imine **6** was determined by integrating the characteristic signal of CH_3 group (δ = 2.30 ppm) relative to the internal standard (CH_2Br_2, δ 4.93 ppm).

Synthesis of Compounds 6a-t (General Procedure)

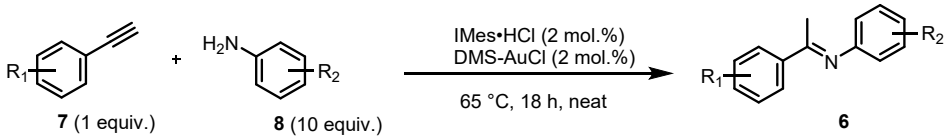

7 (1 equiv.) **8** (10 equiv.) **6**

All the experiments were conducted under an argon atmosphere in 1.5 mL screw-capped glass vials equipped with a magnetic stir bar. A mixture of alkyne (0.4 mmol), the corresponding aromatic amine (0.4 mmol), IMes·HCl (2.7 mg, 0.008 mmol, 2 mol%), and DMS-AuCl (2.4 mg,

0.008 mmol, 2 mol%) was heated at 65 °C for 18 h with stirring and then cooled to room temperature. The resulting crude product obtained was purified via column chromatography on silica gel using a gradient elution by petroleum ether and ethyl acetate (EA:PE = 1:100 → 1:70 → 1:50 → 1:20).

(E)-N-(1-Phenylethylidene)aniline (6a)

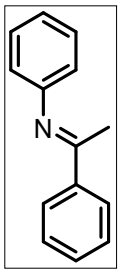

The product was obtained as a light brown liquid, yield 77 mg (99%).**^{1}H NMR ($CDCl_3$, 300 MHz)** δ 8.00-7.95 (m, 2H), 7.45-7.41 (m, 3H), 7.35 (dd, J = 8.0 Hz, 7.6 Hz, 2H), 7.08 (t, J = 7.6 Hz, 1H), 6.81-6.79 (m, 2H), 2.23 (s, 3H). **^{13}C{^{1}H} NMR ($CDCl_3$, 100 MHz)** δ 165.7, 151.9, 139.6, 130.7, 129.1, 128.6, 127.4, 123.4, 119.6, 17.6. The spectral data are consistent with those reported in the literature.[18]

(*E*)-1-(4-ethoxyphenyl)-*N*-mesitylethan-1-imine (6b):

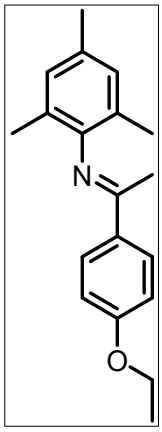

The product was obtained as a light brown liquid, yield 110 mg (98%). **^{1}H NMR ($CDCl_3$, 300 MHz)** *δ* 8.05 – 7.98 (m, 2H), 7.02 – 6.95 (m, 2H), 6.90 (s, 2H), 4.12 (q, *J* = 7.0 Hz, 2H), 2.31 (s, 3H), 2.06 (s, 3H), 2.02 (s, 6H), 1.48 (t, *J* = 7.0 Hz, 3H). **^{13}C{^{1}H} NMR ($CDCl_3$, 76 MHz)** *δ* 164.57, 160.93, 146.68, 131.85, 131.74, 128.75, 128.52, 125.88, 114.15, 63.65, 20.83, 18.03, 17.25, 14.88. **ESI-(+)HRMS**, *m/z*: 282.1849, calcd for $C_{19}H_{23}NO$ = 282.1852 $[M+H]^+$, (Δ = 1.06 ppm).

(*E*)-*N*-(2,6-diisopropylphenyl)-1-(4-ethoxyphenyl)ethan-1-imine (6c):

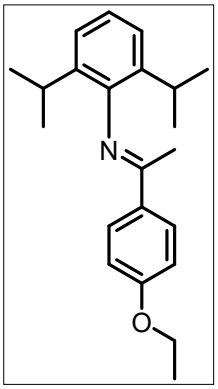

The product was obtained as a light brown liquid, yield 123 mg (95%). **^{1}H NMR ($CDCl_3$, 300 MHz)** δ 8.05 – 7.98 (m, 2H), 7.17 (d, *J* = 1.8 Hz, 1H), 7.15 (s, 1H), 7.08 (dd, *J* = 8.8, 6.3 Hz, 1H), 7.04 – 6.96 (m, 2H), 4.13 (q, *J* = 7.0 Hz, 2H), 2.78 (p, *J* = 6.9 Hz, 2H), 2.08 (s, 3H), 1.48 (t, *J* = 7.0 Hz, 3H), 1.16 (dd, *J* = 6.9, 5.1 Hz, 12H). **^{13}C{^{1}H} NMR ($CDCl_3$, 76 MHz)** δ 163.87, 161.02, 147.09, 136.42, 131.87, 128.86, 123.20, 123.01, 114.27, 63.74, 28.32, 23.35, 23.11, 18.00, 14.93. **ESI-(+)HRMS**, *m/z*: 324.2322, calcd for $C_{22}H_{29}NO$ = 324.2322 $[M+H]^+$, (Δ = 0 ppm).

(*E*)-*N*,*N*-dimethyl-4-(1-((4-(methylthio)phenyl)imino)ethyl)aniline (6d):

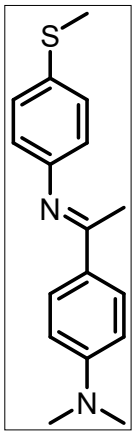

The product was obtained as a brown oil, yield 105 mg (92%). **^{1}H NMR ($CDCl_3$, 300 MHz)** δ 7.96 – 7.82 (m, 2H), 7.33 – 7.21 (m, 2H), 6.83 – 6.64 (m, 4H), 3.03 (s, 6H), 2.49 (s, 3H), 2.18 (s, 3H). **^{13}C{^{1}H} NMR ($CDCl_3$, 76 MHz)** δ 165.02, 152.08, 150.40, 131.35, 128.70, 127.28, 120.83, 111.41, 40.35, 17.37, 17.06. **ESI-(+)HRMS**, *m/z*: 285.1430, calcd for $C_{17}H_{20}N_2S$ = 285.1420 $[M+H]^+$, (Δ = 3.51 ppm).

(*E*)-4-(1-((4-bromonaphthalen-1-yl)imino)ethyl)-*N*,*N*-dimethylaniline (6e):

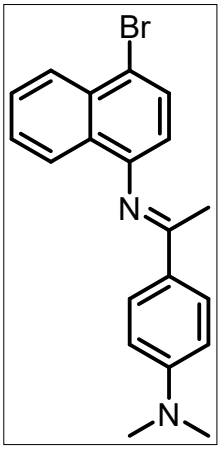

The product was obtained as a light brown solid, yield 132 mg (90%). **^{1}H NMR ($CDCl_3$, 300 MHz)** δ 8.24 (d, *J* = 8.3 Hz, 1H), 8.06 – 8.00 (m, 2H), 7.84 (d, *J* = 8.4 Hz, 1H), 7.73 (d, *J* = 7.9 Hz, 1H), 7.60 (ddd, *J* = 8.3, 6.8, 1.2 Hz, 1H), 7.45 (ddd, *J* = 8.1, 6.9, 1.1 Hz, 1H), 6.81 – 6.74 (m, 2H), 6.67 (d, *J* = 7.9 Hz, 1H), 3.07 (s, 6H), 2.15 (s, 3H). **^{13}C{^{1}H} NMR ($CDCl_3$,76 MHz)** δ 166.08, 152.27, 148.85, 132.44, 129.96, 128.94, 127.90, 127.51, 127.23, 126.74, 126.05, 124.55, 116.11, 114.61, 111.40, 40.36, 17.43. **ESI-(+)HRMS**, *m/z*: 367.0804, calcd $C_{20}H_{18}BrN_2$ = 367.0804 $[M+H]^+$, (Δ = 0 ppm).

(*E*)-*N*-(4-bromonaphthalen-1-yl)-1-(4-ethoxyphenyl)ethan-1-imine (6f):

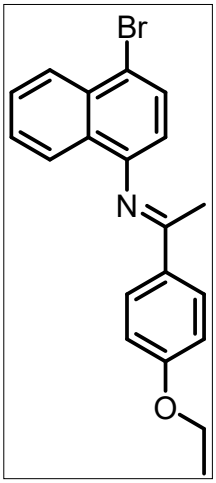

The product was obtained as a yellow solid, yield 126 mg (86%). **^{1}H NMR (CD_2Cl_2, 300 MHz)** δ 8.23 (d, *J* = 8.5 Hz, 1H), 8.07 (d, *J* = 8.8 Hz, 2H), 7.81 (d, *J* = 8.3 Hz, 1H), 7.75 (d, *J* = 7.9 Hz, 1H), 7.66 – 7.58 (m, 1H), 7.52 – 7.44 (m, 1H), 7.00 (d, *J* = 8.8 Hz, 2H), 6.66 (d, *J* = 7.9 Hz, 1H), 4.12 (q, *J* = 7.0 Hz, 2H), 2.17 (s, 3H), 1.45 (t, *J* = 7.0 Hz, 3H). **^{13}C{^{1}H} NMR (CD_2Cl_2, 76 MHz)** δ 166.54, 161.89, 148.99, 132.85, 132.10, 130.43, 129.60, 128.10, 127.56, 126.63, 124.86, 116.63, 114.72, 64.28, 17.85, 15.14. **ESI-(+)HRMS**, *m/z*: 368.0645, calcd for $C_{20}H_{18}NOBr$ = 368.0645 $[M+H]^+$, (Δ = 0 ppm).

(*E*)-4-(1-((4-bromophenyl)imino)ethyl)-*N*,*N*-dimethylaniline (6g):

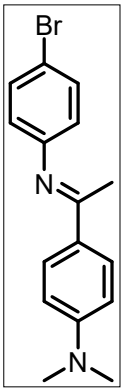

The product was obtained as a yellow solid, yield 101 mg (80%). **^{1}H NMR ($CDCl_3$, 300 MHz)** δ 7.92 – 7.79 (m, 2H), 7.48 – 7.38 (m, 2H), 6.81 – 6.55 (m, 4H), 3.04 (s, 6H), 2.17 (s, 4H). **^{13}C{^{1}H} NMR ($CDCl_3$, 76 MHz)** δ 165.24, 152.14, 151.49, 131.90, 128.73, 126.93, 121.90, 115.58, 111.35, 40.30, 17.04. **ESI-(+)HRMS**, *m/z*: 317.0645, calcd for $C_{16}H_{17}N_2Br$ = 317.0648 $[M+H]^+$, (Δ = 0.95 ppm).

(*E*)-1-(4-ethoxyphenyl)-*N*-(4-methoxyphenyl)ethan-1-imine (6h):

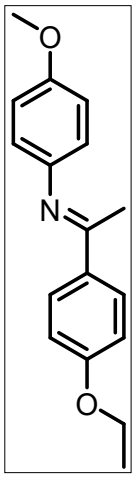

The product was obtained as a pale-yellow crystals, yield 86 mg (80%). **^{1}H NMR ($CDCl_3$, 300 MHz)** δ 7.95 – 7.89 (m, 2H), 7.02 – 6.83 (m, 4H), 6.79 – 6.70 (m, 2H), 4.09 (q, *J* = 7.0 Hz, 2H), 3.81 (s, 3H), 2.21 (s, 3H), 1.44 (t, *J* = 7.0 Hz, 3H). **^{13}C{^{1}H} NMR ($CDCl_3$, 76 MHz)** δ 164.92, 160.91, 155.85, 145.17, 132.38, 128.82, 120.98, 114.29, 114.16, 63.64, 55.56, 17.15, 14.87. **ESI-(+)HRMS**, *m/z*: 270.1489, calcd for $C_{17}H_{19}NO_2$ = 270.1502 $[M+H]^+$, (Δ = 4.81 ppm).

(*E*)-*N*-(4-bromophenyl)-1-(4-ethoxyphenyl)ethan-1-imine (6i):

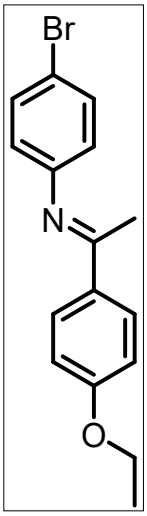

The product was obtained as a yellow crystalline powder, yield 99 mg (78%). **^{1}H NMR ($CDCl_3$, 300 MHz)** δ 7.91 (d, *J* = 8.8 Hz, 2H), 7.44 (d, *J* = 8.5 Hz, 2H), 6.94 (d, *J* = 8.8 Hz, 2H), 6.67 (d, *J* = 8.5 Hz, 2H), 4.10 (q, *J* = 7.0 Hz, 2H), 2.19 (s, 2H), 1.45 (t, *J* = 7.0 Hz, 3H). **^{13}C{^{1}H} NMR ($CDCl_3$, 76 MHz)** δ 165.33, 161.24, 151.05, 132.03, 131.80, 129.00, 121.60, 116.01, 114.27, 63.73, 17.32, 14.89. **ESI-(+)HRMS**, *m/z*: 318.0491, calcd for $C_{16}H_{16}NBr$ = 318.0488 $[M+H]^+$, (Δ = 0.94 ppm).

(*E*)-1-(4-fluorophenyl)-*N*-mesitylethan-1-imine (6j):

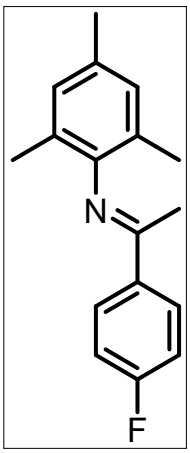

The product was obtained as a light brown solid, yield 76 mg (75%). **^{1}H NMR ($CDCl_3$, 300 MHz)** δ 8.08 – 7.99 (m, 2H), 7.19 – 7.10 (m, 2H), 6.91 – 6.87 (m, 2H), 2.30 (s, 3H), 2.06 (s, 3H), 2.00 (s, 6H). **^{13}C{^{1}H} NMR ($CDCl_3$, 76 MHz)** δ 164.40 (d, $^{1}J_{C\text{-}F}$ = 250.4 Hz), 164.22, 146.43, 135.56 (d, $^{4}J_{C\text{-}F}$ = 3.1 Hz), 132.11, 129.23 (d, $^{3}J_{C\text{-}F}$ = 8.5 Hz), 128.65, 125.67, 115.38 (d, $^{2}J_{C\text{-}F}$ = 21.5 Hz), 20.85, 18.00, 17.44. **^{19}F{^{1}H} NMR ($CDCl_3$, 282 MHz)** δ -113.85. **ESI-(+)HRMS**, *m/z*: 256.1500, calcd for $C_{20}H_{16}NO_2Br$ = 256.1496 $[M+H]^+$, (Δ = 1.63 ppm).

(*E*)-*N*,*N*-dimethyl-4-(1-((4-(trifluoromethyl)phenyl)imino)ethyl)aniline (6k):

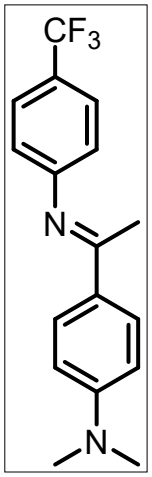

The product was obtained as a yellow solid, yield 84 mg (69%). **^{1}H NMR ($CDCl_3$, 300 MHz)**: δ 7.95 – 7.84 (m, 2H), 7.58 (d, J = 8.4 Hz, 2H), 6.87 (d, J = 8.3 Hz, 2H), 6.79 – 6.67 (m, 2H), 3.05 (s, 6H), 2.18 (s, 3H). **^{13}C{^{1}H} NMR ($CDCl_3$, 76 MHz)**: δ 165.09, 155.67 (q, $^{4}J_{C-F}$ = 1.2 Hz), 152.18, 128.76, 126.53, 126.48, 126.13 (q, $^{3}J_{C-F}$= 3.8 Hz), 124.68 (d, $^{1}J_{C-F}$ = 271.1 Hz, CF_3), 124.67 (q, $^{2}J_{C-F}$ = 32.4 Hz), 119.99, 111.26, 40.19, 17.10. **^{19}F{^{1}H} NMR ($CDCl_3$, 282 MHz)**: δ -64.78. **ESI-(+)HRMS**, *m/z*: 307.1422, calcd for $C_{17}H_{18}N_2F_3$ = 1.76 ppm $[M+H]^+$, (Δ = 1.06 ppm).

(*E*)-*N*-(4-bromonaphthalen-1-yl)-1-(4-propylphenyl)ethan-1-imine (6l):

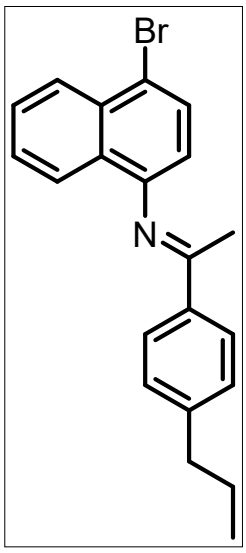

The product was obtained as a light brown solid, yield 96 mg (66%). **^{1}H NMR ($CDCl_3$, 300 MHz)** δ 8.24 (d, J = 8.4 Hz, 1H), 8.03 (d, J = 8.2 Hz, 2H), 7.79 (d, J = 8.3 Hz, 1H), 7.74 (d, J = 7.8 Hz, 1H), 7.64 – 7.56 (m, 1H), 7.50 – 7.41 (m, 1H), 7.32 (d, J = 8.2 Hz, 2H), 6.65 (d, J = 7.8 Hz, 1H), 2.69 (t, 2H), 2.19 (s, 3H), 1.71 (h, J = 7.4 Hz, 2H), 0.99 (t, J = 7.3 Hz, 3H). **^{13}C{^{1}H} NMR ($CDCl_3$, 76 MHz)** δ 166.95, 148.29, 146.18, 136.68, 132.50, 129.94, 128.79, 127.66, 127.48, 127.37, 126.27, 124.34, 116.71, 114.20, 38.06, 24.59, 17.86, 13.95. **ESI-(+)HRMS**, *m/z*: 366.0854, calcd for $C_{21}H_{20}NBr$ = 366.0852 $[M+H]^+$, (Δ = 0.55 ppm).

(*E*)-*N*-(4-bromonaphthalen-1-yl)-1-(4-bromophenyl)ethan-1-imine (6m):

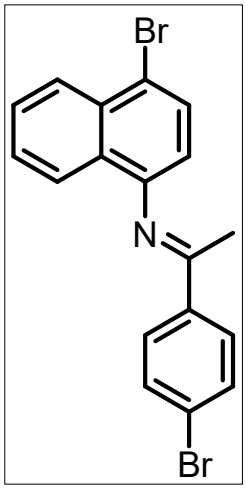

The product was obtained as a yellow solid, yield 97 mg (60%). **^{1}H NMR ($CDCl_3$, 300 MHz)** δ 8.26 (d, *J* = 8.4 Hz, 1H), 8.02 – 7.93 (m, 2H), 7.75 (dd, *J* = 8.1, 2.7 Hz, 2H), 7.70 – 7.55 (m, 3H), 7.48 (ddd, *J* = 8.3, 6.8, 1.3 Hz, 1H), 6.64 (d, *J* = 7.8 Hz, 1H), 2.19 (s, 3H). **^{13}C{^{1}H} NMR ($CDCl_3$, 76 MHz)** δ 165.97, 147.71, 137.89, 132.48, 131.82, 129.87, 129.05, 127.76, 127.43, 127.31, 126.42, 125.74, 124.13, 117.14, 114.02, 17.71. **ESI-(+)HRMS**, *m/z*: 403.9464, calcd for $C_{18}H_{13}NBr_2$ = 403.9468 $[M+H]^+$, (Δ = 0.99 ppm).

(*E*)-*N*-(4-bromonaphthalen-1-yl)-1-phenylethan-1-imine (6n):

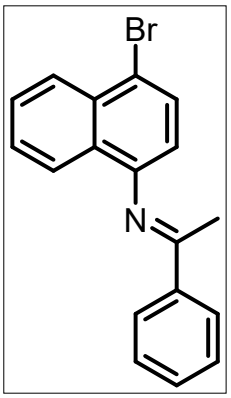

The product was obtained as a light brown solid, yield 76 mg (59%). **^{1}H NMR ($CDCl_3$, 300 MHz)** δ 8.27 (d, *J* = 8.4 Hz, 1H), 8.15 – 8.10 (m, 2H), 7.81 (d, *J* = 8.4 Hz, 1H), 7.76 (d, *J* = 7.9 Hz, 1H), 7.62 (ddd, *J* = 8.4, 6.9, 1.3 Hz, 1H), 7.56 – 7.45 (m, 4H), 6.68 (d, *J* = 7.9 Hz, 1H), 2.22 (s, 3H). **^{13}C{^{1}H} NMR ($CDCl_3$, 76 MHz)** δ 167.11, 148.05, 139.04, 132.44, 131.04, 129.90, 128.64, 127.69, 127.45, 127.36, 126.32, 124.24, 121.36, 116.86, 114.11, 110.26, 17.91. **ESI-(+)HRMS**, *m/z*: 324.0392, calcd for $C_{18}H_{14}NBr$ = 324.0382 $[M+H]^+$, (Δ = 3.09 ppm).

(*E*)-1-(4-ethoxyphenyl)-*N*-(4-(trifluoromethyl)phenyl)ethan-1-imine (6o):

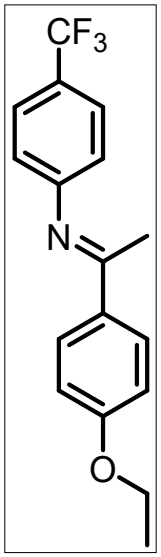

The product was obtained as a yellow crystalline powder, yield 71 mg (58%). **^{1}H NMR ($CDCl_3$, 300 MHz)** δ 7.94 (d, *J* = 8.8 Hz, 2H), 7.59 (d, *J* = 8.3 Hz, 2H), 6.95 (d, *J* = 8.8 Hz, 2H), 6.87 (d, *J* = 8.2 Hz, 2H), 4.10 (q, *J* = 7.0 Hz, 2H), 2.20 (s, 3H), 1.46 (t, *J* = 7.0 Hz, 3H). **^{13}C{^{1}H} NMR ($CDCl_3$, 76 MHz)** δ 165.31, 161.36, 155.22 (d, $^{4}J_{C\text{-}F}$ = 1.2 Hz), 131.42, 129.08, 127.08, 126.32 (q, $^{3}J_{C\text{-}F}$= 3.7 Hz), 125.13 (q, $^{2}J_{C\text{-}F}$ = 32.5 Hz), 124.67 (CF_3, q, $J_{C\text{-}F}$ = 271.3 Hz), 119.77, 114.27, 63.72, 17.46, 14.85. **^{19}F{^{1}H} NMR ($CDCl_3$, 282 MHz)** δ -64.87. **ESI-(+)HRMS**, *m/z*: 308.1263, calcd for $C_{17}H_{16}NOF_3$ = 308.1257 $[M+H]^+$, (Δ = 1.95 ppm).

(*E*)-*N*-(4-bromonaphthalen-1-yl)-1-(4-(trifluoromethyl)phenyl)ethan-1-imine (6p):

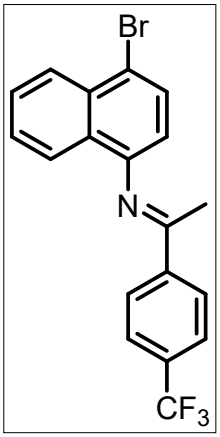

The product was obtained as a light brown liquid, yield 48 mg (30%). **^{1}H NMR ($CDCl_3$, 300 MHz)** δ 8.26 (d, *J* = 8.4 Hz, 1H), 8.22 (d, *J* = 8.1 Hz, 2H), 7.79 – 7.76 (m, 2H), 7.74 (d, *J* = 4.9 Hz, 2H), 7.63 (ddd, *J* = 8.4, 6.9, 1.3 Hz, 1H), 7.48 (ddd, *J* = 8.2, 6.9, 1.2 Hz, 1H), 6.66 (d, *J* = 7.8 Hz, 1H), 2.25 (s, 3H). **^{13}C{^{1}H} NMR ($CDCl_3$, 76 MHz)** δ 165.94, 147.48, 142.20, 132.66 (d, $^{2}J_{C\text{-}F}$ = 32.5 Hz), 132.53, 129.87, 127.85, 127.51, 127.22, 126.55, 125.64 (q, $^{3}J_{C\text{-}F}$ = 3.8 Hz), 124.11 (CF_3, d, $^{1}J_{C\text{-}F}$ = 272.3 Hz), 124.05, 117.45, 113.93, 17.97. **^{19}F{^{1}H} NMR ($CDCl_3$, 282 MHz)** δ -65.96. **ESI-(+)HRMS**, *m/z*: 392.0260, calcd for $C_{19}H_{13}NBrF_3$ = 392.0256 $[M+H]^+$, (Δ = 1.02 ppm).

(*E*)-*N*-(2,5-di-tert-butylphenyl)-1-phenylethan-1-imine (6q):

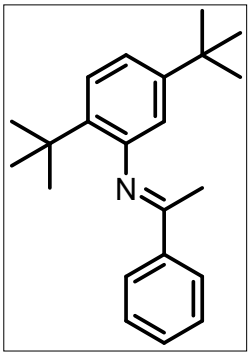

The product was obtained as a yellow solid, yield 37 mg (30%). **^{1}H NMR ($CDCl_3$,300 MHz)** δ 8.08 – 8.00 (m, 2H), 7.51 – 7.43 (m, 3H), 7.33 (d, *J* = 8.3 Hz, 1H), 7.06 (dd, *J* = 8.3, 2.3 Hz, 1H), 6.49 (d, *J* = 2.2 Hz, 1H), 2.23 (s, 3H), 1.34 (s, 9H), 1.30 (s, 9H). **^{13}C{^{1}H} NMR ($CDCl_3$, 76 MHz)** δ 163.17, 149.76, 149.34, 139.75, 136.92, 130.41, 128.56, 127.37, 126.06, 120.09, 117.55, 34.88, 34.39, 31.44, 29.78, 18.02. **ESI-(+)HRMS**, *m/z*: 308.2370, calcd for $C_{22}H_{29}N$ = 308.2373 $[M+H]^+$, (Δ = 0.97 ppm).

Methyl (*E*)-4-(1-((4-bromonaphthalen-1-yl)imino)ethyl)benzoate (6r):

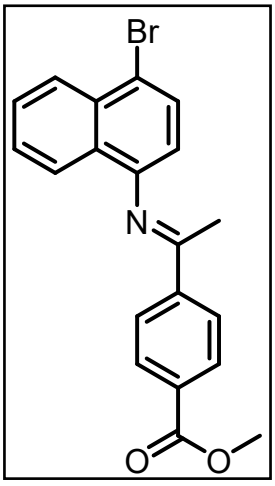

The product was obtained as a brown solid, yield 42 mg (28%). **^{1}H NMR ($CDCl_3$, 300 MHz)** δ 8.26 (d, *J* = 8.2 Hz, 1H), 8.16 (s, 4H), 7.80 – 7.73 (m, 2H), 7.62 (ddd, *J* = 8.4, 6.9, 1.3 Hz, 1H), 7.48 (ddd, *J* = 8.2, 6.9, 1.2 Hz, 1H), 6.66 (d, *J* = 7.9 Hz, 1H), 3.98 (s, 3H), 2.25 (s, 3H). **^{13}C{^{1}H} NMR ($CDCl_3$, 76 MHz)** δ 166.80, 166.45, 147.64, 142.96, 132.52, 132.18, 129.90, 129.88, 127.82, 127.48, 127.25, 126.51, 124.13, 117.35, 113.94, 52.50, 18.07. **ESI-(+)HRMS**, *m/z*: 382.0436, calcd for $C_{20}H_{16}NO_2Br$ = 382.0437 $[M+H]^+$, (Δ = 0.26 ppm).

S3. TEM investigation of Cu and Au nanoparticles

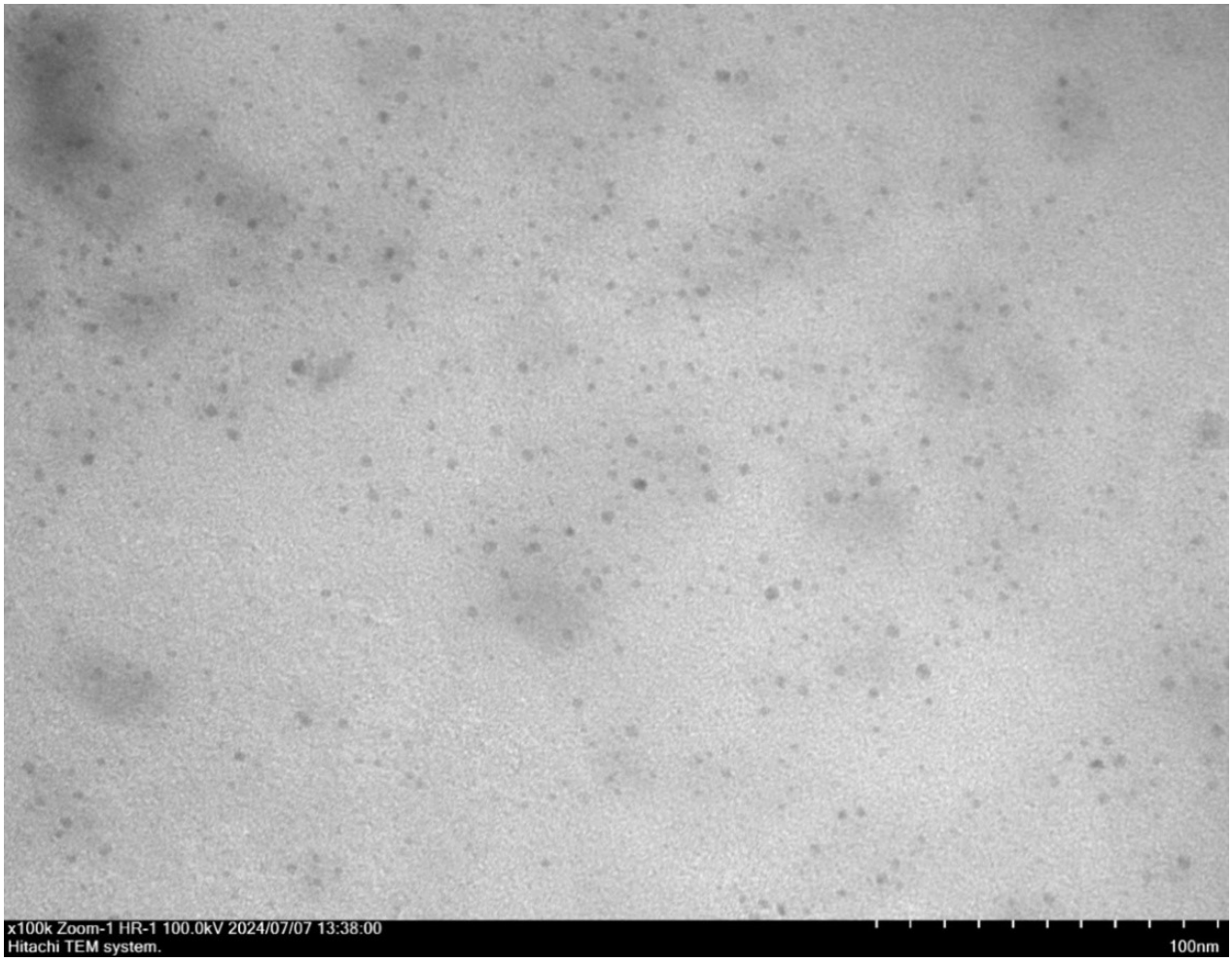

Figure S1. TEM image of Cu NPs obtained in Chan-Evans-Lam type reaction between phenylboronic acid and aniline catalyzed with **Ph_3PCuCl** complex.

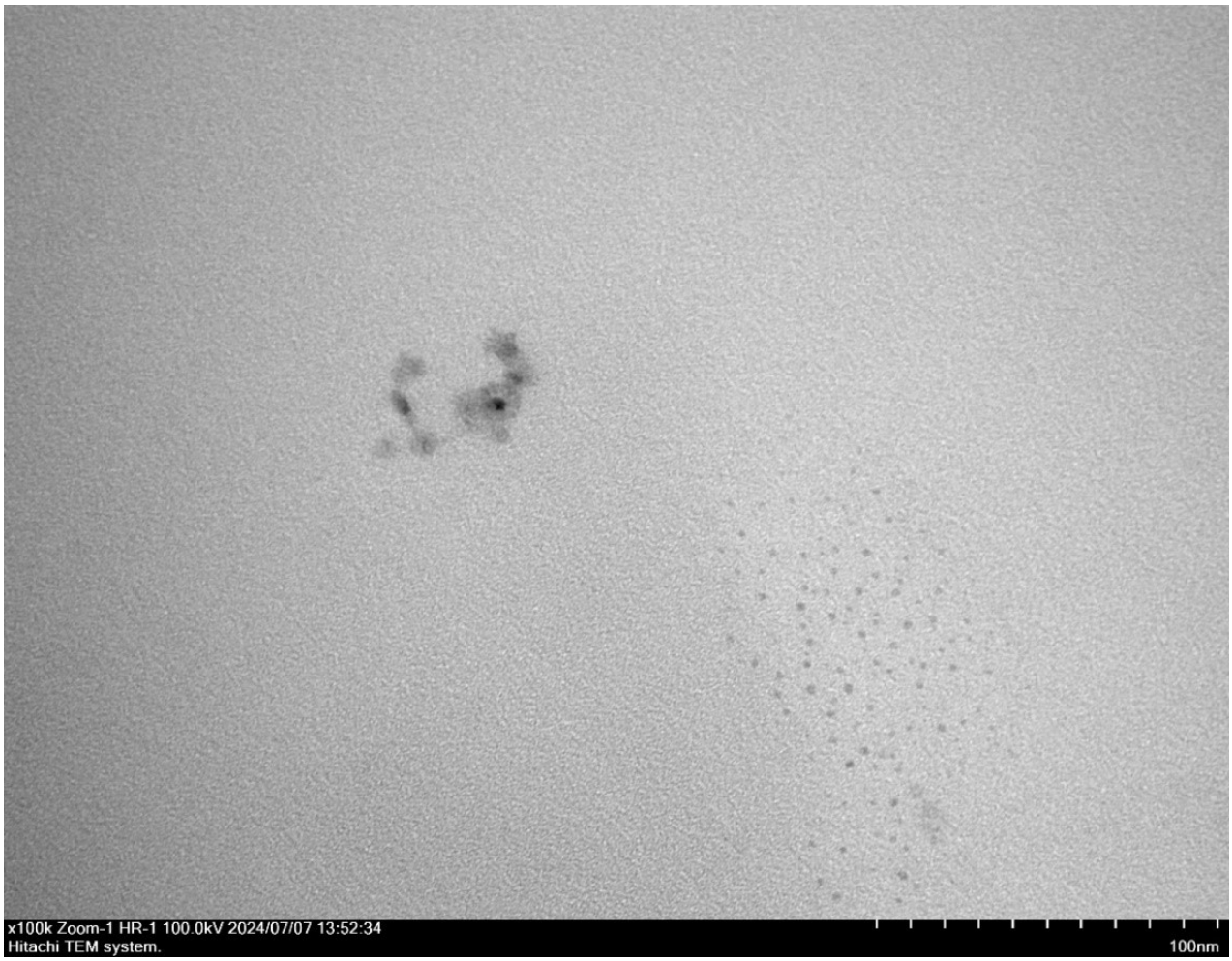

Figure S2. TEM image of Cu NPs obtained in Chan-Evans-Lam type reaction between phenylboronic acid and aniline catalyzed with **IMesCuCl** complex.

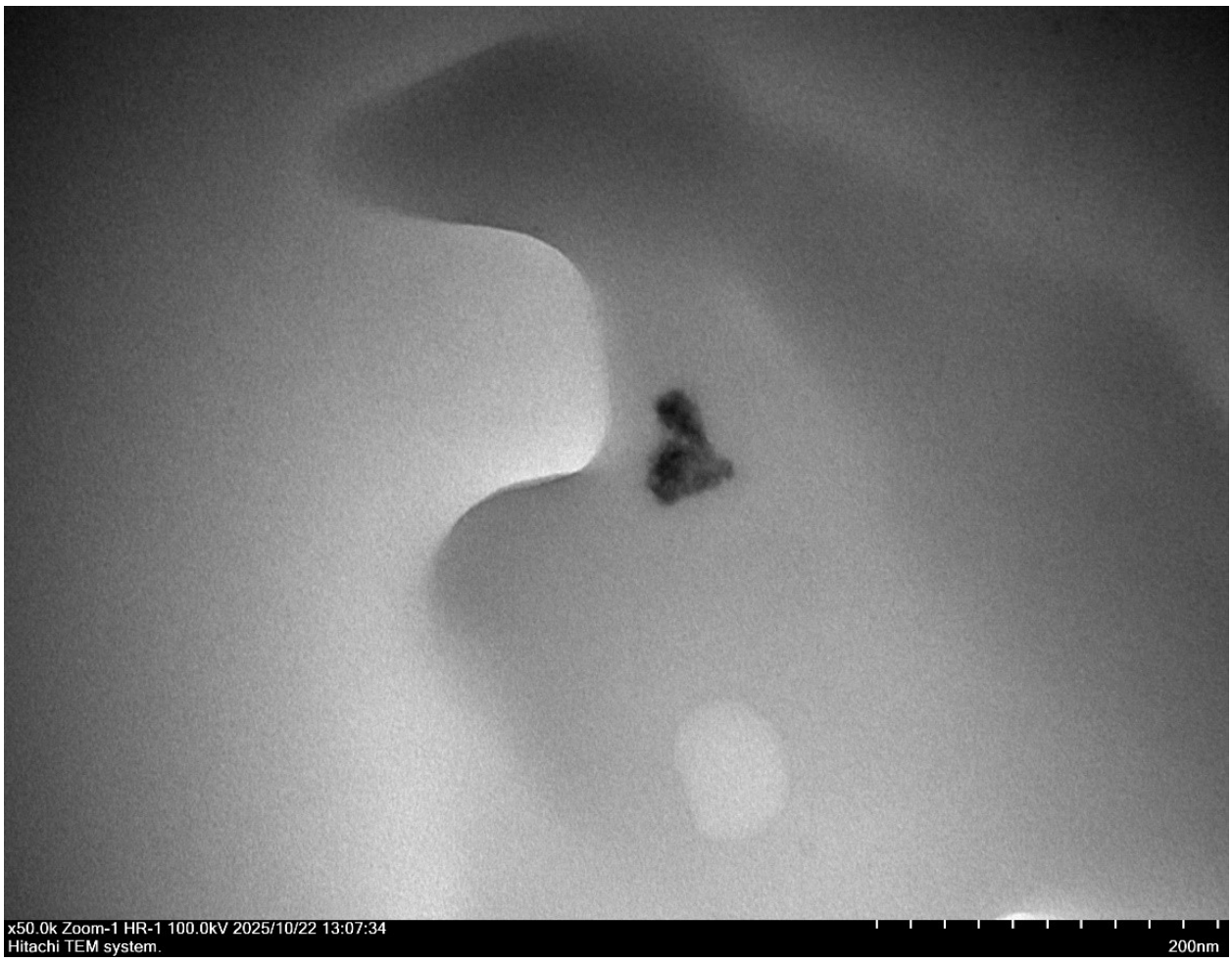

Figure S3. TEM image of Cu NPs obtained in Chan-Evans-Lam type reaction between phenylboronic acid and aniline catalyzed with **[IMesH][$CuCl_2$]** complex.

Figure S4. TEM image of Cu NPs obtained in Chan-Evans-Lam type reaction between phenylboronic acid and aniline catalyzed with **CuCl** salt.

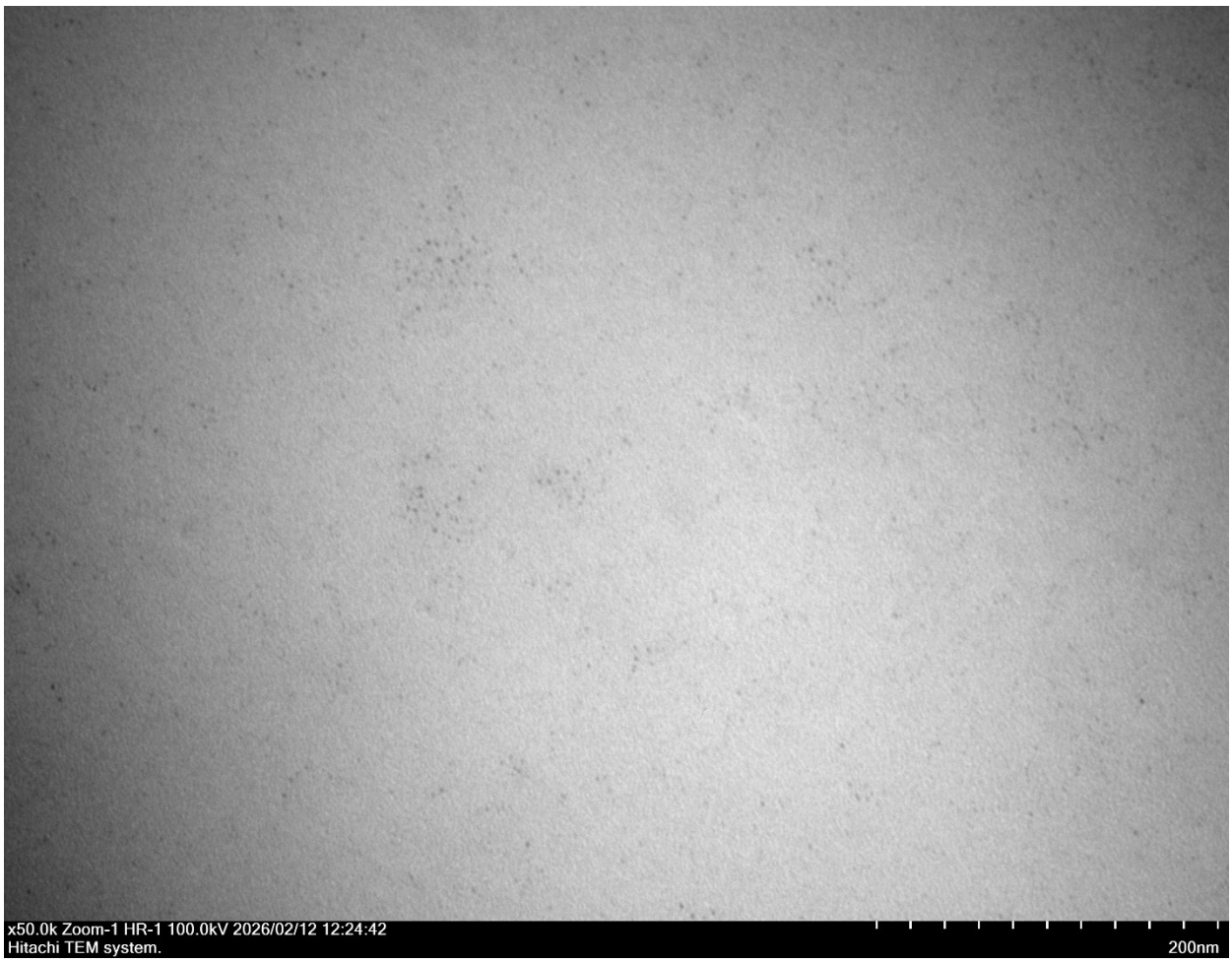

Figure S5. TEM image of Cu NPs obtained in Chan-Evans-Lam type reaction between phenylboronic acid and aniline catalyzed with **$Cu(OAc)_2$** salt.

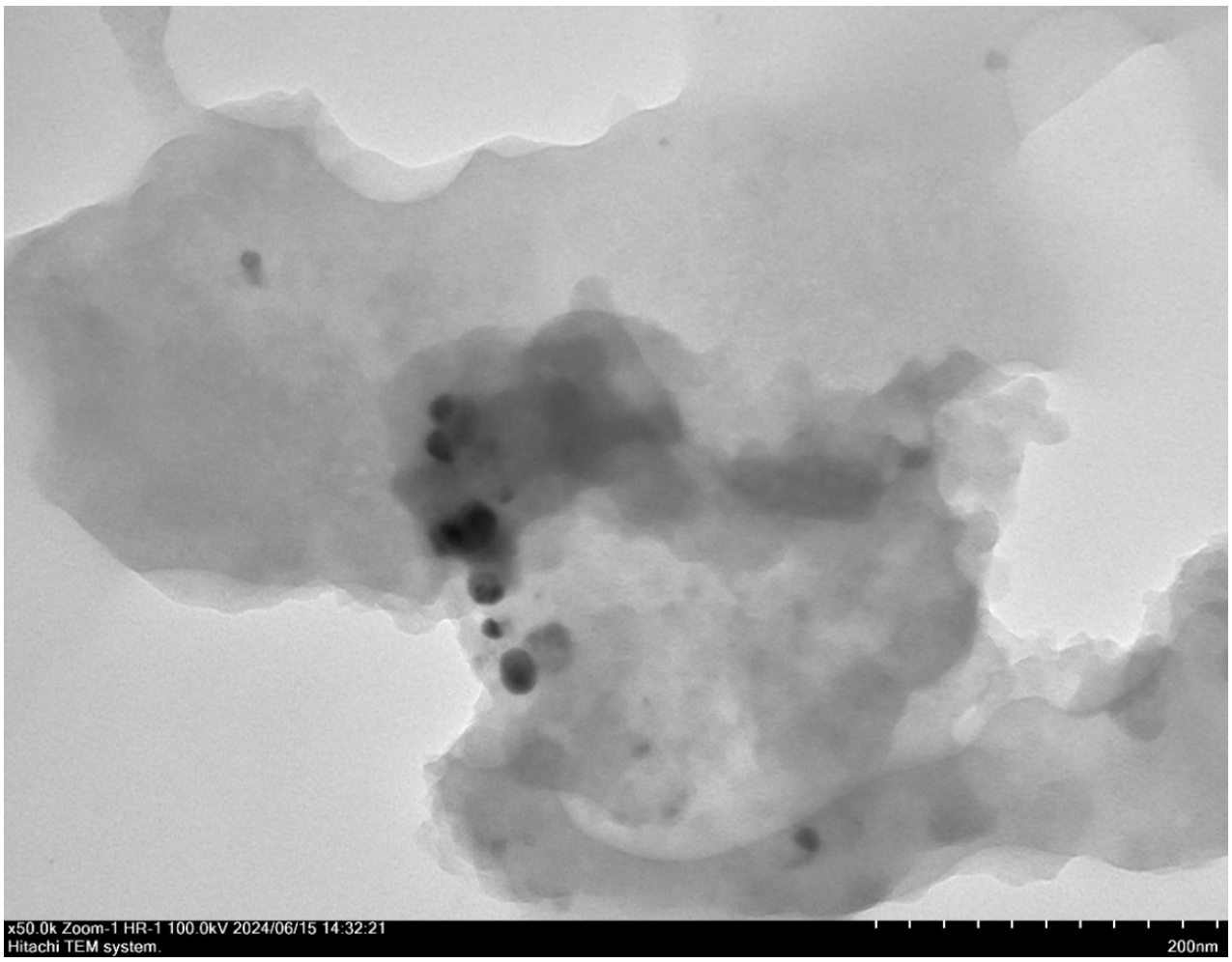

Figure S6. TEM image of Cu NPs obtained in "click" azide-alkyne coupling reaction between 4-azidotoluene and phenylacetylene catalyzed with **Ph_3PCuCl** complex.

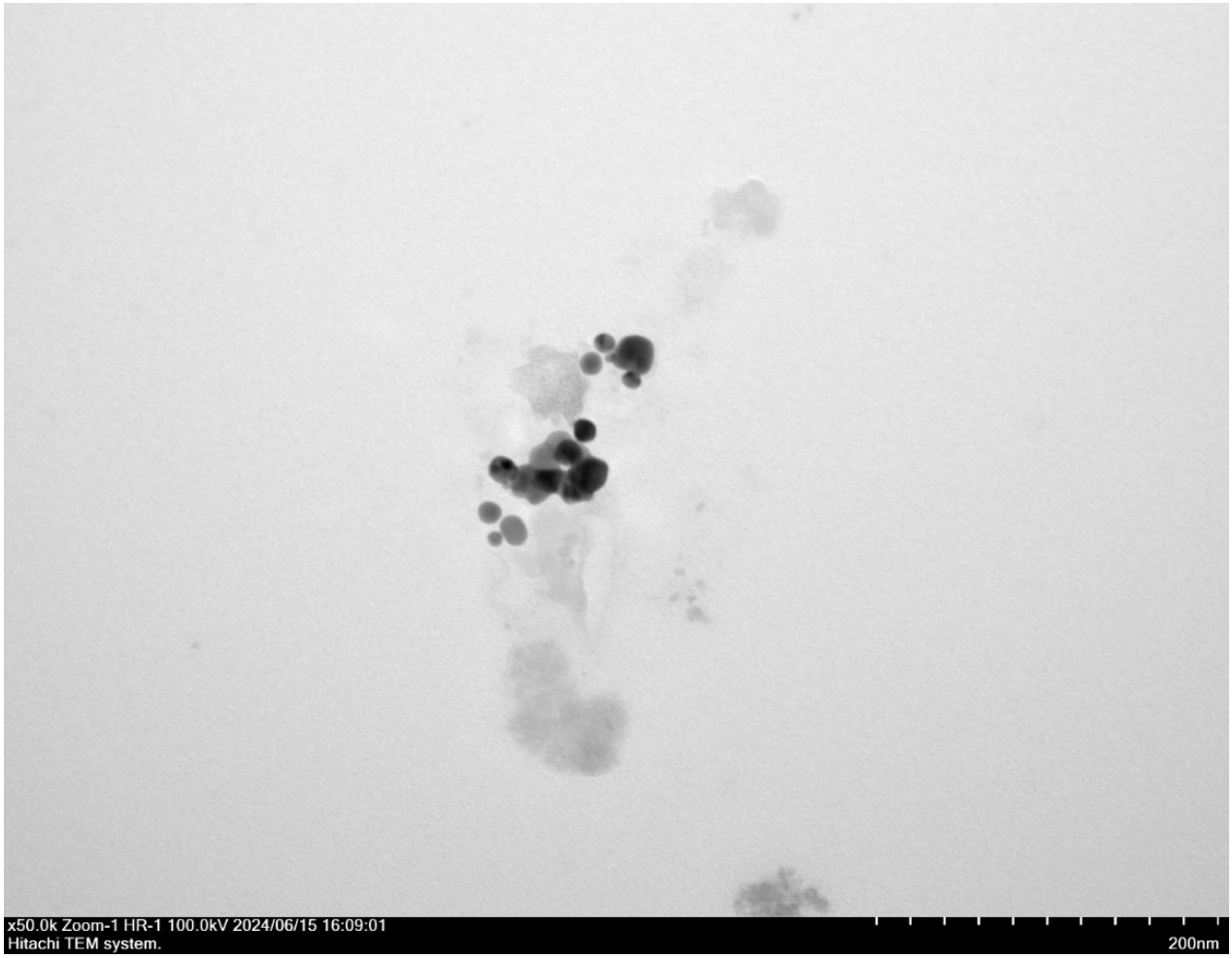

Figure S7. TEM image of Cu NPs obtained in "click" azide-alkyne coupling reaction between 4-azidotoluene and phenylacetylene catalyzed with **IMesCuCl** complex.

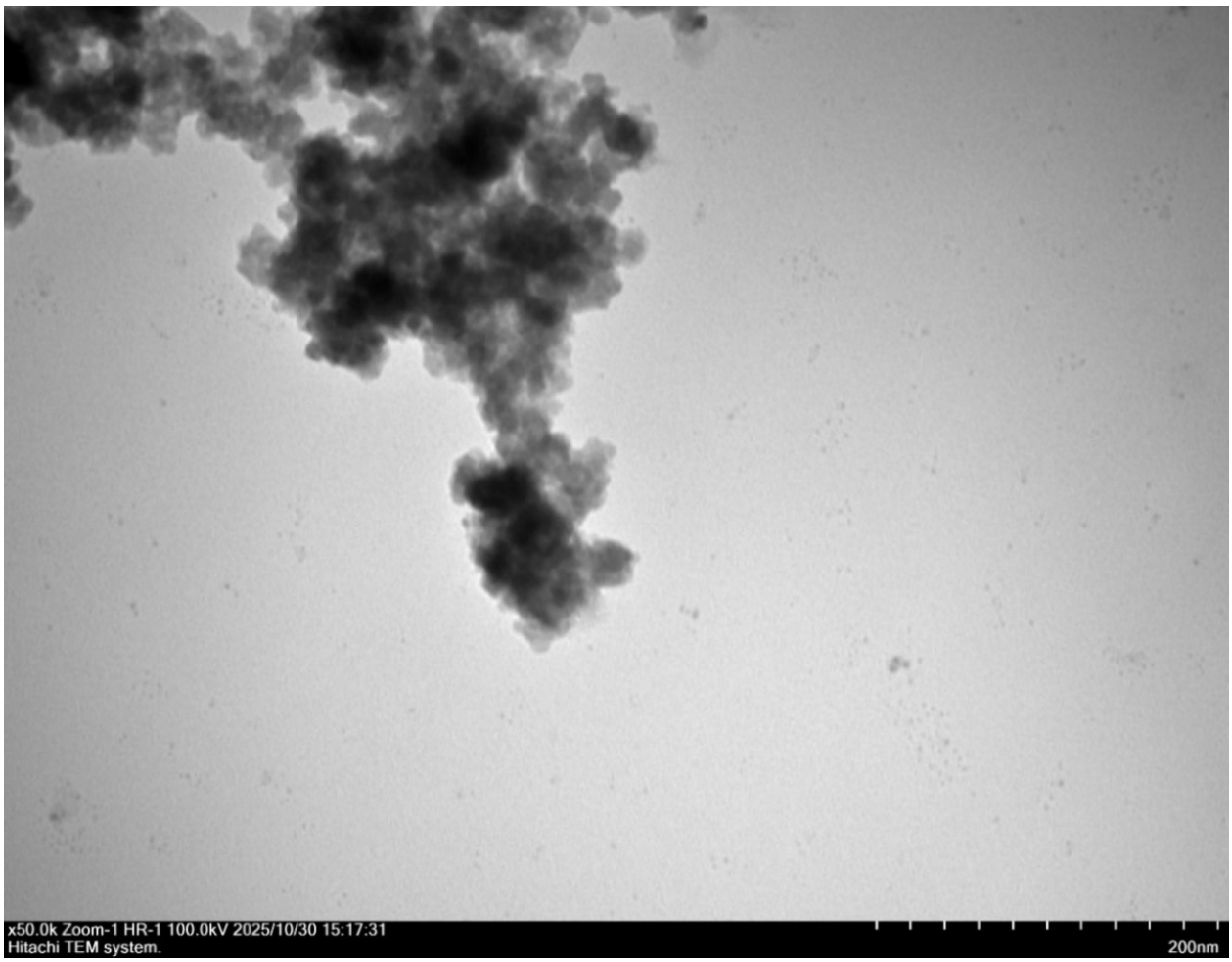

Figure S8. TEM image of Cu NPs obtained in "click" azide-alkyne coupling reaction between 4-azidotoluene and phenylacetylene catalyzed with [**IMesH][CuCl$_2$]** complex.

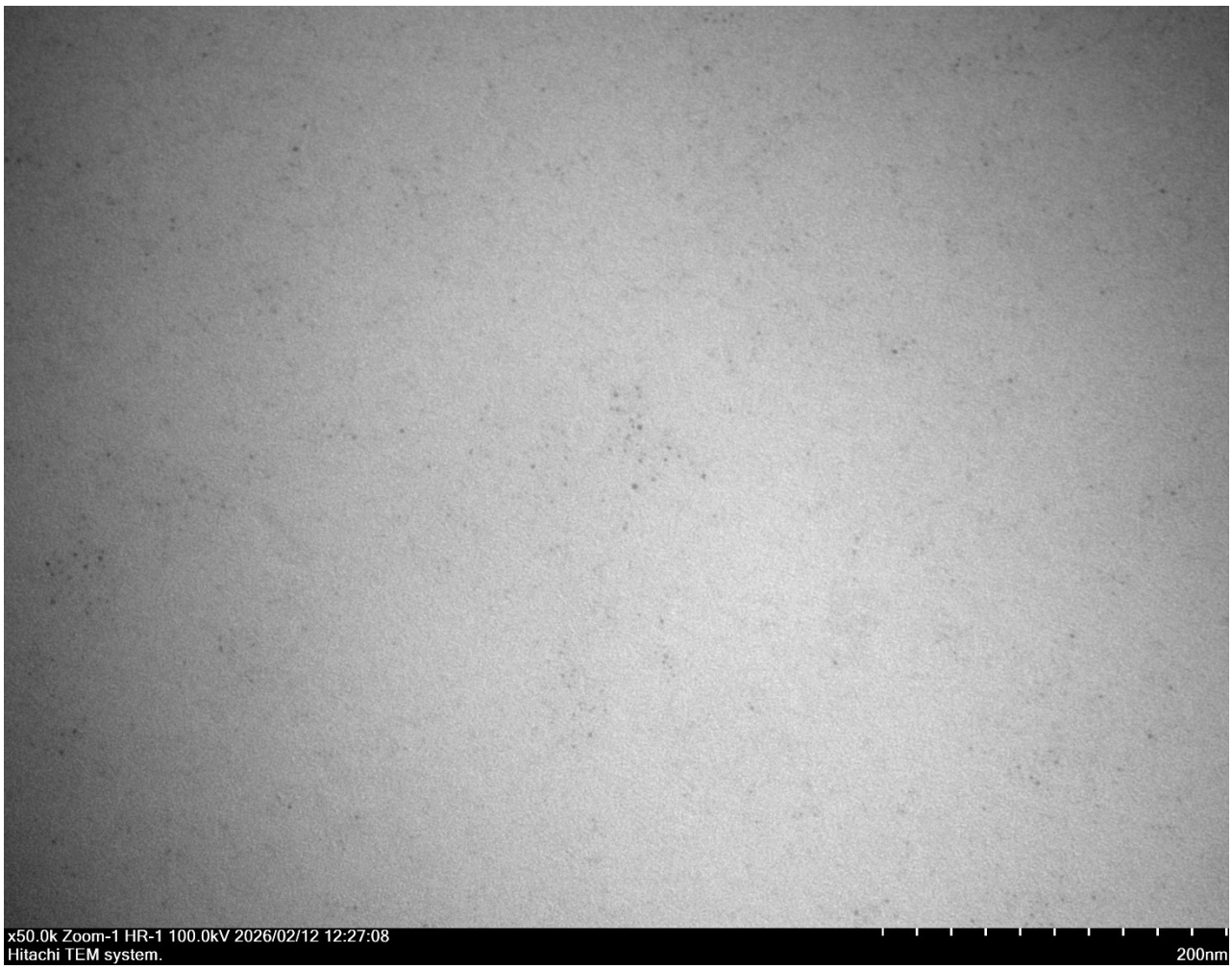

Figure S9. TEM image of Cu NPs obtained in “click” azide-alkyne coupling reaction between 4-azidotoluene and phenylacetylene catalyzed with **CuCl** salt.

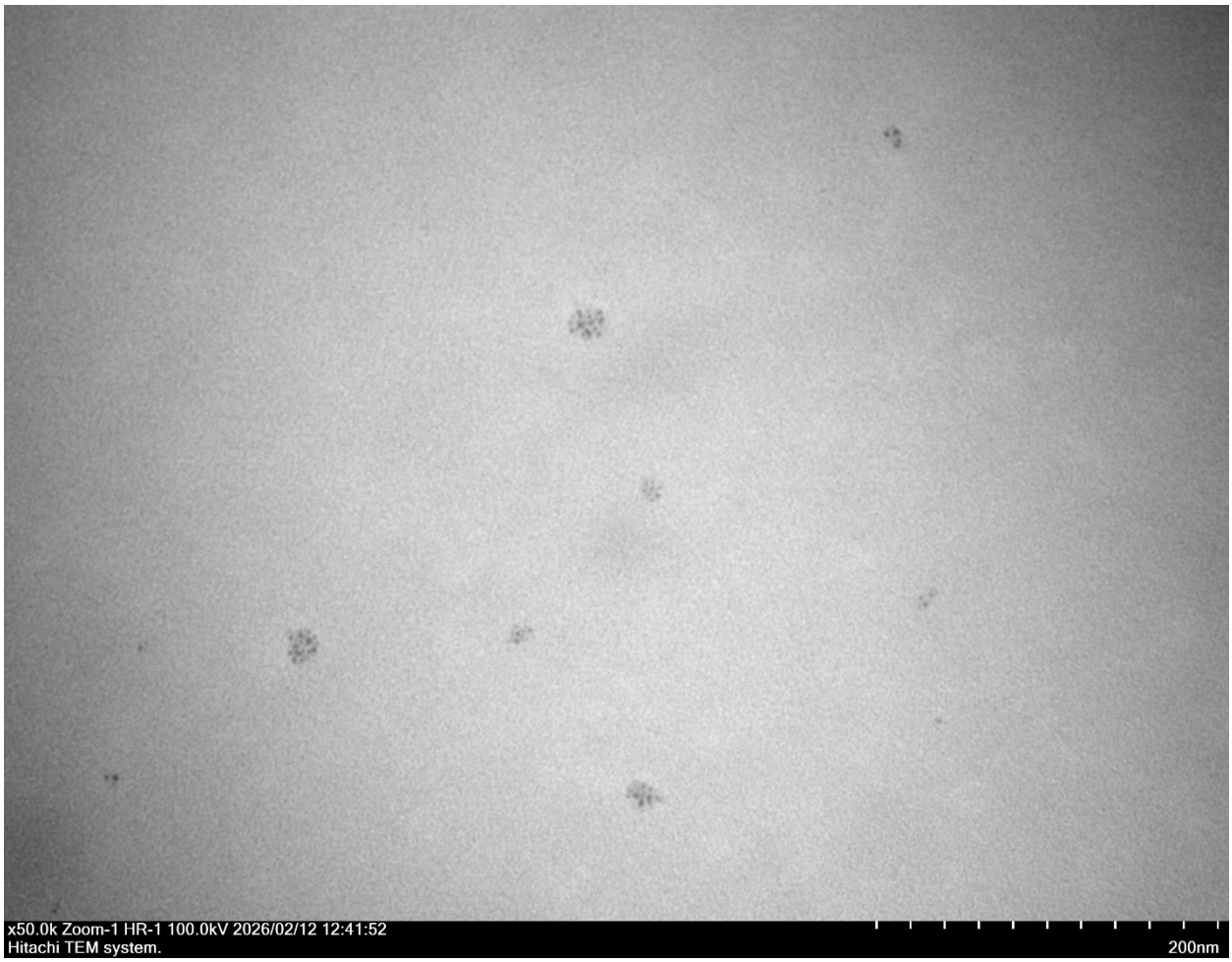

Figure S10 TEM image of Au NPs obtained in Ullmann type C-S coupling reaction between phenyliodide and aniline catalyzed with **CuCl** salt.

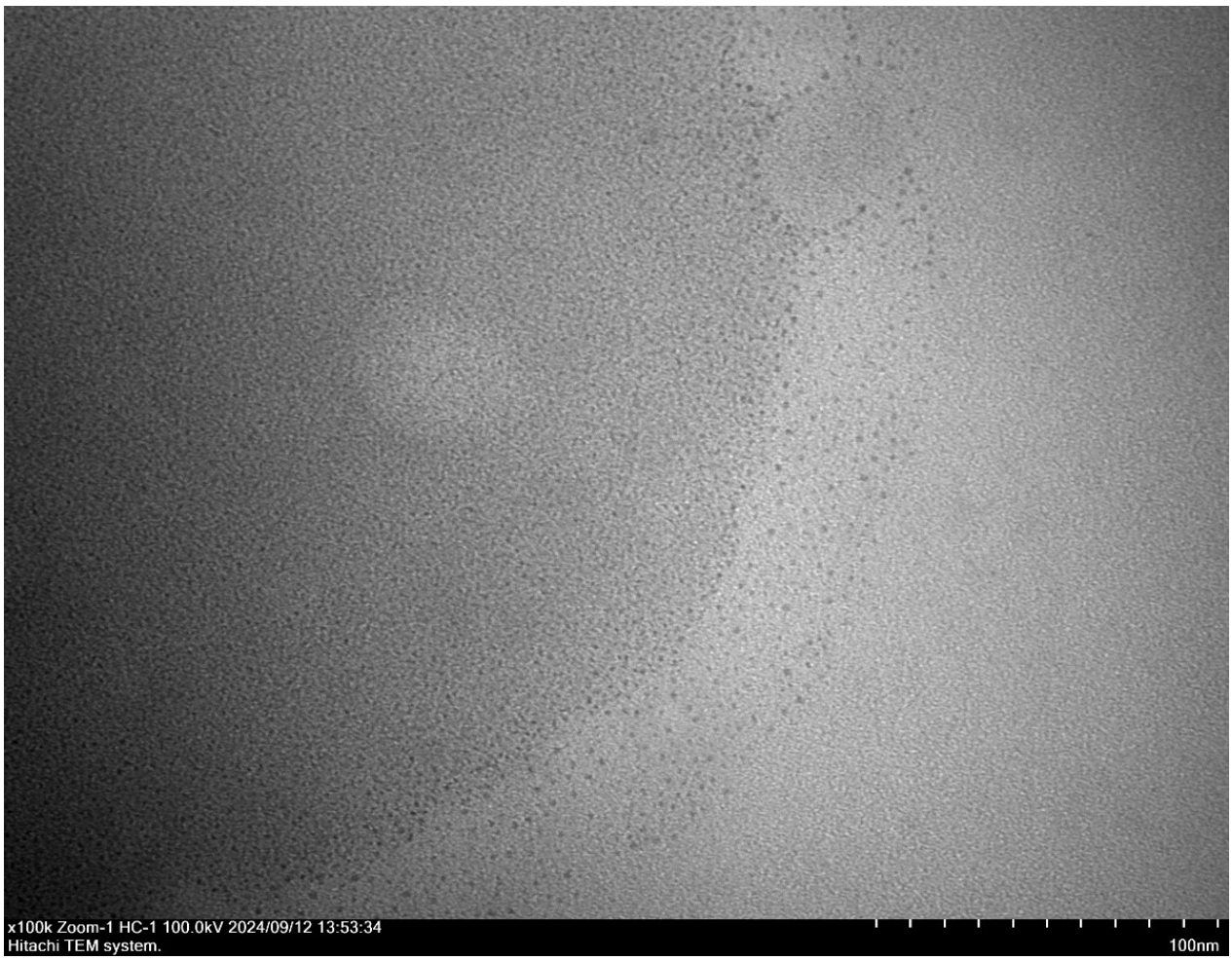

Figure S11. TEM image of Au NPs obtained in Ullmann type C-S coupling reaction between phenyliodide and aniline catalyzed with **Ph_3PAuCl** complex.

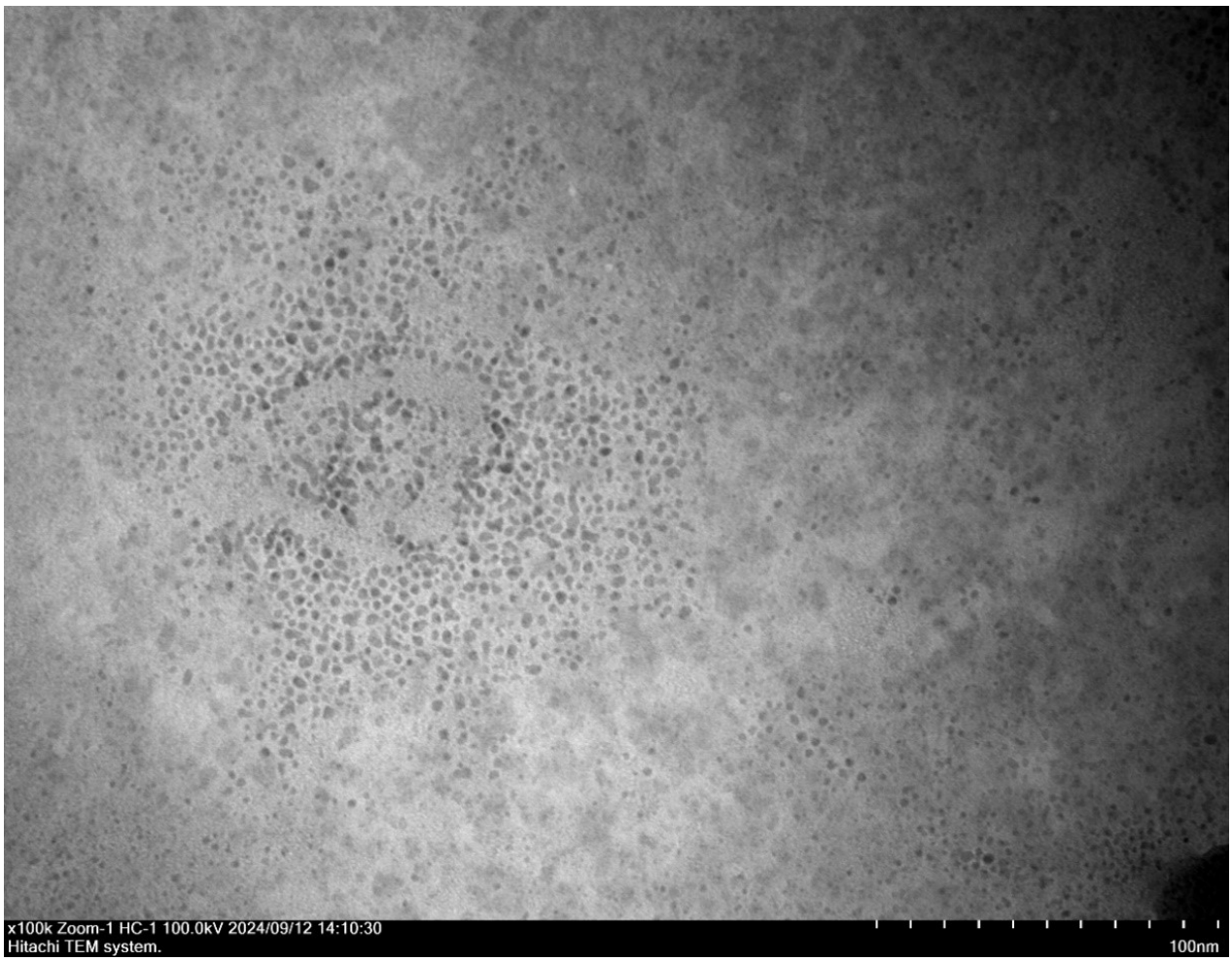

Figure S12. TEM image of Au NPs obtained in Ullmann type C-S coupling reaction between phenyliodide and aniline catalyzed with **IMesAuCl** complex.

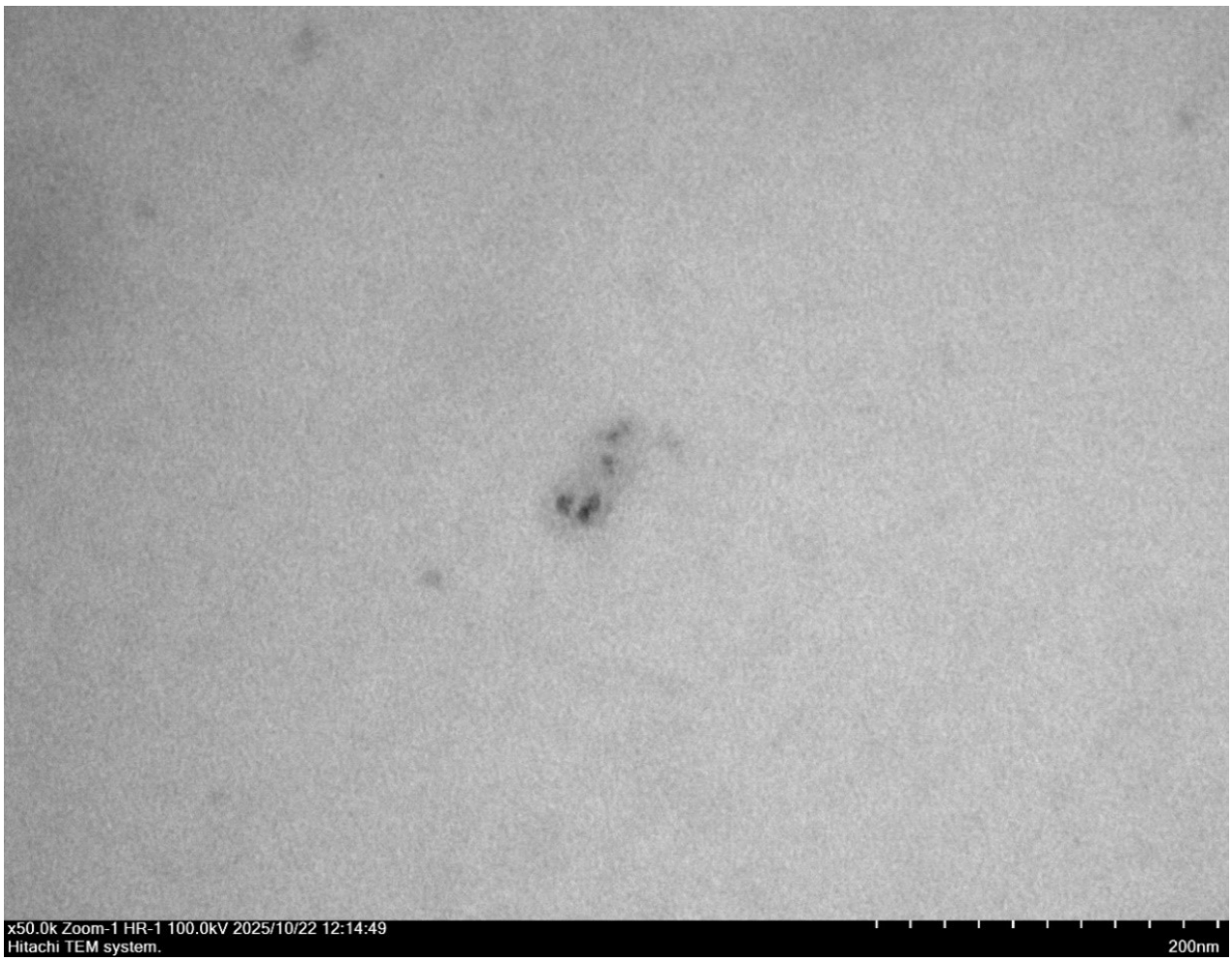

Figure S13. TEM image of Au NPs obtained in Ullmann type C-S coupling reaction between phenyliodide and aniline catalyzed with **[IMesH][$AuCl_2$]** complex.

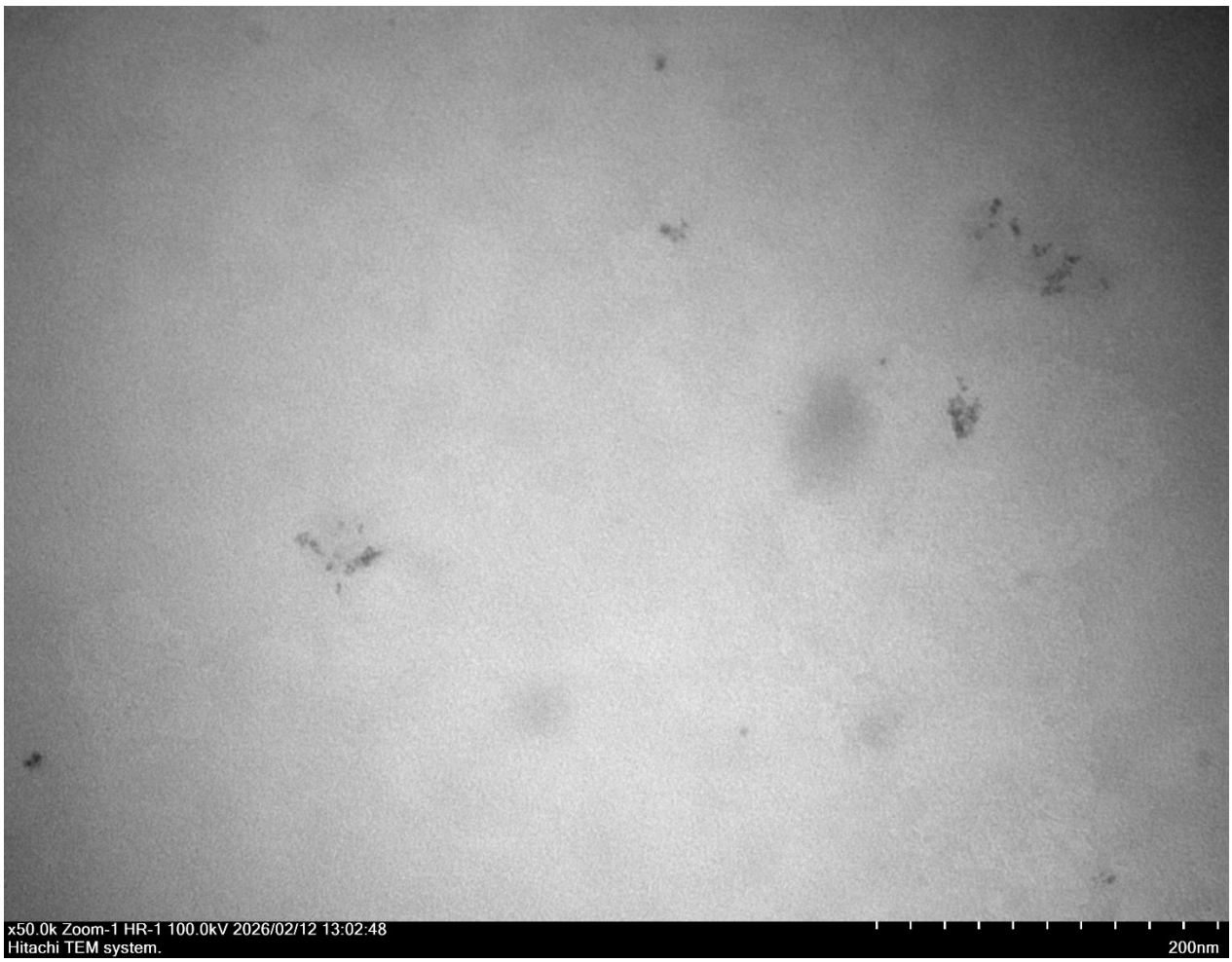

Figure S14. TEM image of Au NPs obtained in Ullmann type C-S coupling reaction between phenyliodide and aniline catalyzed with **AuCl** salt.

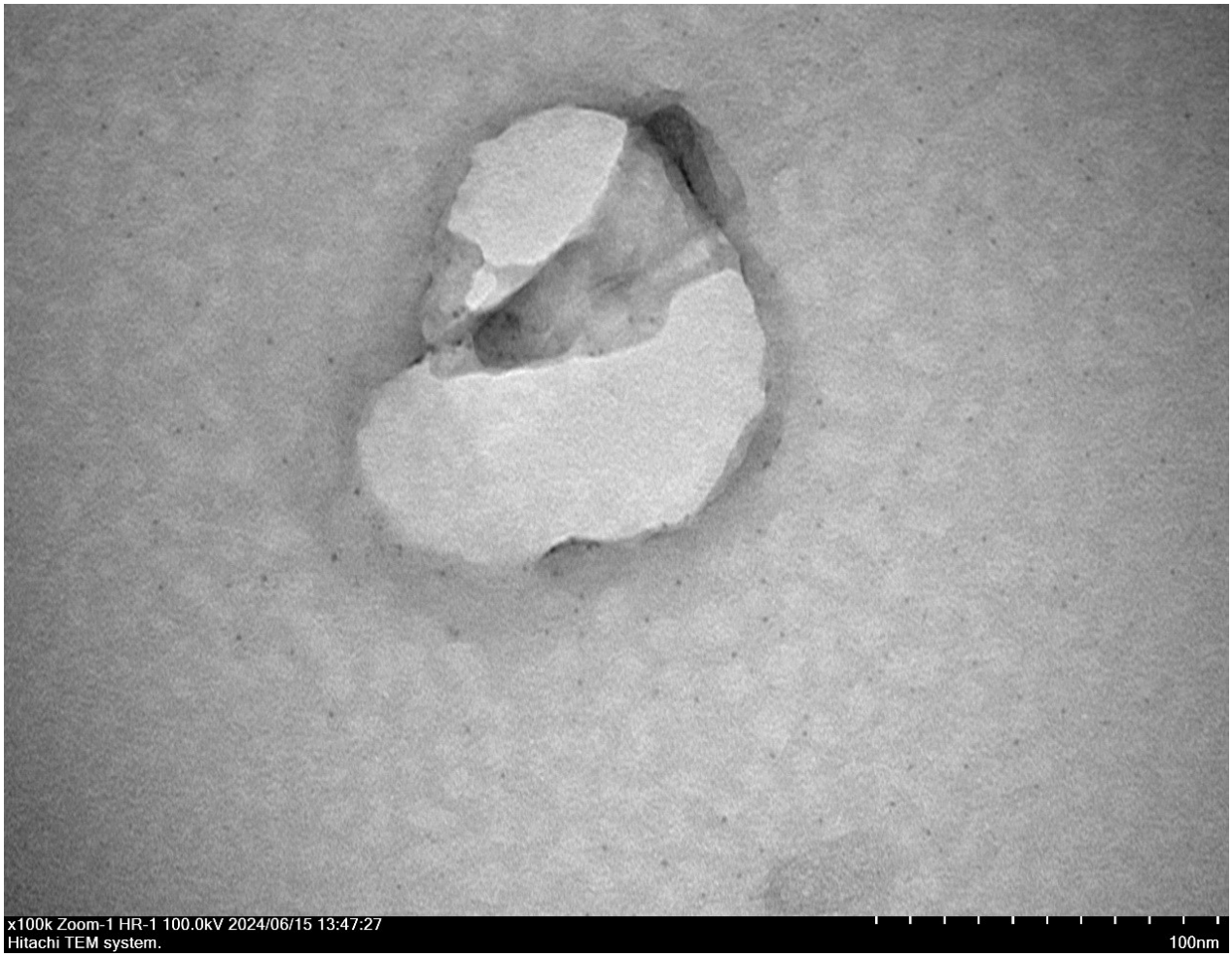

Figure S15. TEM image of Au NPs obtained in A^3 (aldehyde-alkyne-amine) coupling reaction between 4-methoxybenzaldehyde, phenylacetylene and morpholine catalyzed with **Ph_3PAuCl** complex.

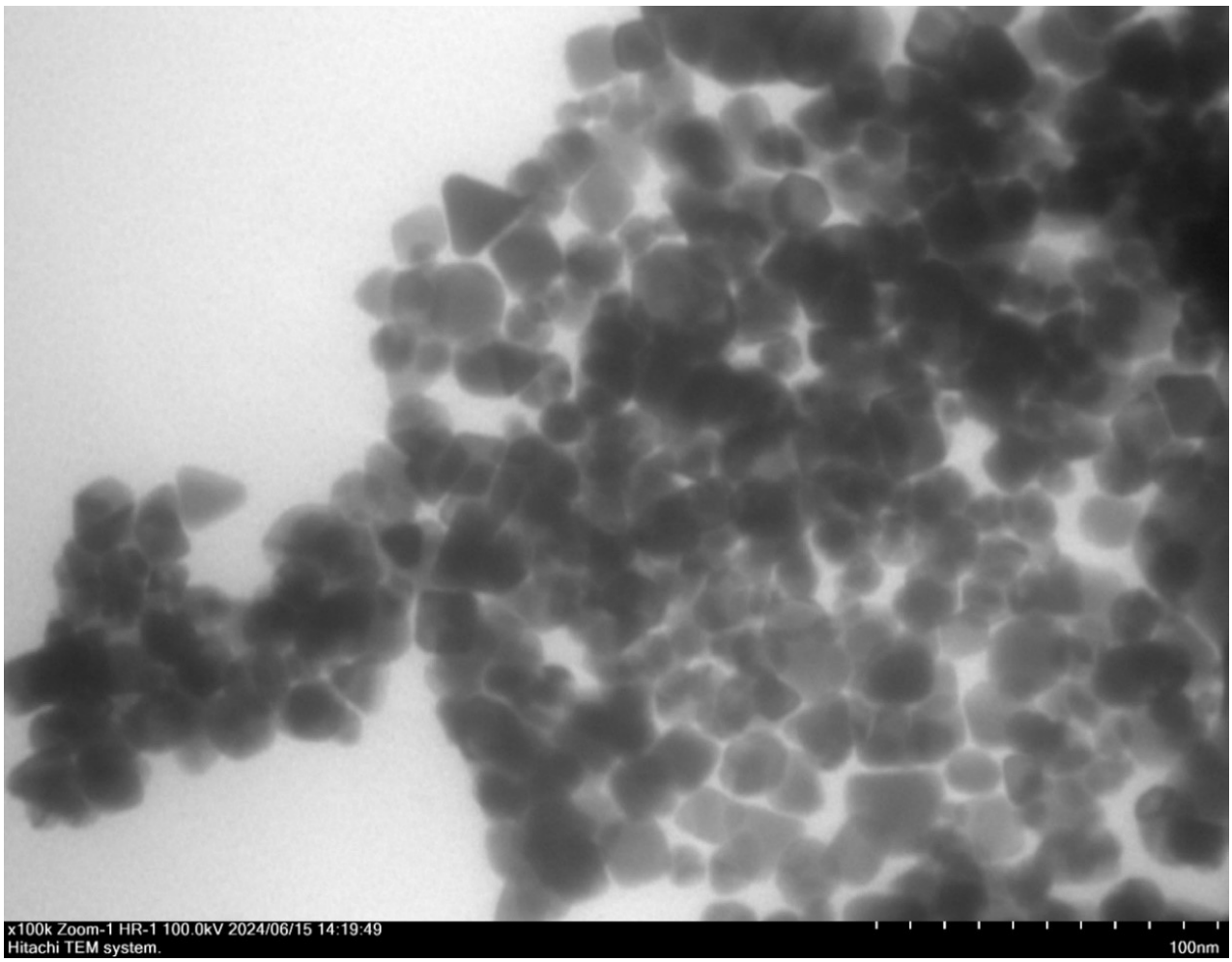

Figure S16. TEM image of Au NPs obtained in A^3 (aldehyde-alkyne-amine) coupling reaction between 4-methoxybenzaldehyde, phenylacetylene and morpholine catalyzed with **IMesAuCl** complex.

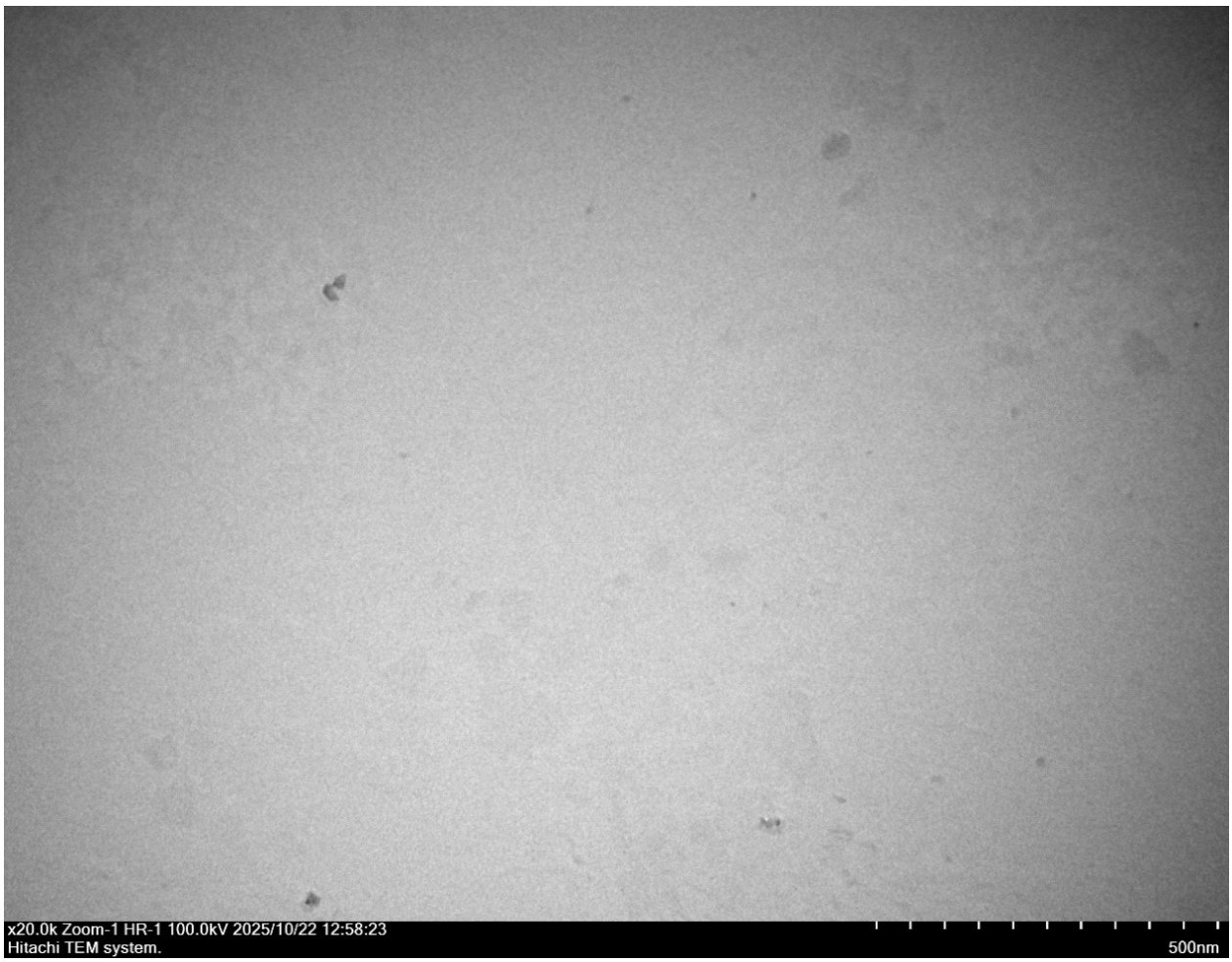

Figure S17. TEM image of Au NPs obtained in A^3 (aldehyde-alkyne-amine) coupling reaction between 4-methoxybenzaldehyde, phenylacetylene and morpholine catalyzed with **[IMesH][$AuCl_2$]** complex.

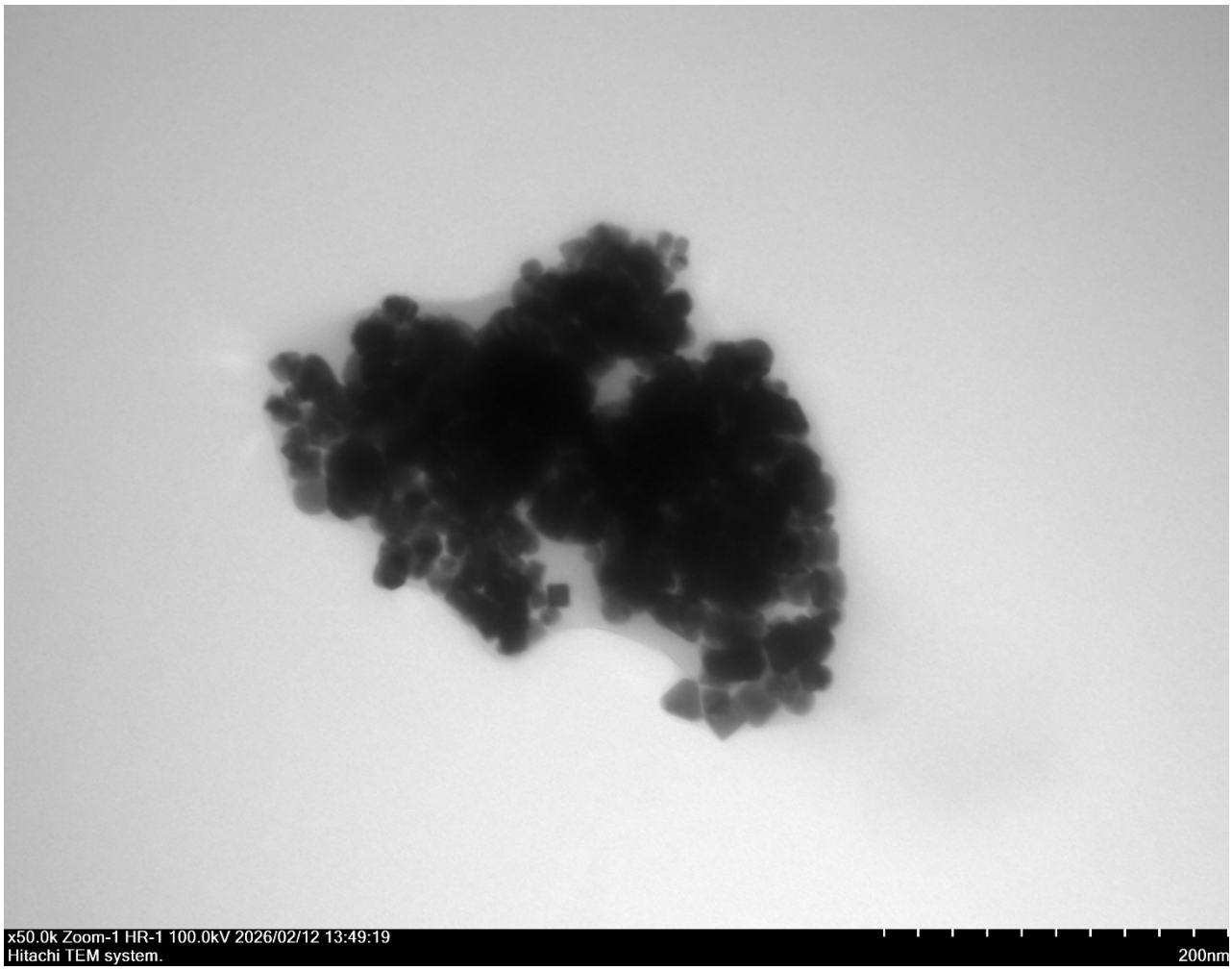

Figure S18. TEM image of Au NPs obtained in A^3 (aldehyde-alkyne-amine) coupling reaction between 4-methoxybenzaldehyde, phenylacetylene and morpholine catalyzed with **AuCl** salt.

Figure S19. TEM image of Au NPs obtained in hydration of phenylacetylene reaction with **Ph_3PAuCl** complex.

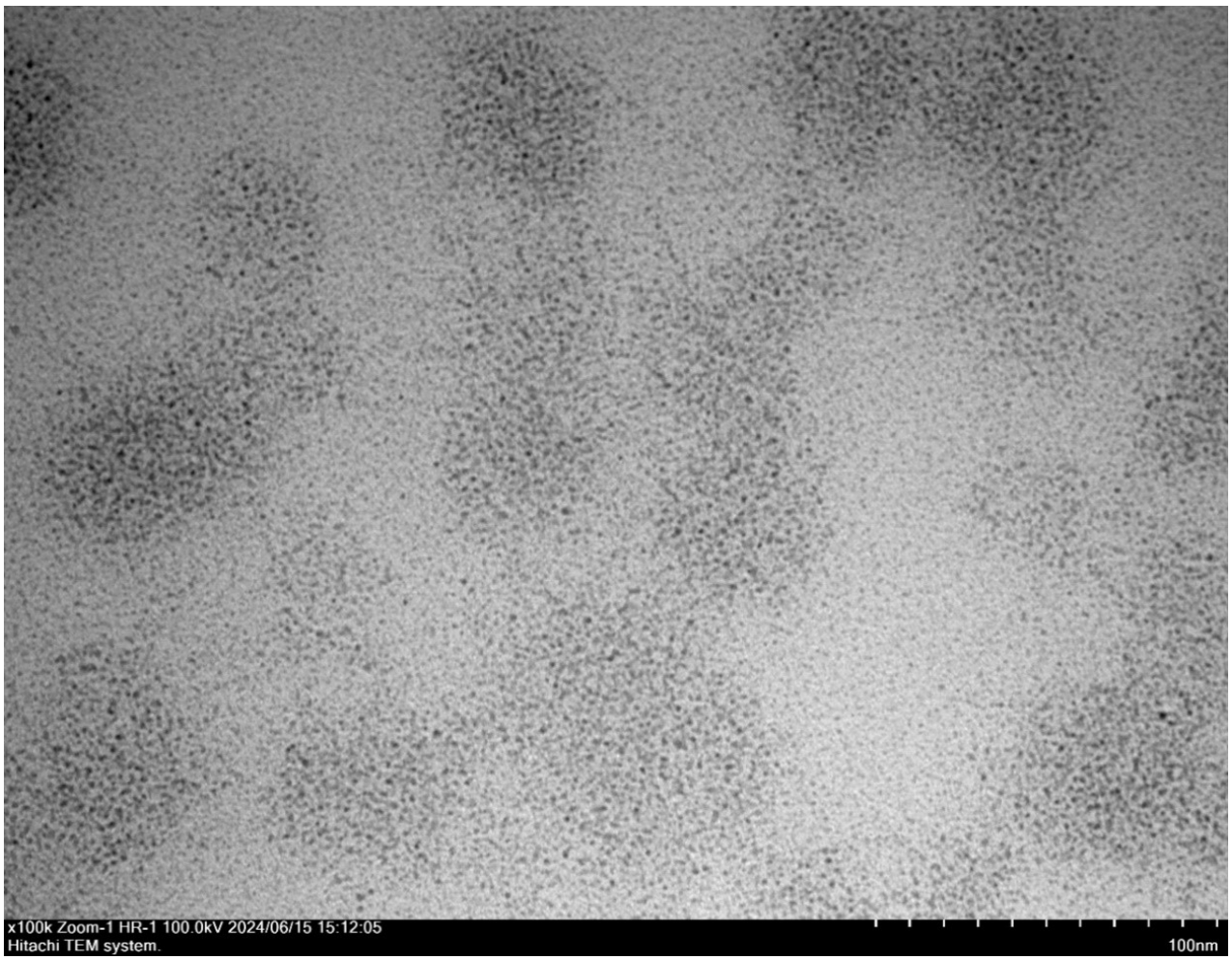

Figure S20. TEM image of Au NPs obtained in hydration of phenylacetylene reaction catalyzed with **IMesAuCl** complex.

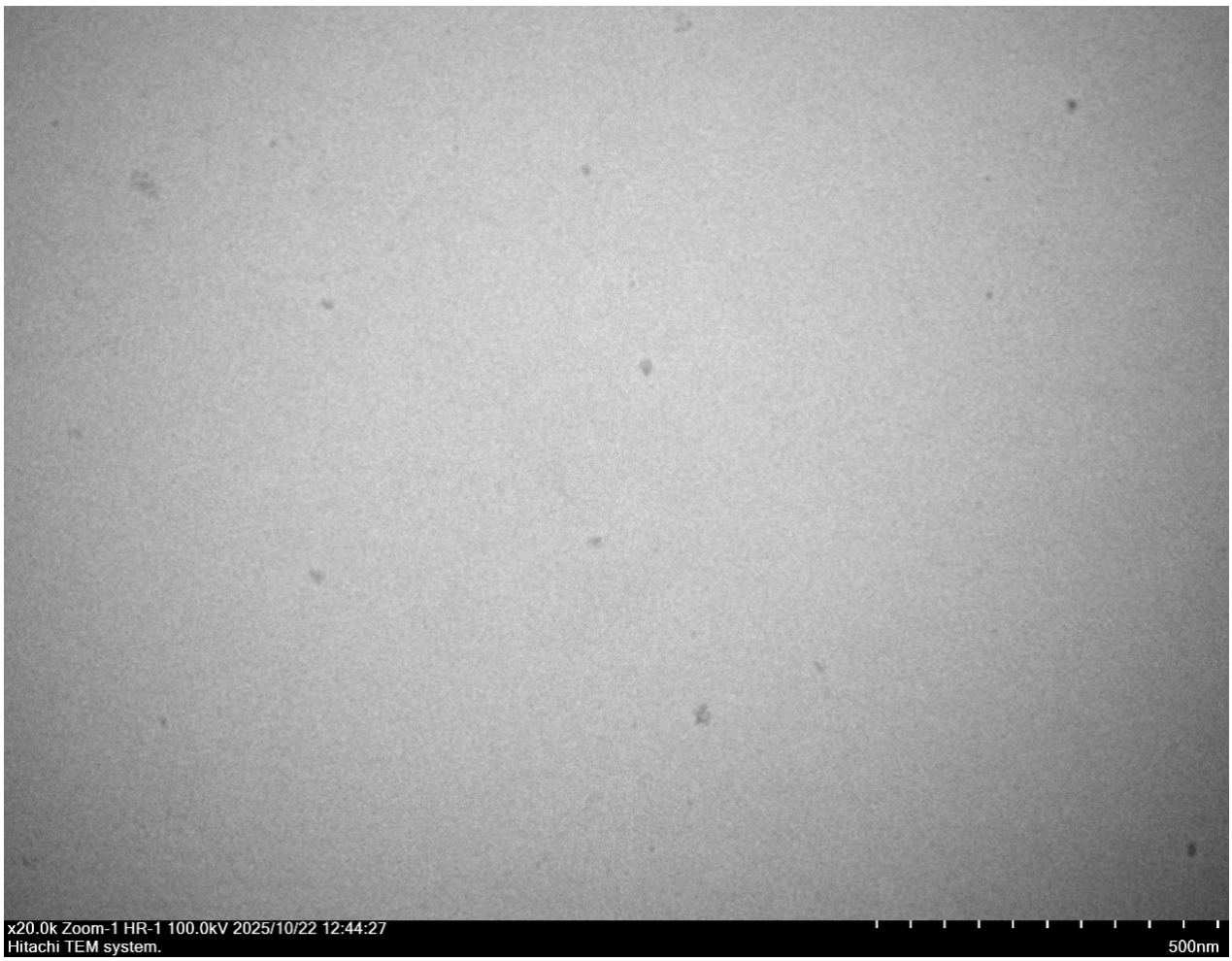

Figure S21. TEM image of Au NPs obtained in hydration of phenylacetylene reaction catalyzed with **[IMesH][AuCl$_2$]** complex.

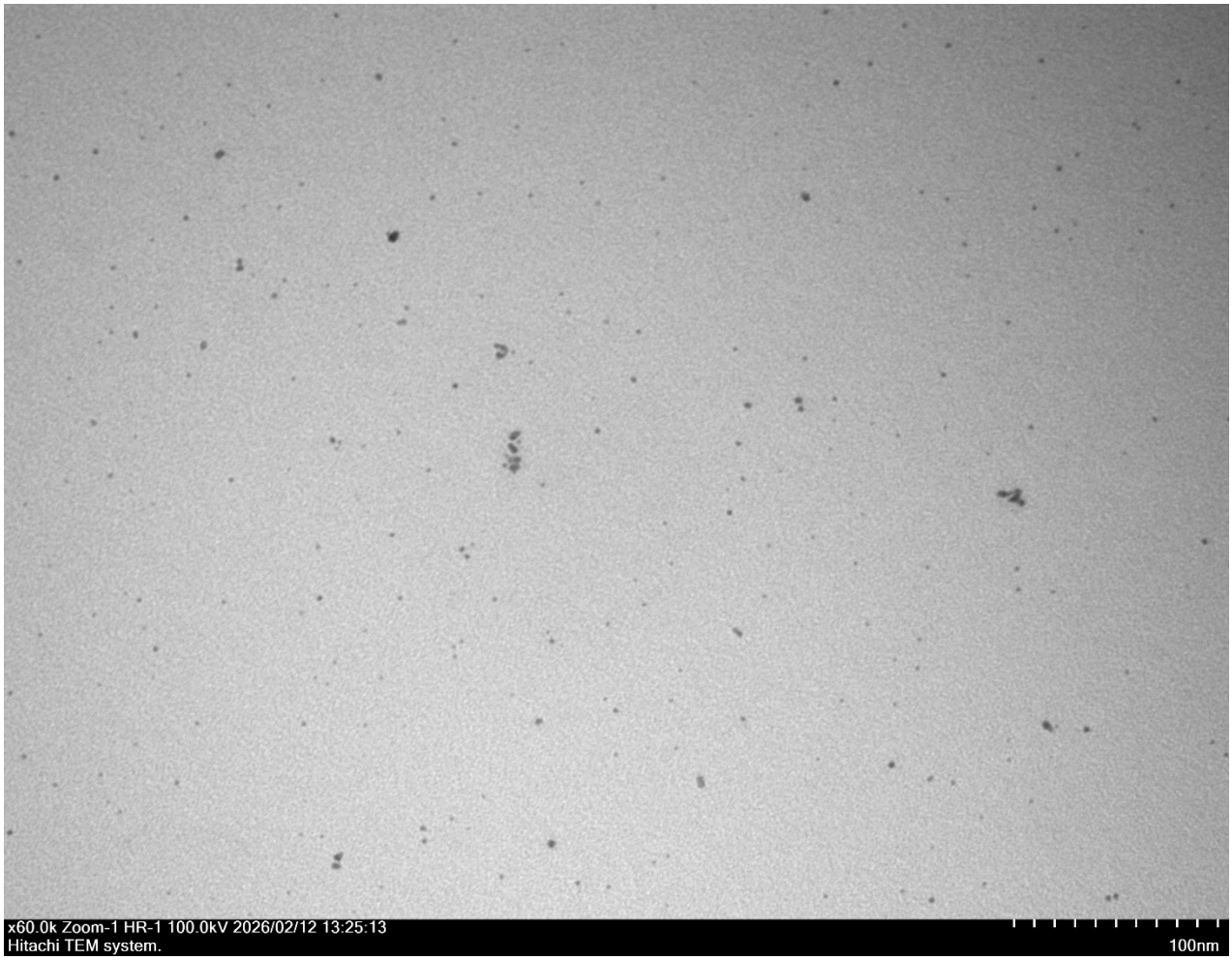

Figure S22. TEM image of Au NPs obtained in hydration of phenylacetylene reaction catalyzed with **AuCl** salt.

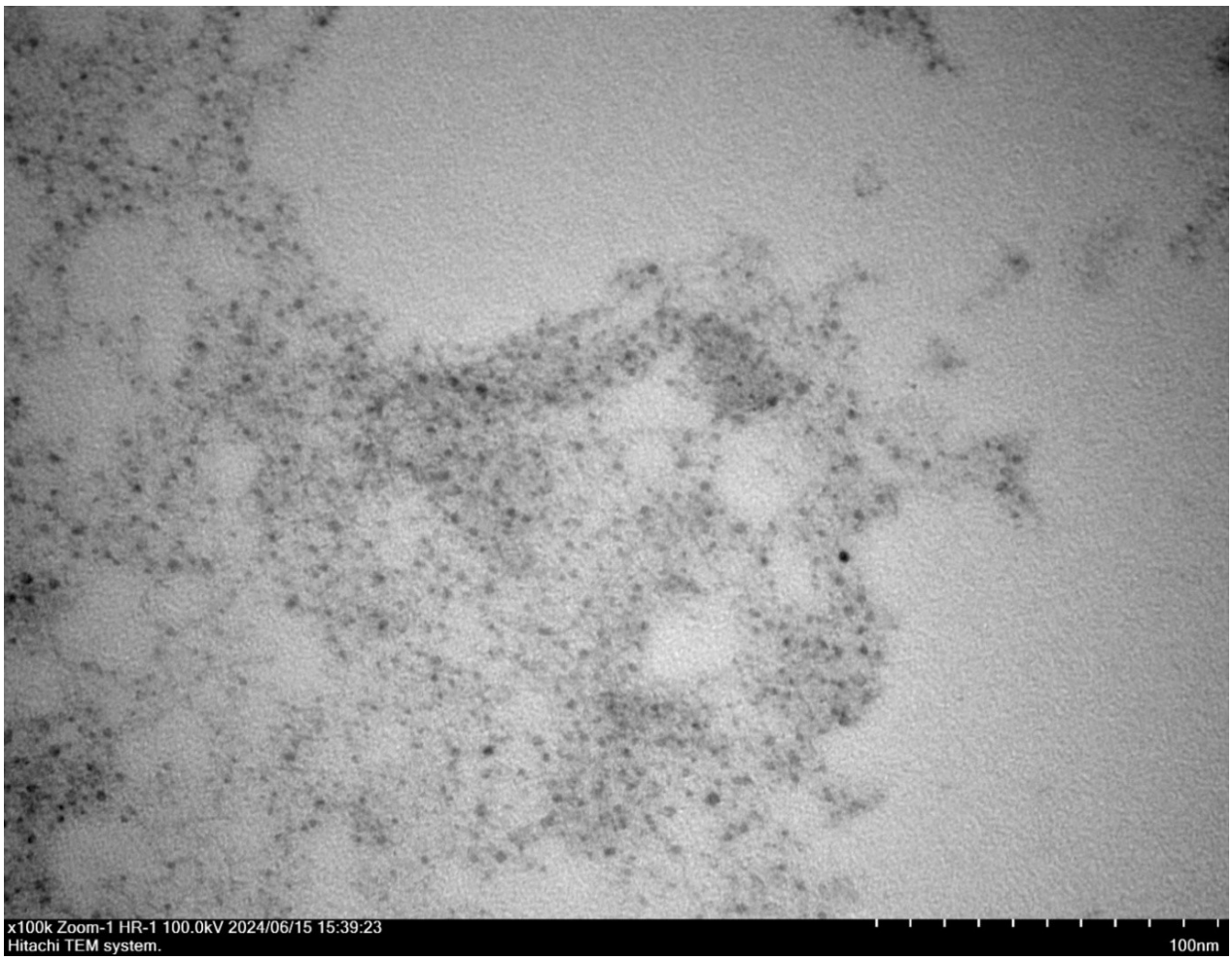

Figure S23. TEM image of Au NPs obtained in nucleophilic addition of aniline to phenylacetylene reaction catalyzed with **Ph_3PAuCl** complex.

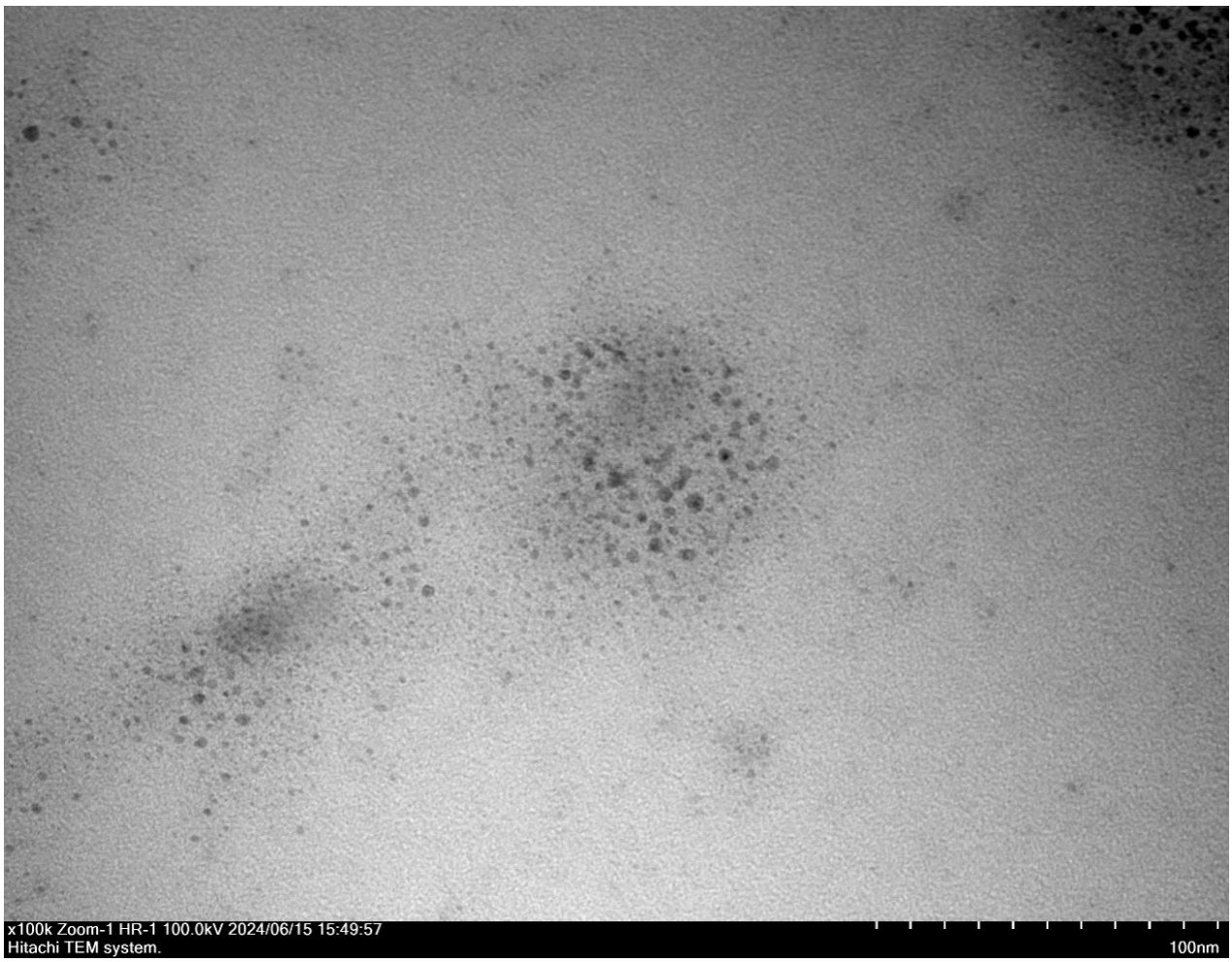

Figure S24. TEM image of Au NPs obtained in nucleophilic addition of aniline to phenylacetylene reaction catalyzed with **IMesAuCl** complex.

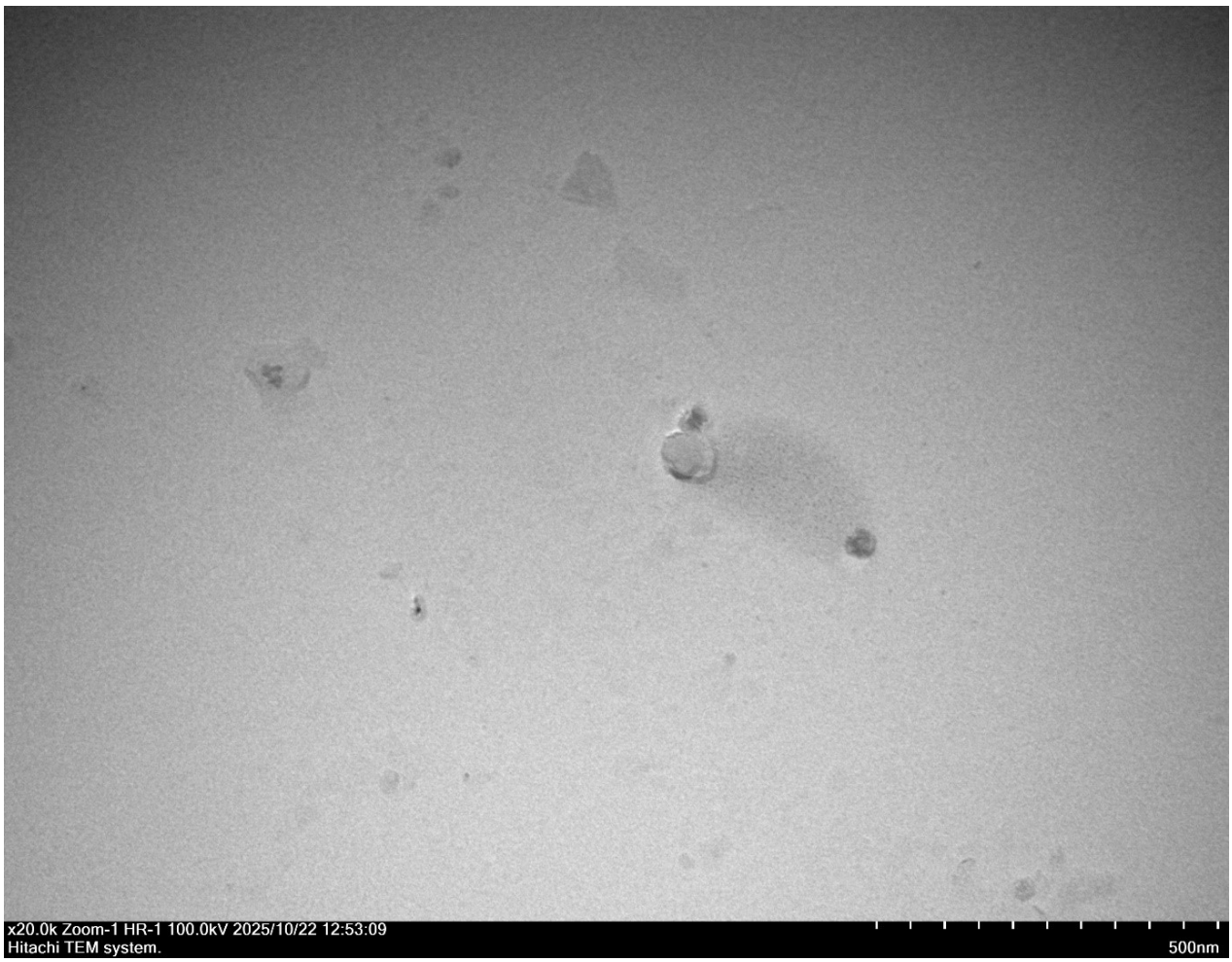

Figure S25. TEM image of Au NPs obtained in nucleophilic addition of aniline to phenylacetylene reaction catalyzed with **[IMesH][AuCl$_2$]** complex.

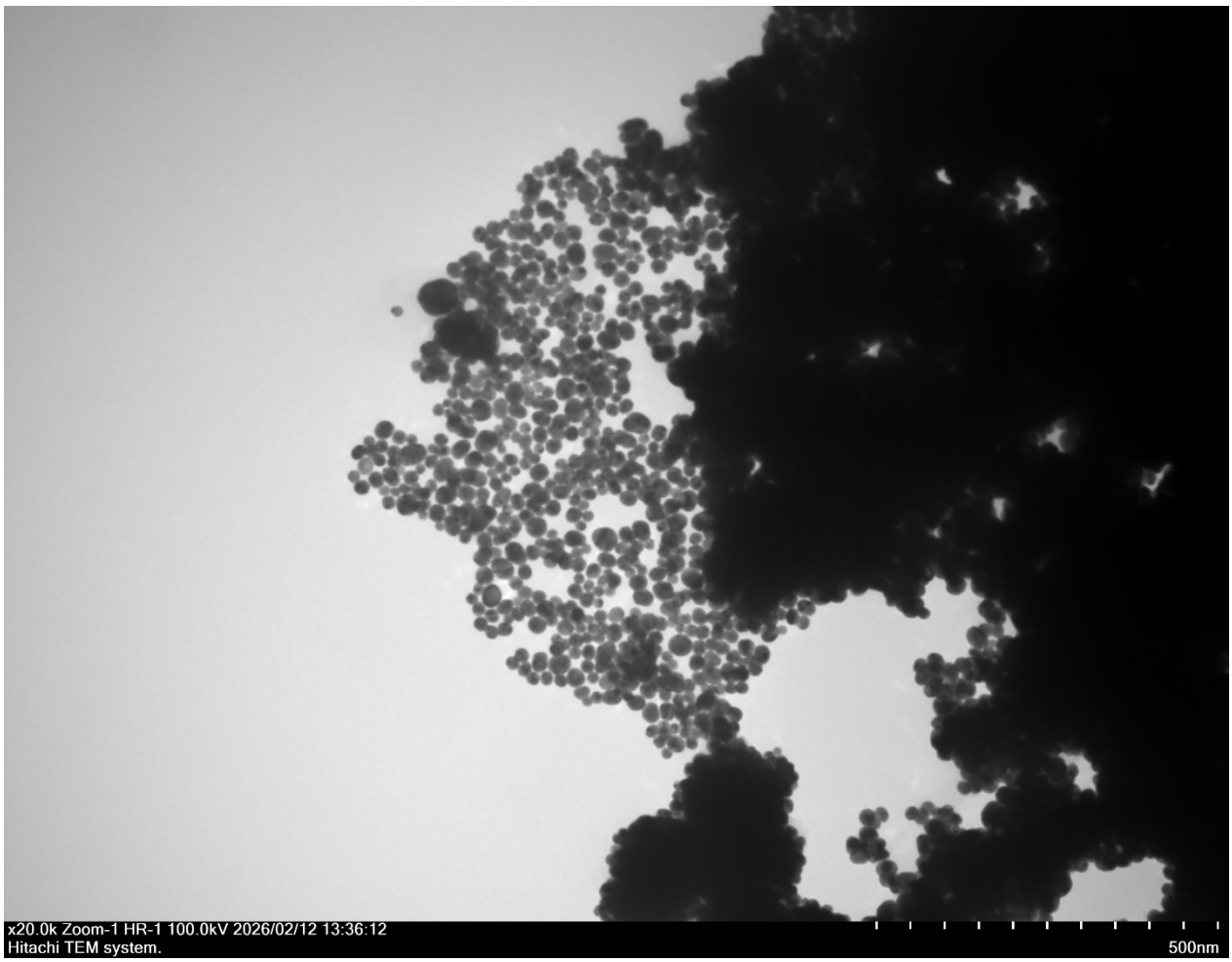

Figure S26. TEM image of Au NPs obtained in nucleophilic addition of aniline to phenylacetylene reaction catalyzed with **AuCl** salt.

S4. ESI-HRMS spectra

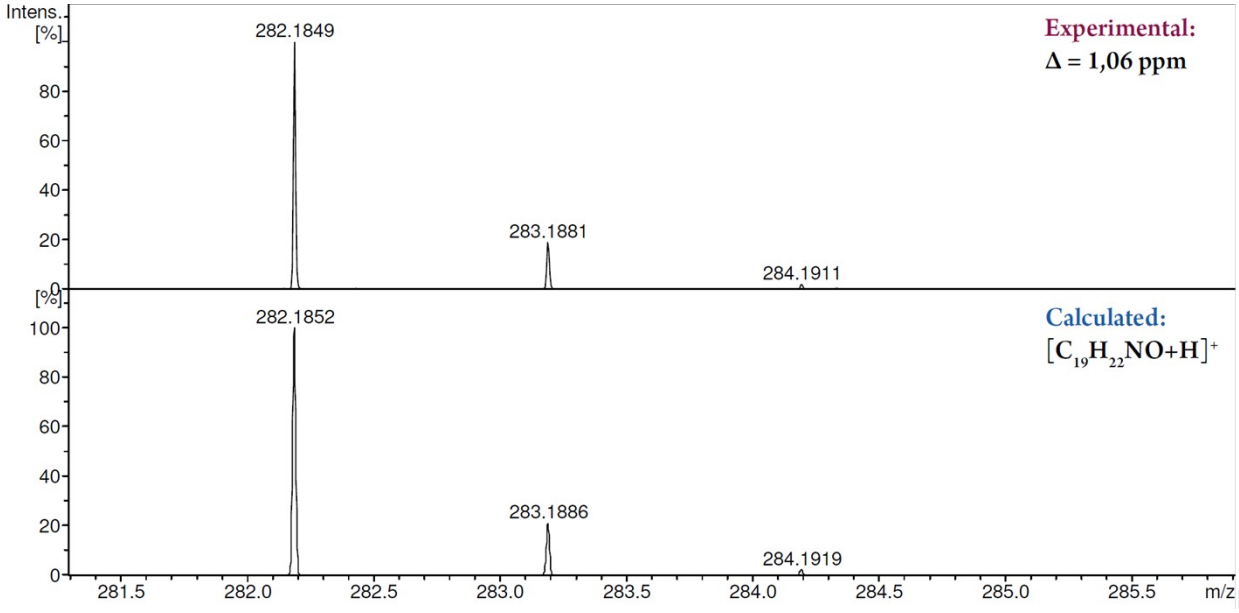

Figure S27. Experimental and theoretical ESI-(+)HRMS spectrum of **6b** in CH_3CN solution: experimental peak $[M+H]^+$ = 282.1849 Da, calculated for $C_{19}H_{23}NO$ = 282.1852, Δ = 1.06 ppm.

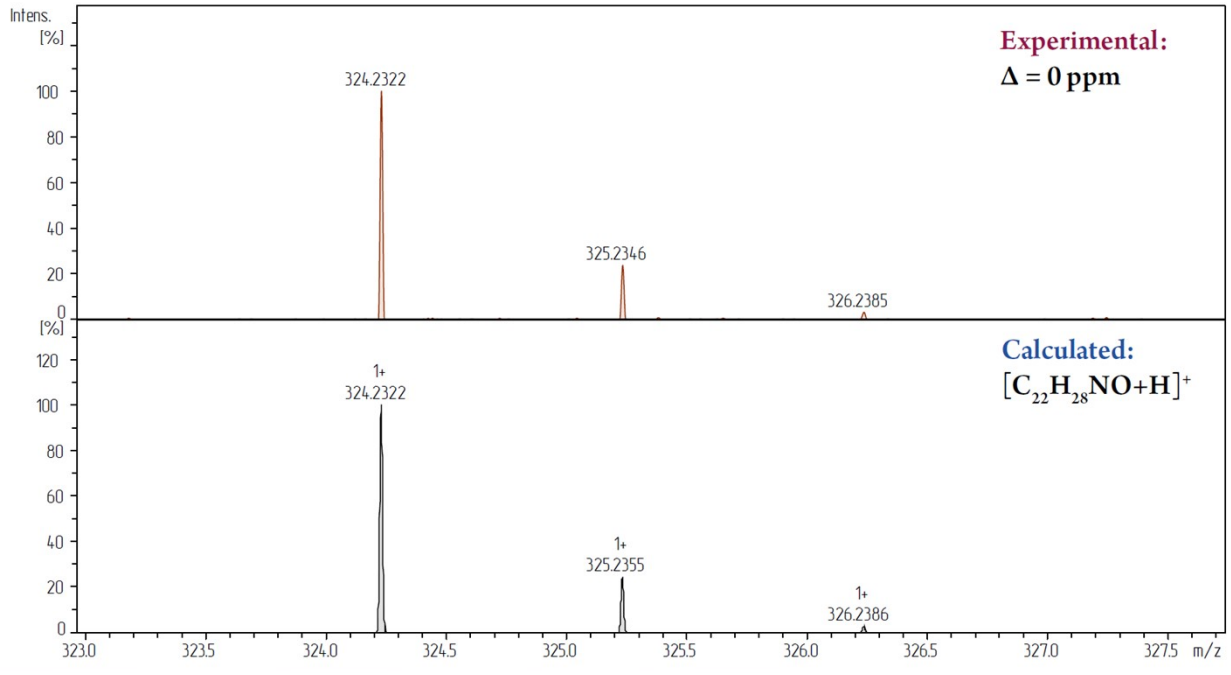

Figure S28. Experimental and theoretical ESI-(+)HRMS spectrum of **6c** in CH_3CN solution: experimental peak $[M+H]^+$ = 324.2322 Da, calculated for $C_{22}H_{28}NO$ = 324.2322, Δ = 0 ppm.

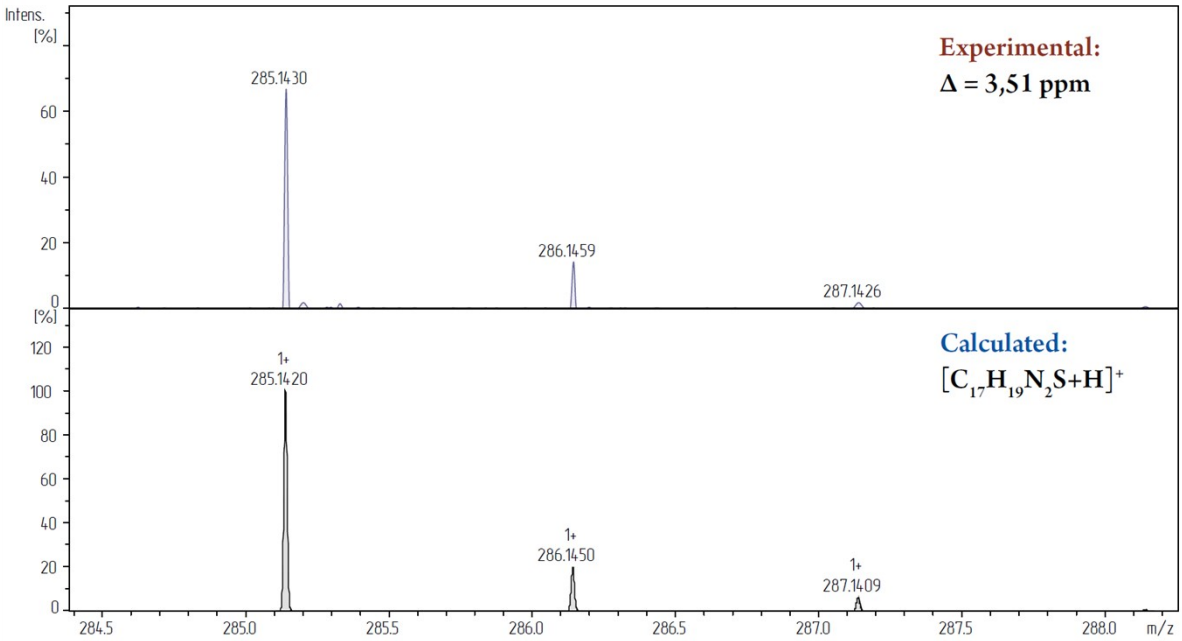

Figure S29. Experimental and theoretical ESI-(+)HRMS spectrum of **6d** in CH_3CN solution: experimental peak $[M+H]^+$ = 285.1430 Da, calculated for $C_{17}H_{20}N_2S$ = 285.1420, Δ = 3.51 ppm.

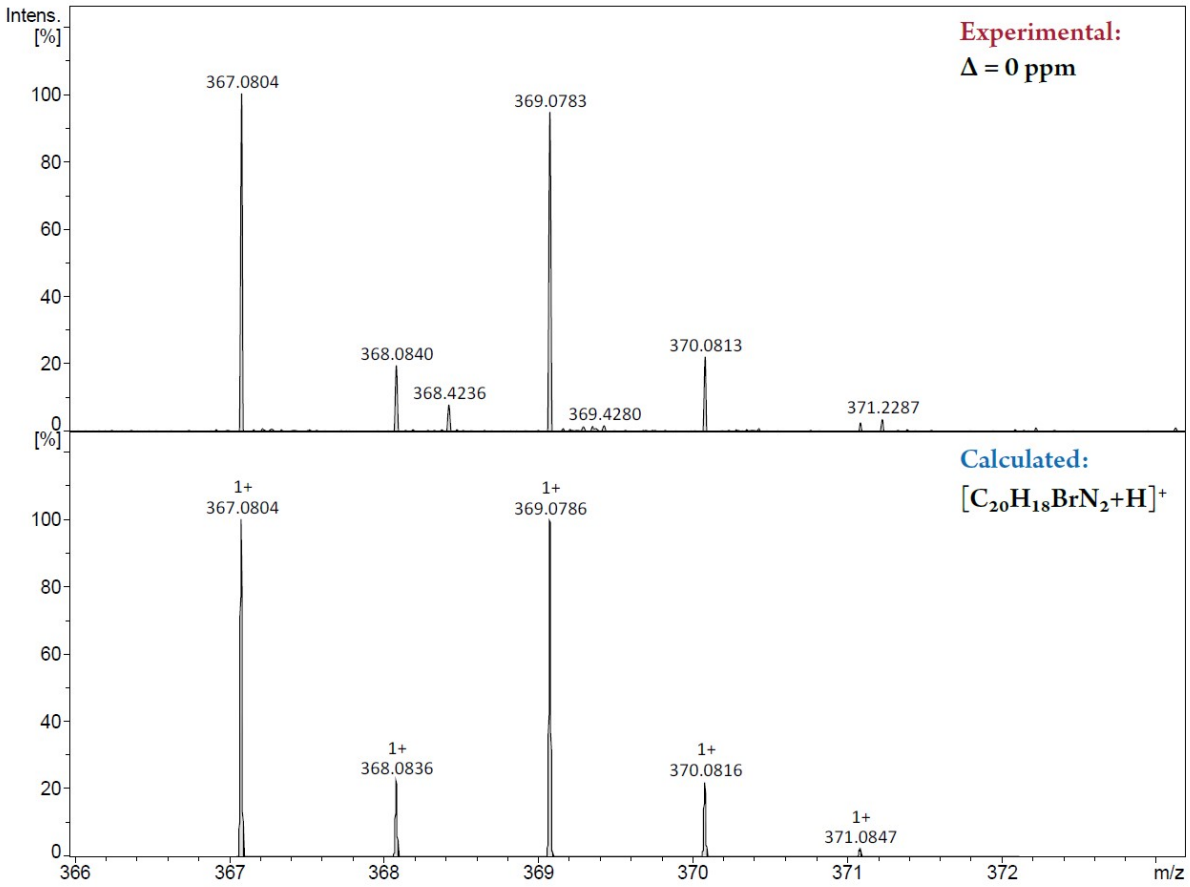

Figure S30. Experimental and theoretical ESI-(+)HRMS spectrum of **6e** in CH_3CN solution: experimental peak $[M+H]^+$ = 367.0804 Da, calculated for $C_{20}H_{18}BrN_2$ = 367.0804, Δ = 0 ppm.

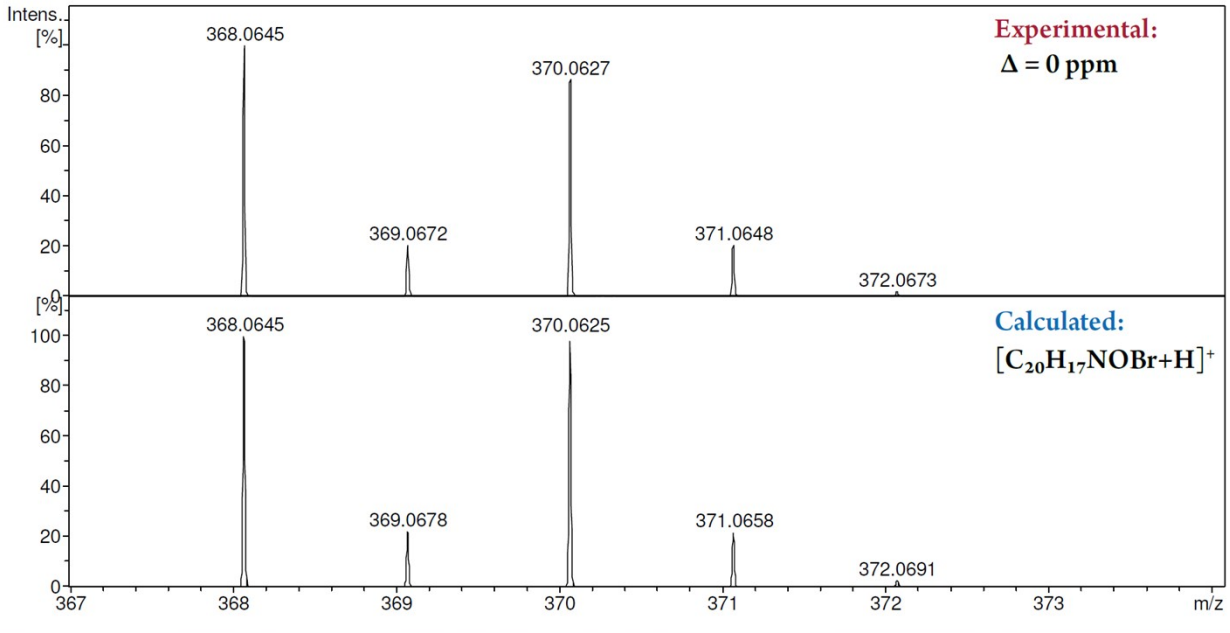

Figure S31. Experimental and theoretical ESI-(+)HRMS spectrum of **6f** in CH_3CN solution: experimental peak $[M+H]^+$ = 368.0645 Da, calculated for $C_{20}H_{18}NOBr$ = 368.0645, Δ = 0 ppm.

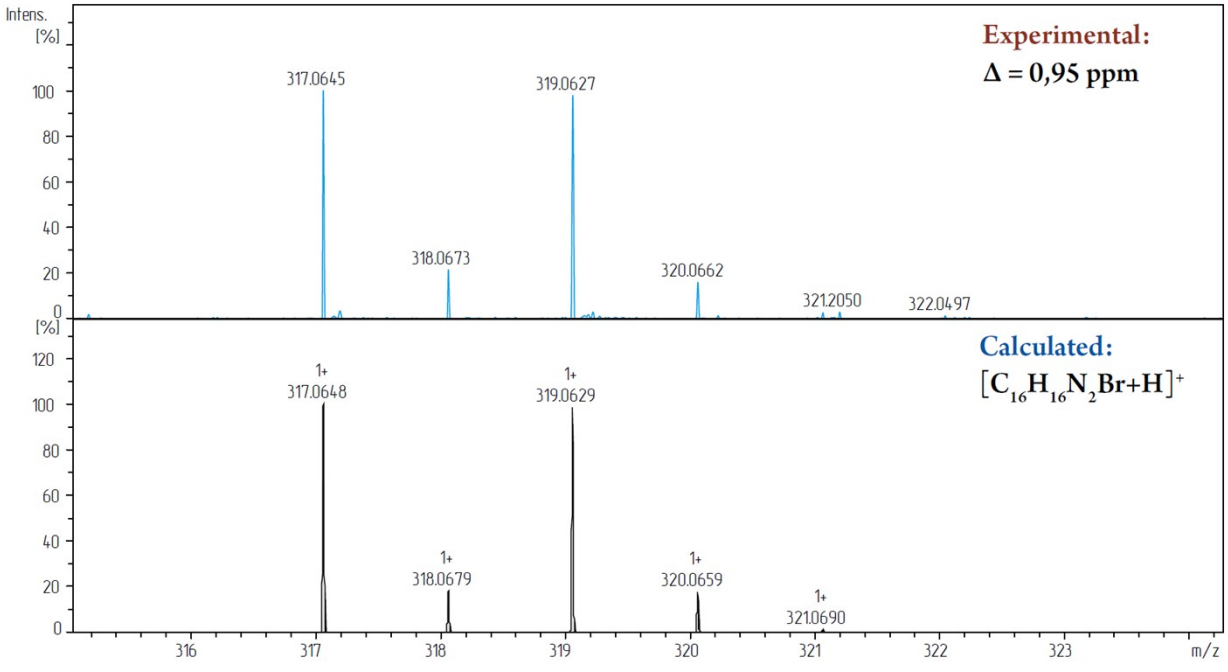

Figure S32. Experimental and theoretical ESI-(+)HRMS spectrum of **6g** in CH_3CN solution: experimental peak $[M+H]^+$ = 317.0645 Da, calculated for $C_{16}H_{17}N_2Br$ = 317.0648, Δ = 0.95 ppm.

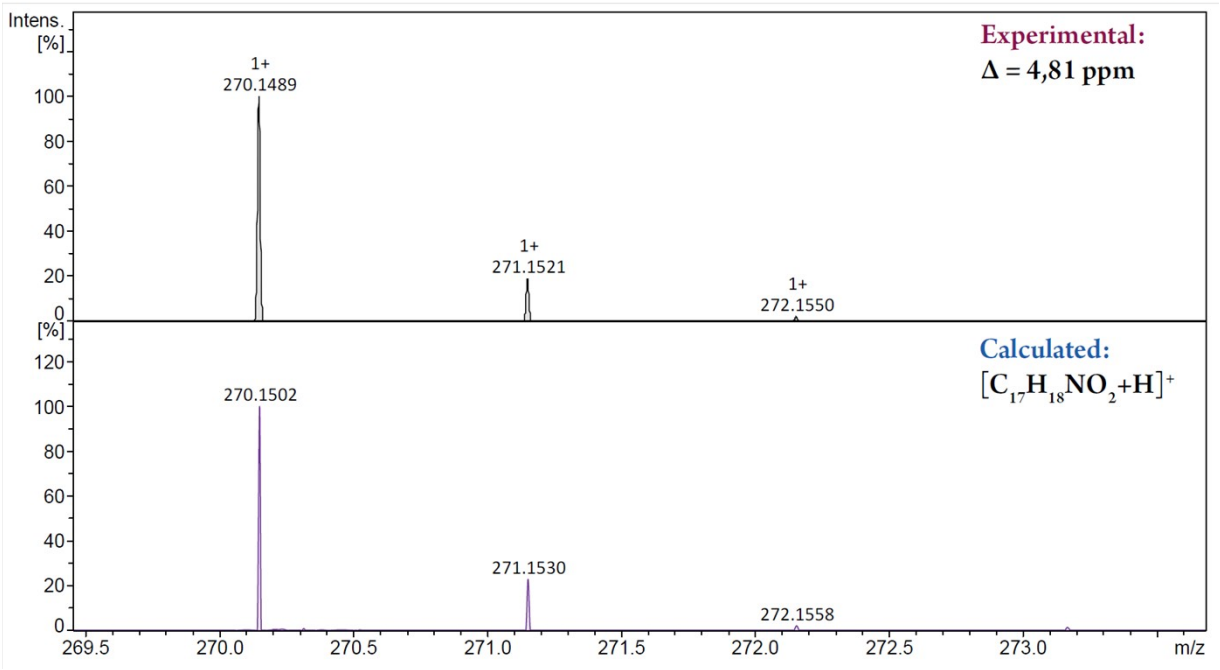

Figure S33. Experimental and theoretical ESI-(+)HRMS spectrum of **6h** in CH_3CN solution: experimental peak $[M+H]^+$ = 270.1489 Da, calculated for $C_{17}H_{19}NO_2$ = 270.1502, Δ = 4.81 ppm.

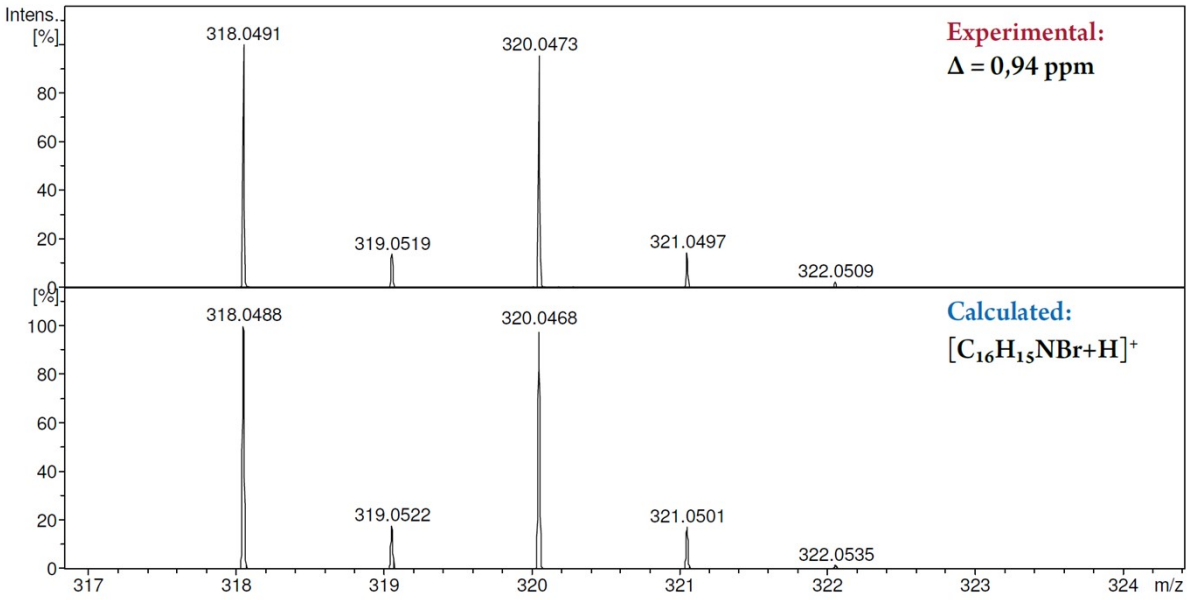

Figure S34. Experimental and theoretical ESI-(+)HRMS spectrum of **6i** in CH_3CN solution: experimental peak $[M+H]^+$ = 318.0491 Da, calculated for $C_{16}H_{16}NBr$ = 318.0488, Δ = 0.94 ppm.

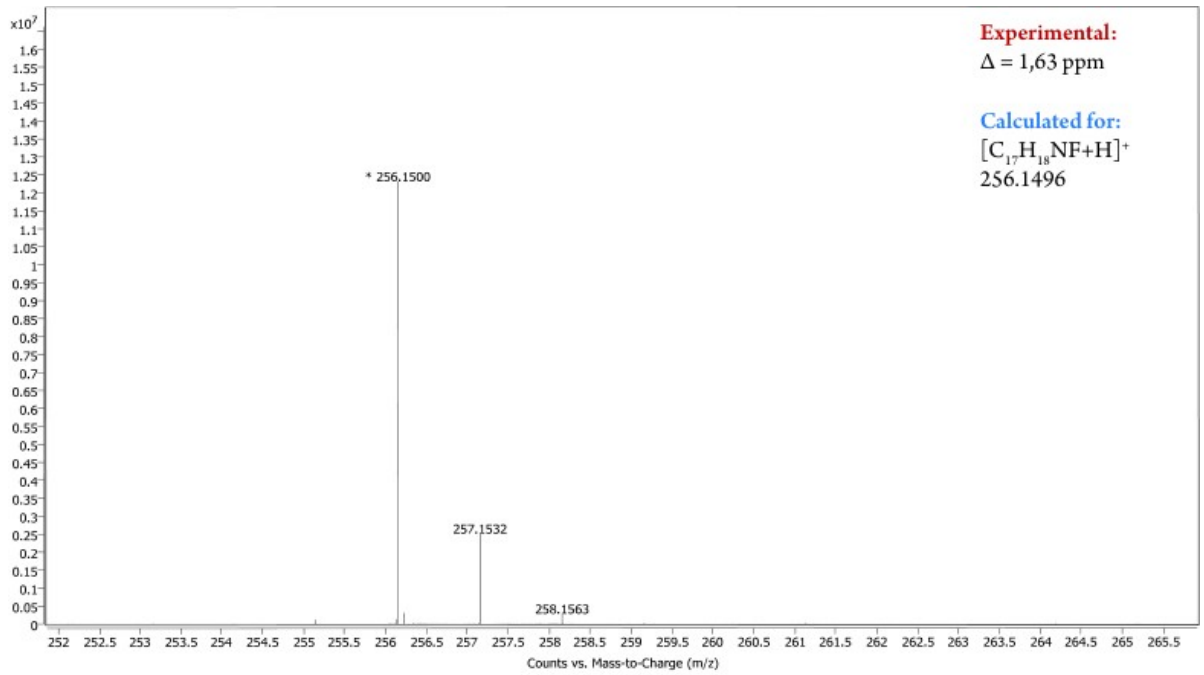

Figure S35. Experimental and theoretical ESI-(+)HRMS spectrum of **6j** in CH_3CN solution: experimental peak $[M+H]^+$ = 256.1500 Da, calculated for $C_{20}H_{16}NO_2Br$ = 256.1496, Δ = 1.63 ppm.

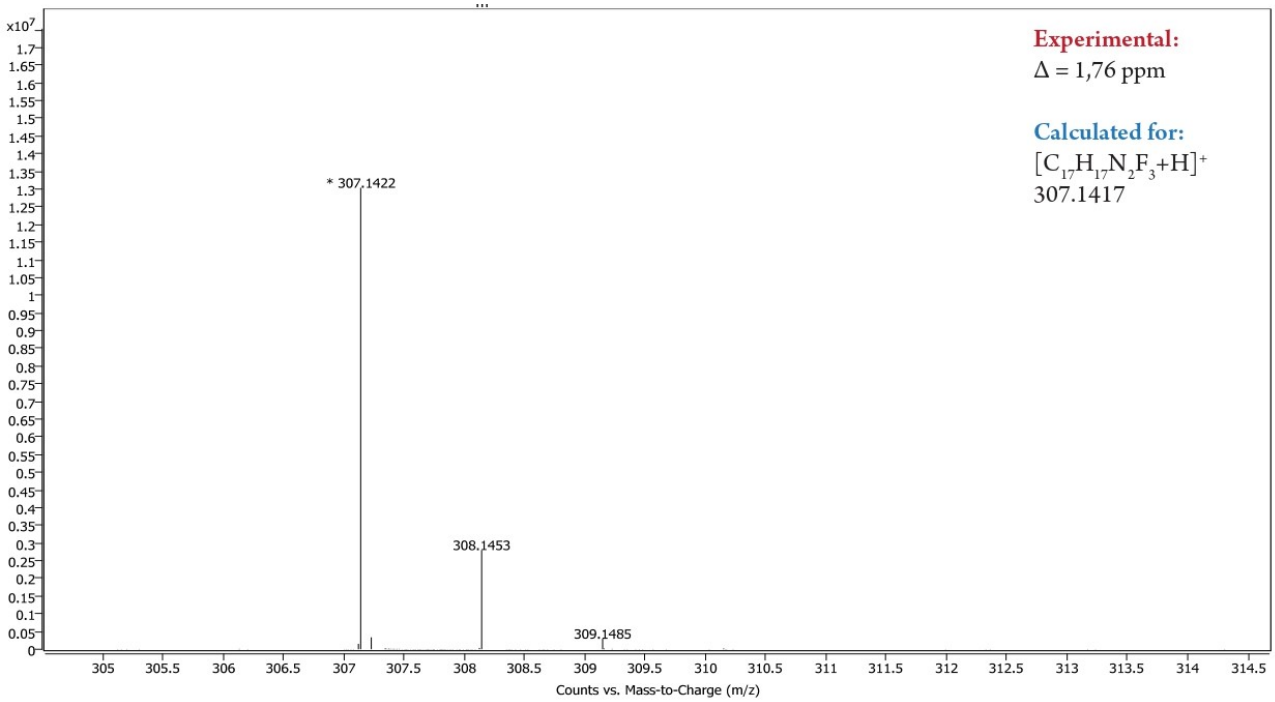

Figure S36. Experimental and theoretical ESI-(+)HRMS spectrum of **6k** in CH_3CN solution: experimental peak $[M+H]^+$ = 307.1422 Da, calculated for $C_{17}H_{17}N_2F_3$ = 307.1422, Δ = 1.76 ppm.

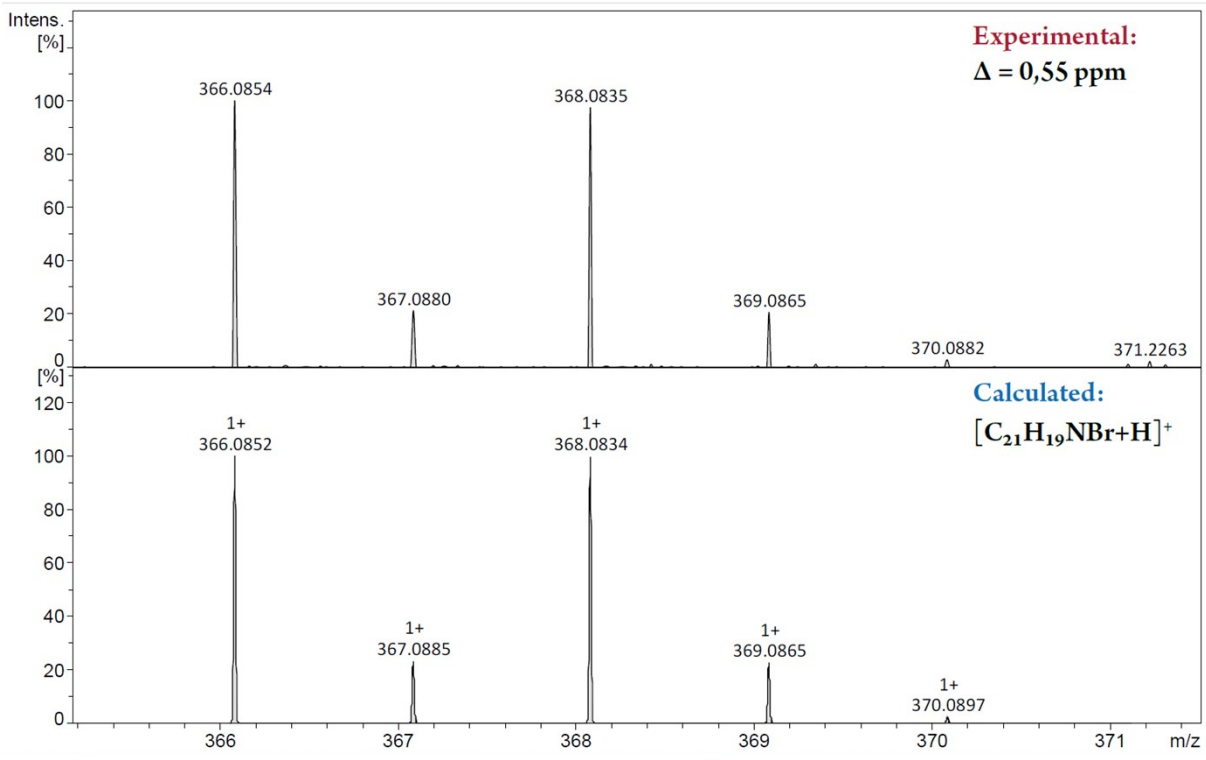

Figure S37. Experimental and theoretical ESI-(+)HRMS spectrum of **6l** in CH_3CN solution: experimental peak $[M+H]^+$ = 366.0854 Da, calculated for $C_{21}H_{20}NBr$ = 366.0852, Δ = 0.55 ppm.

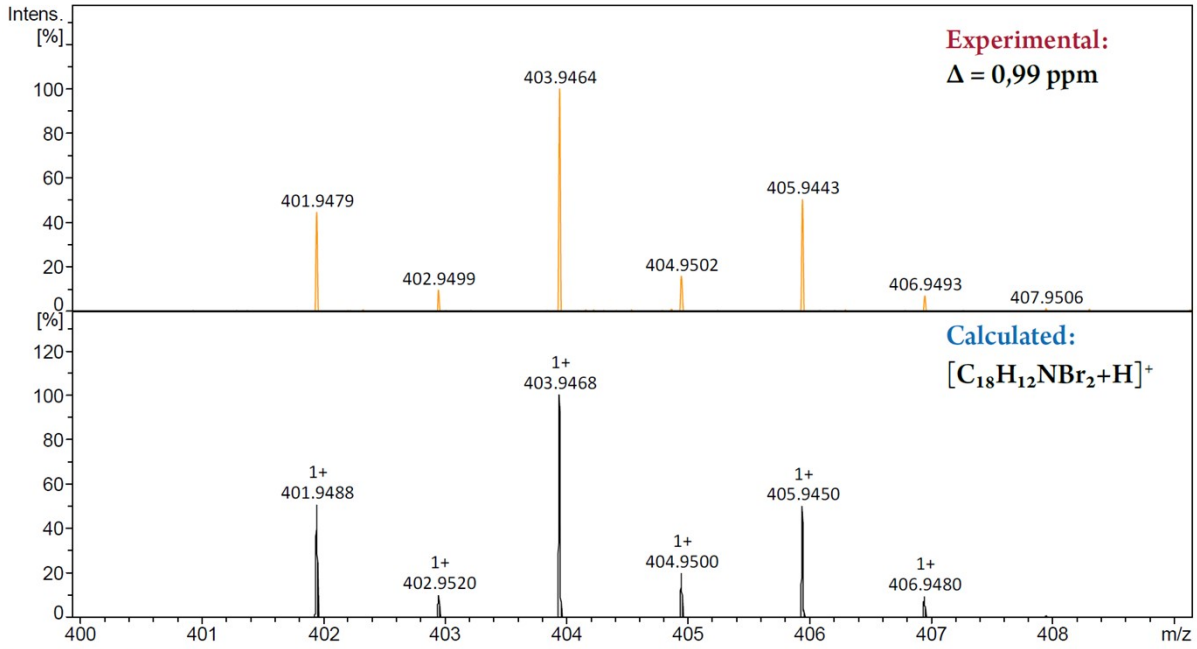

Figure S38. Experimental and theoretical ESI-(+)HRMS spectrum of **6m** in CH_3CN solution: experimental peak $[M+H]^+$ = 403.9464 Da, calculated for $C_{18}H_{13}NBr_2$ = 403.9468, Δ = 0.99 ppm.

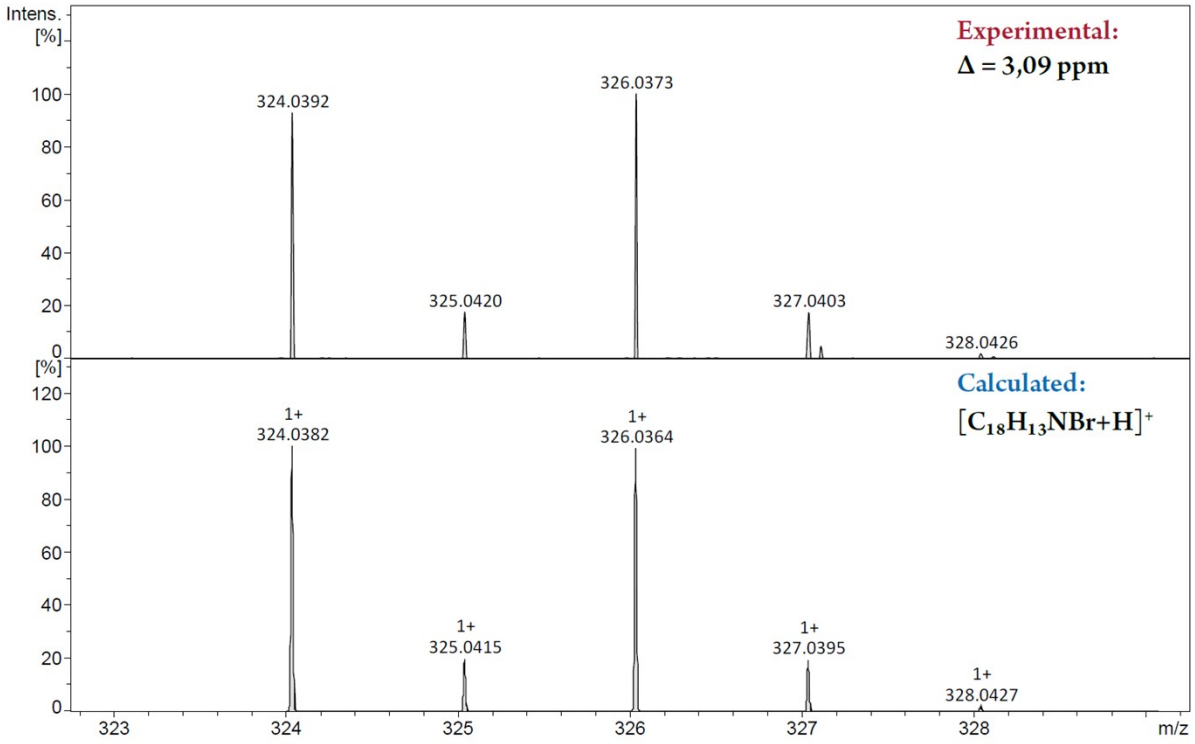

Figure S39. Experimental and theoretical ESI-(+)HRMS spectrum of **6n** in CH_3CN solution: experimental peak $[M+H]^+$ = 324.0392 Da, calculated for $C_{18}H_{14}NBr$ = 324.0382, Δ = 3.09 ppm.

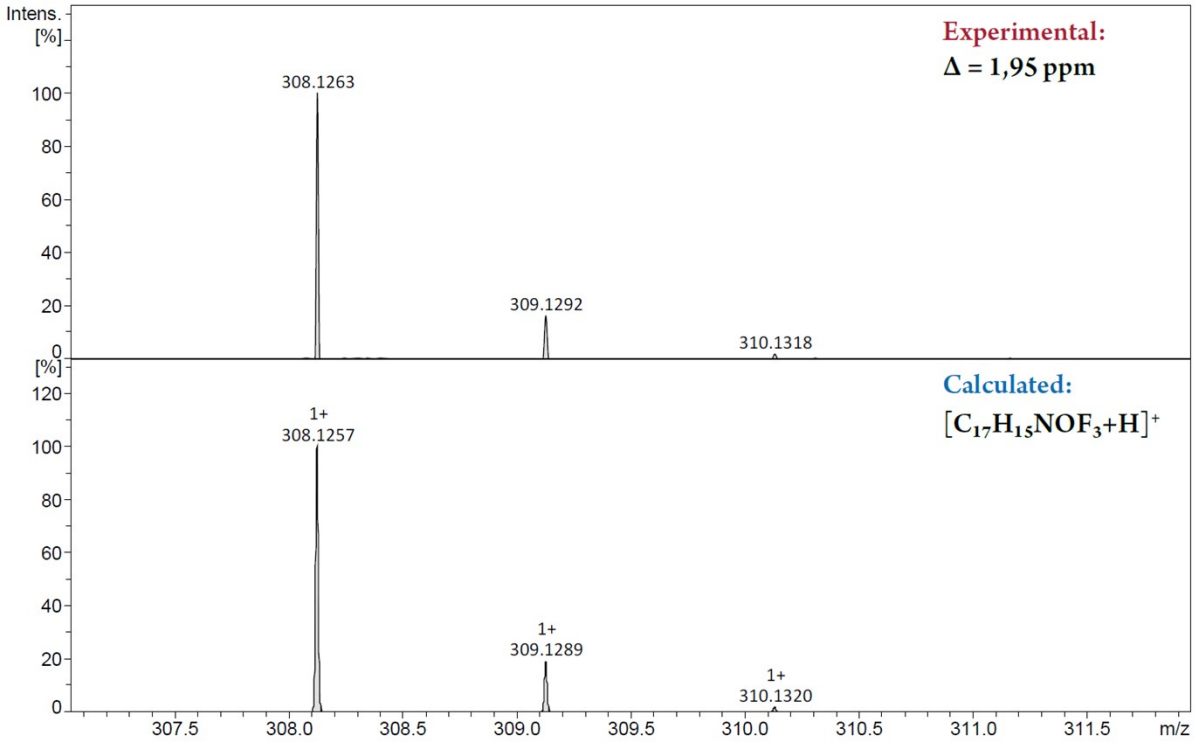

Figure S40. Experimental and theoretical ESI-(+)HRMS spectrum of **6o** in CH_3CN solution: experimental

peak $[M+H]^+$ = 308.1263 Da, calculated for $C_{17}H_{16}NOF_3$ = 308.1257, Δ = 1.95 ppm.

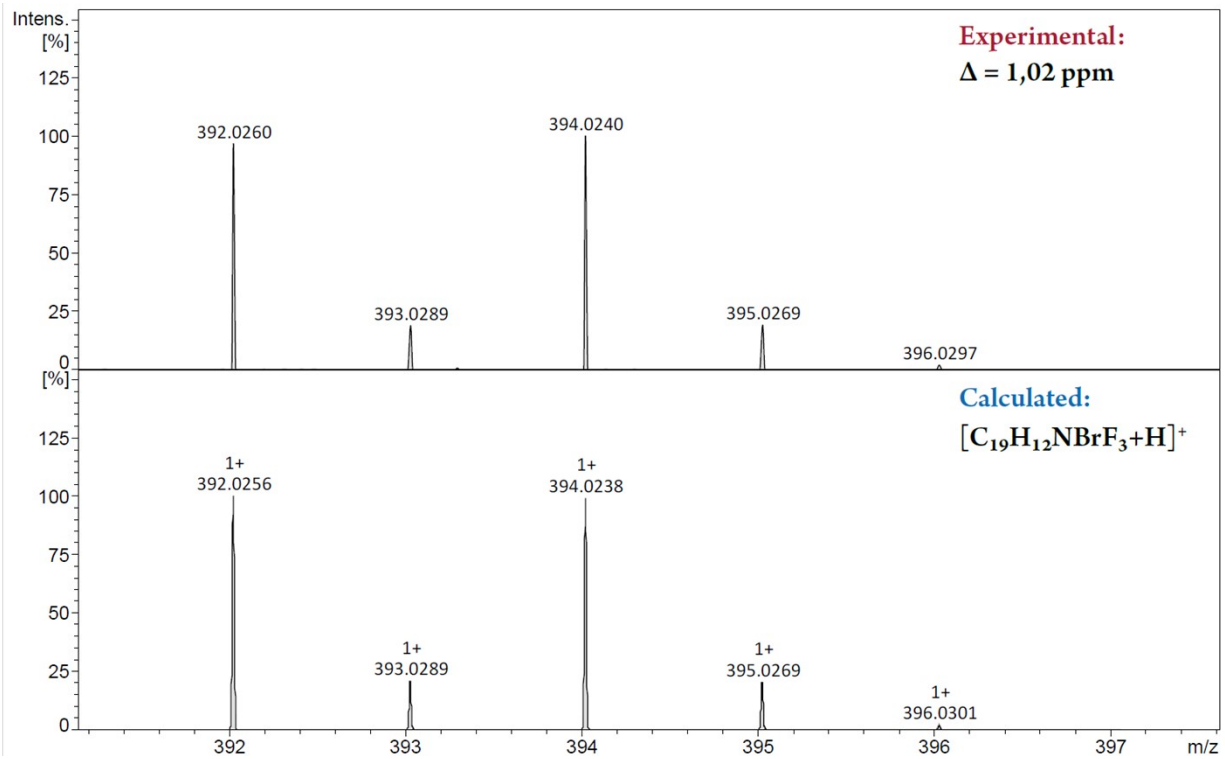

Figure S41. Experimental and theoretical ESI-(+)HRMS spectrum of **6p** in CH_3CN solution: experimental peak $[M+H]^+$ = 392.0260 Da, calculated for $C_{19}H_{13}NBrF_3$ = 392.0256, Δ = 1.02 ppm.

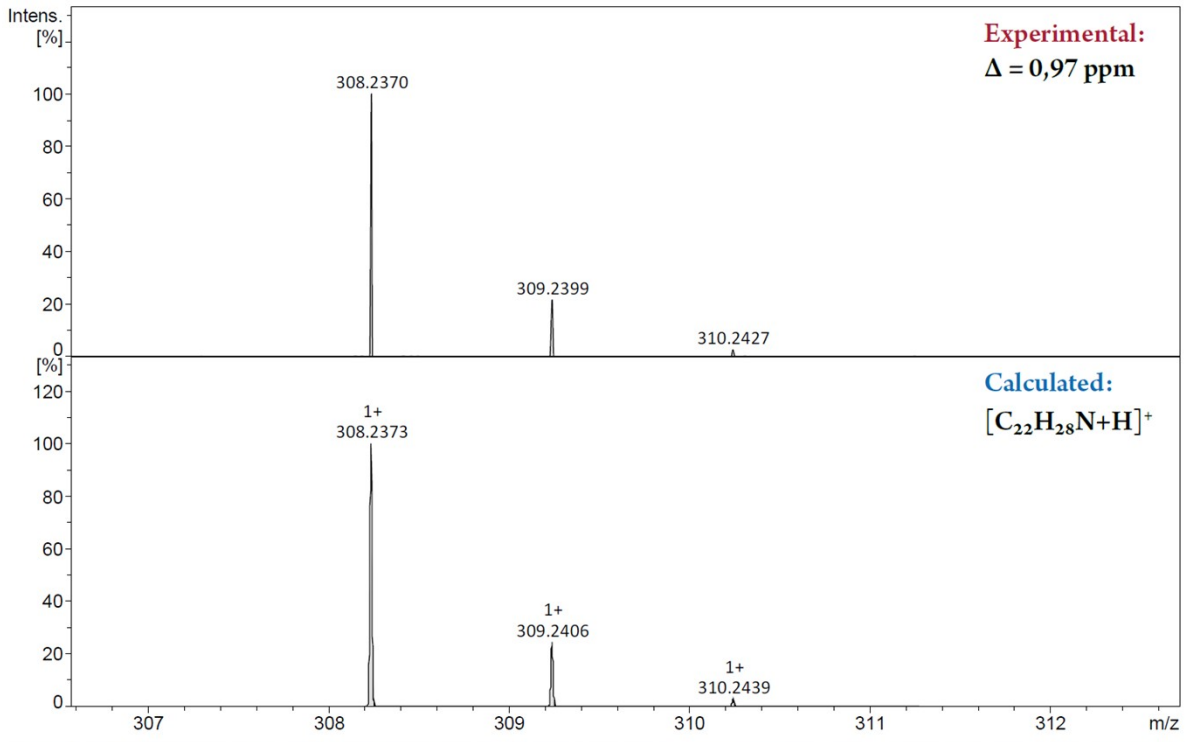

Figur

e S42. Experimental and theoretical ESI-(+)HRMS spectrum of **6q** in CH_3CN solution: experimental peak $[M+H]^+$ = 308.2370 Da, calculated for $C_{22}H_{29}N$ = 308.2373, Δ = 0.97 ppm.

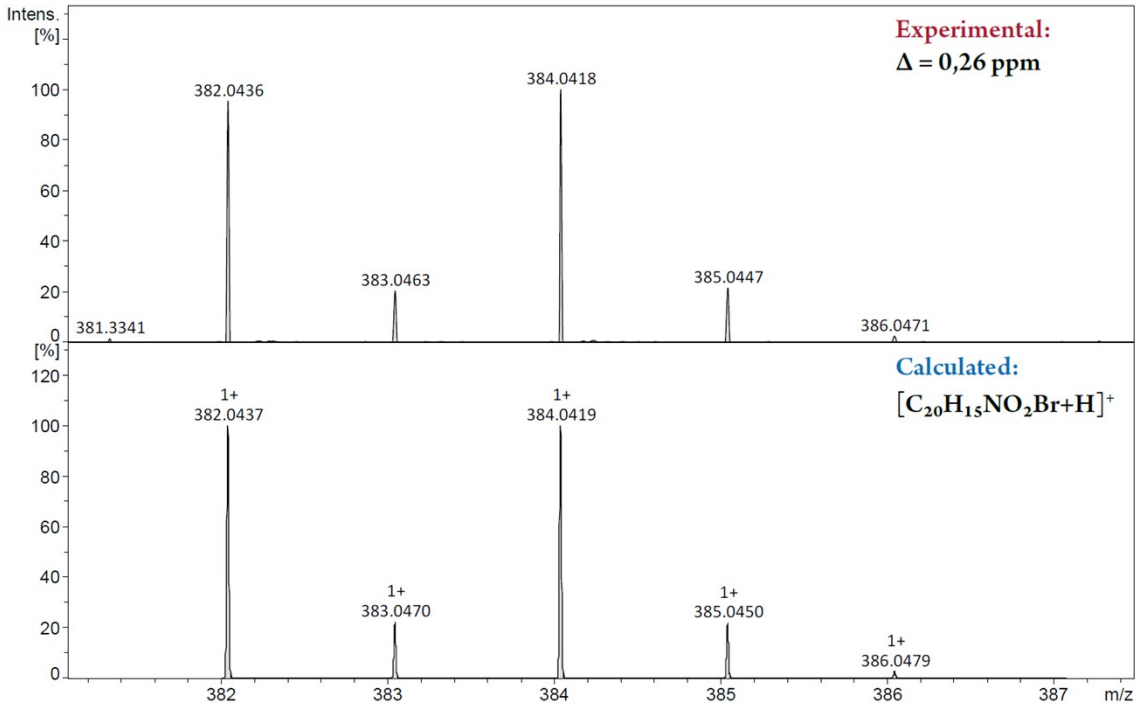

Figure S43. Experimental and theoretical ESI-(+)HRMS spectrum of **6r** in CH_3CN solution: experimental peak $[M+H]^+$ = 382.0436 Da, calculated for $C_{20}H_{16}NO_2Br$ = 382.0437, Δ = 0.26 ppm.

S5. NMR spectra of synthesized compounds

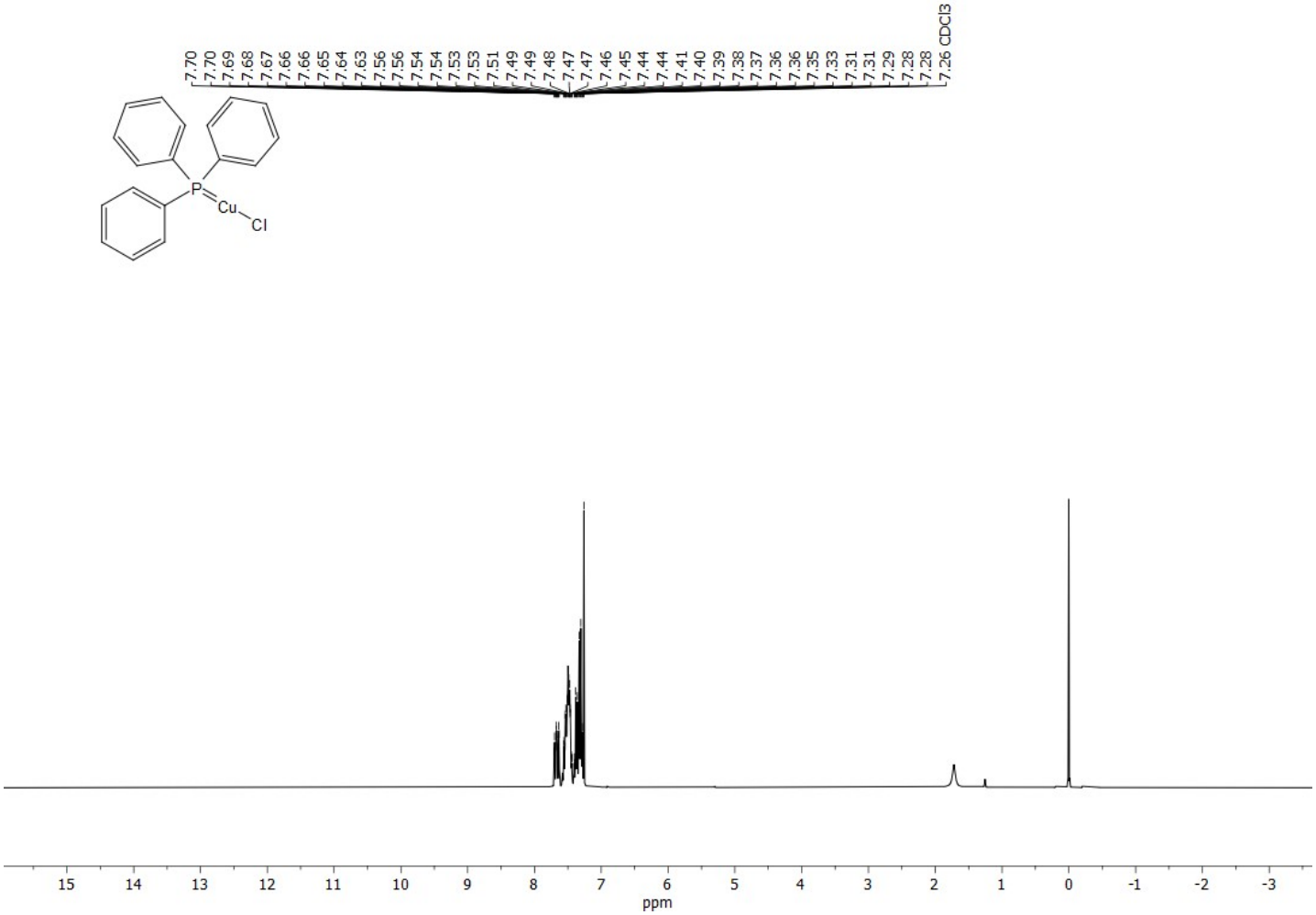

Figure S44. ^{1}H NMR spectrum of **Ph_3PCuCl** ($CDCl_3$, 300 MHz).

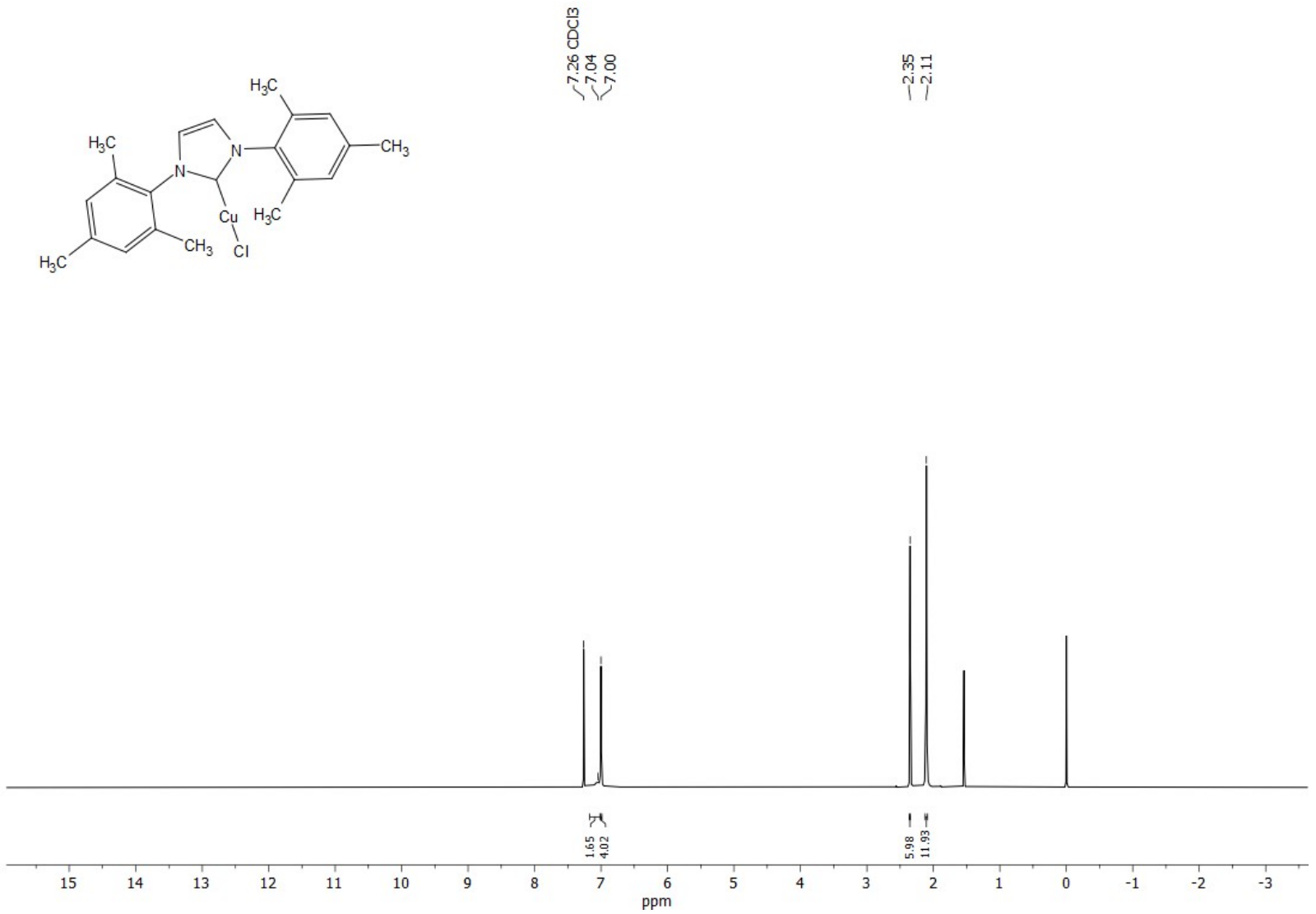

Figure S45. ^{1}H NMR spectrum of **IMesCuCl** ($CDCl_3$, 300 MHz).

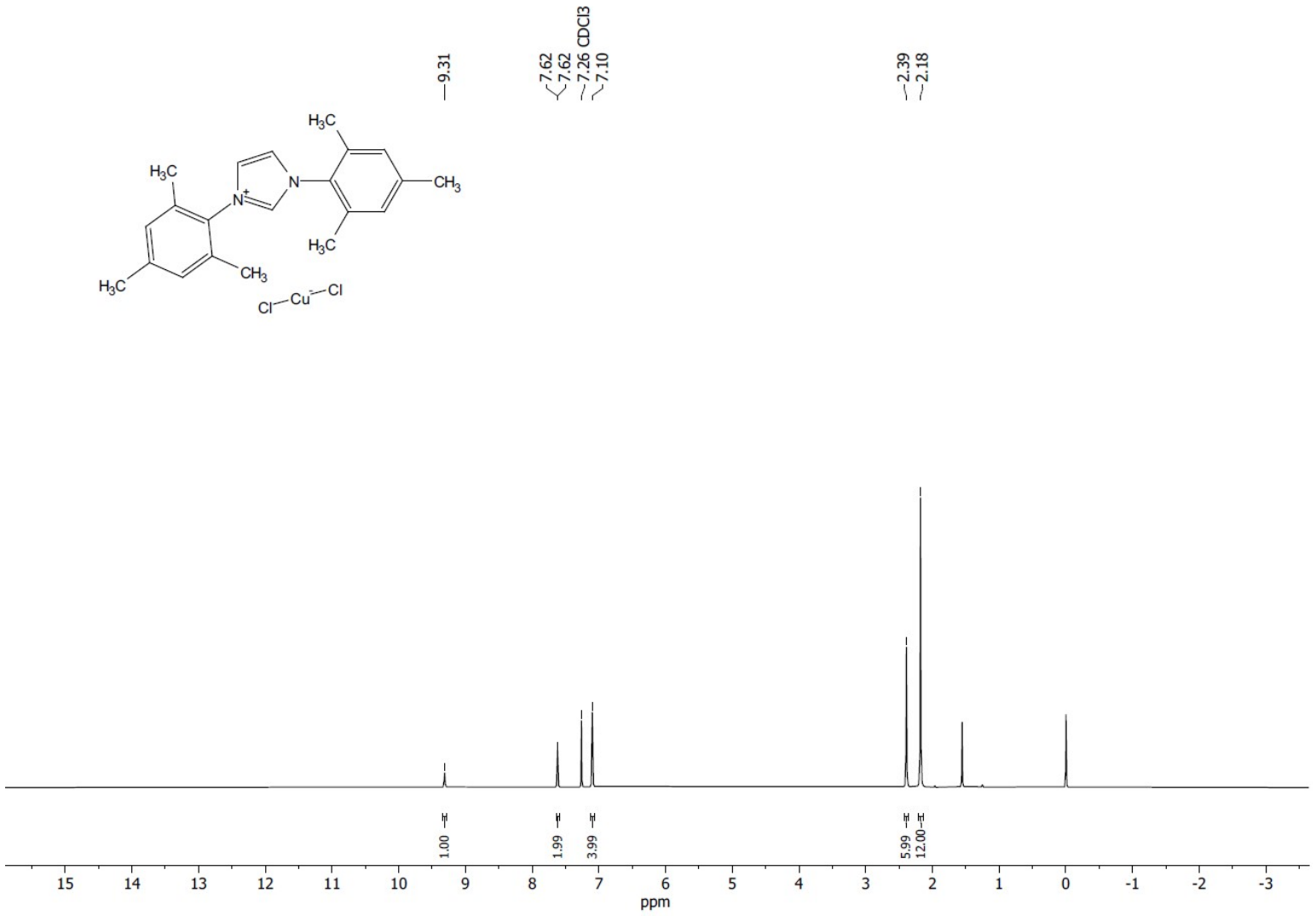

Figure S46. ^{1}H NMR spectrum of [**IMesH][CuCl$_2$]** ($CDCl_3$, 300 MHz).

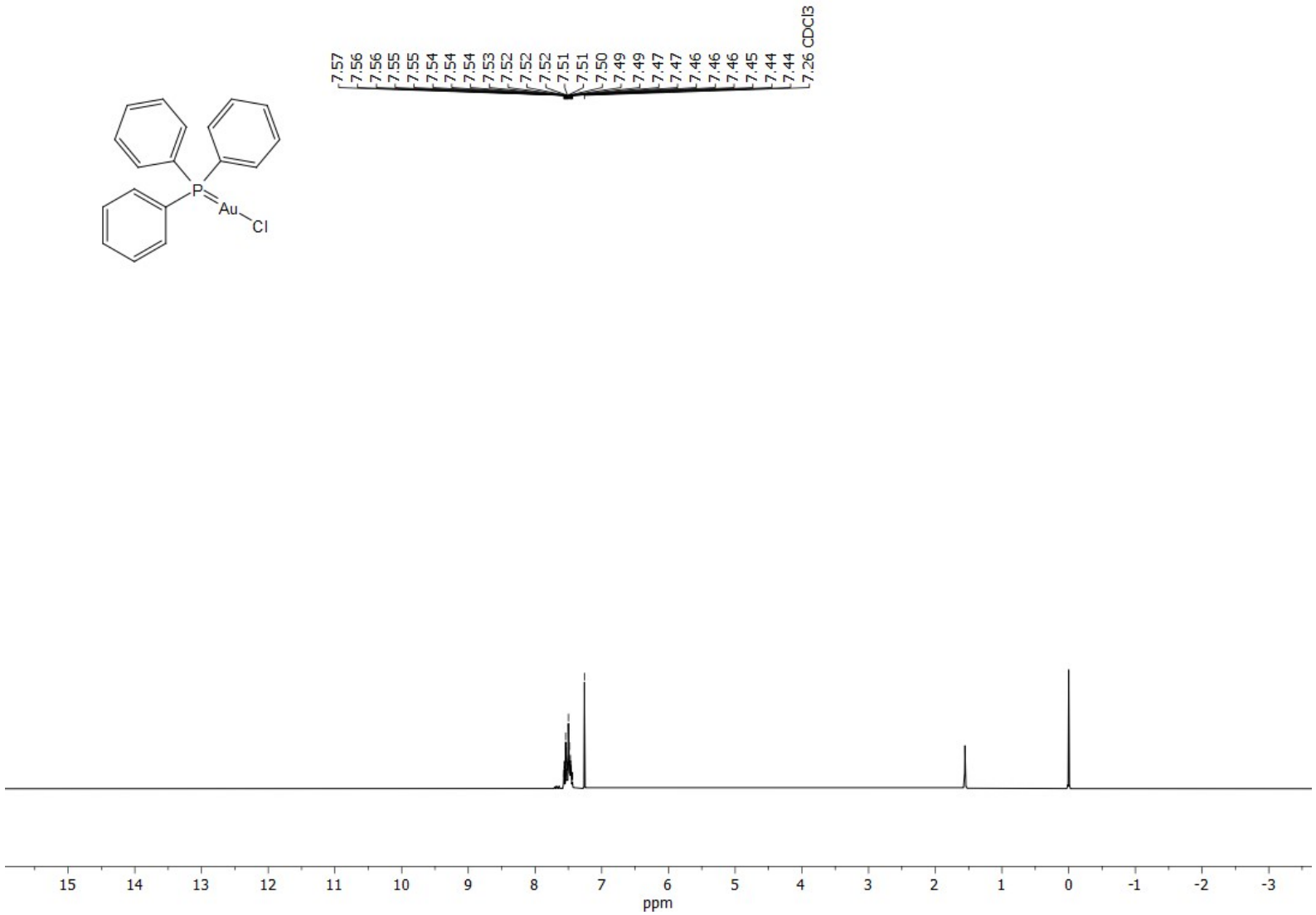

Figure S47. ^{1}H NMR spectrum of **Ph_3PAuCl** ($CDCl_3$, 300 MHz).

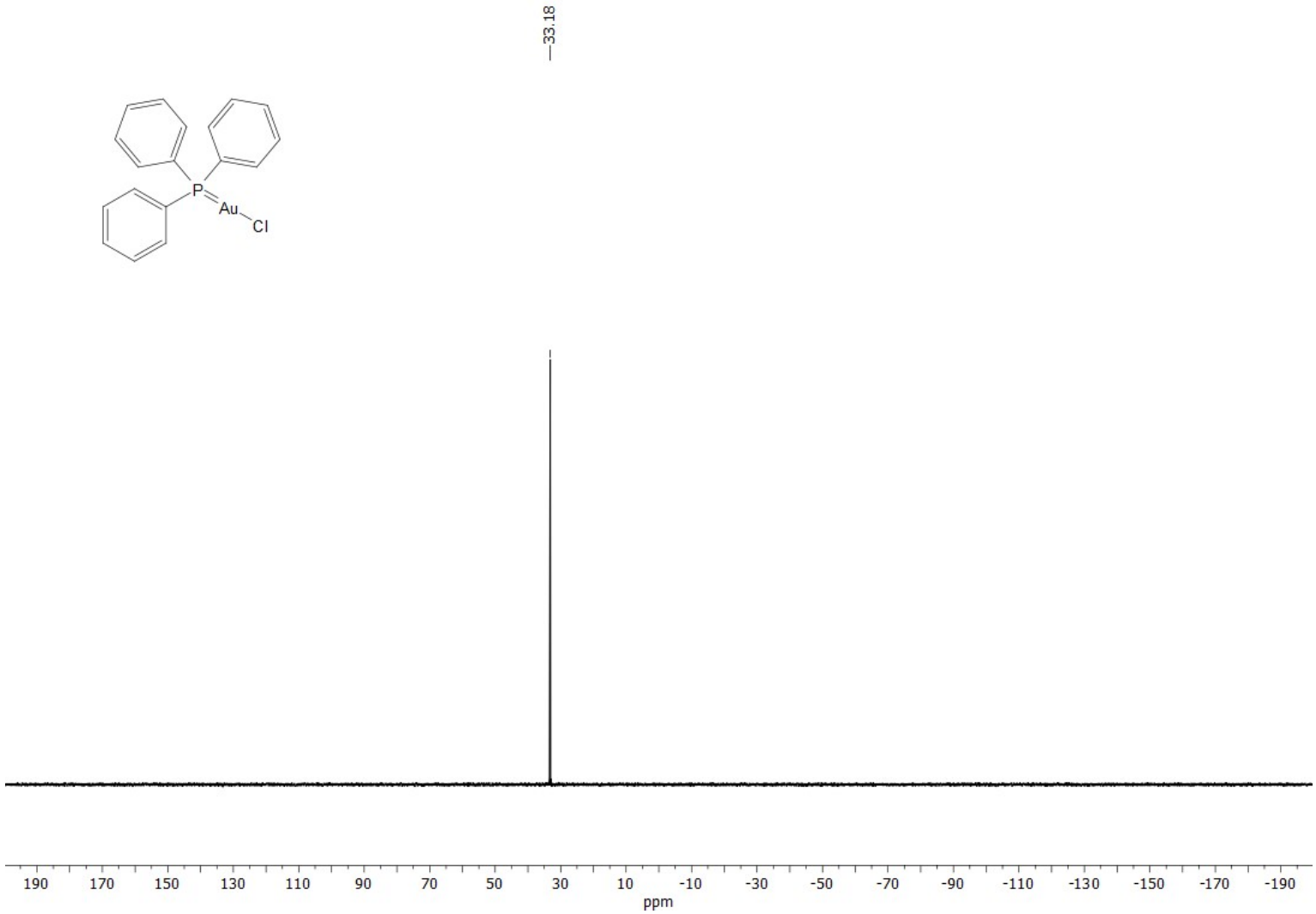

Figure S48. ^{31}P $\{^{1}H\}$ NMR spectrum of **Ph_3PAuCl** ($CDCl_3$, 121.5 MHz, 85% H_3PO_4 was used as external reference).

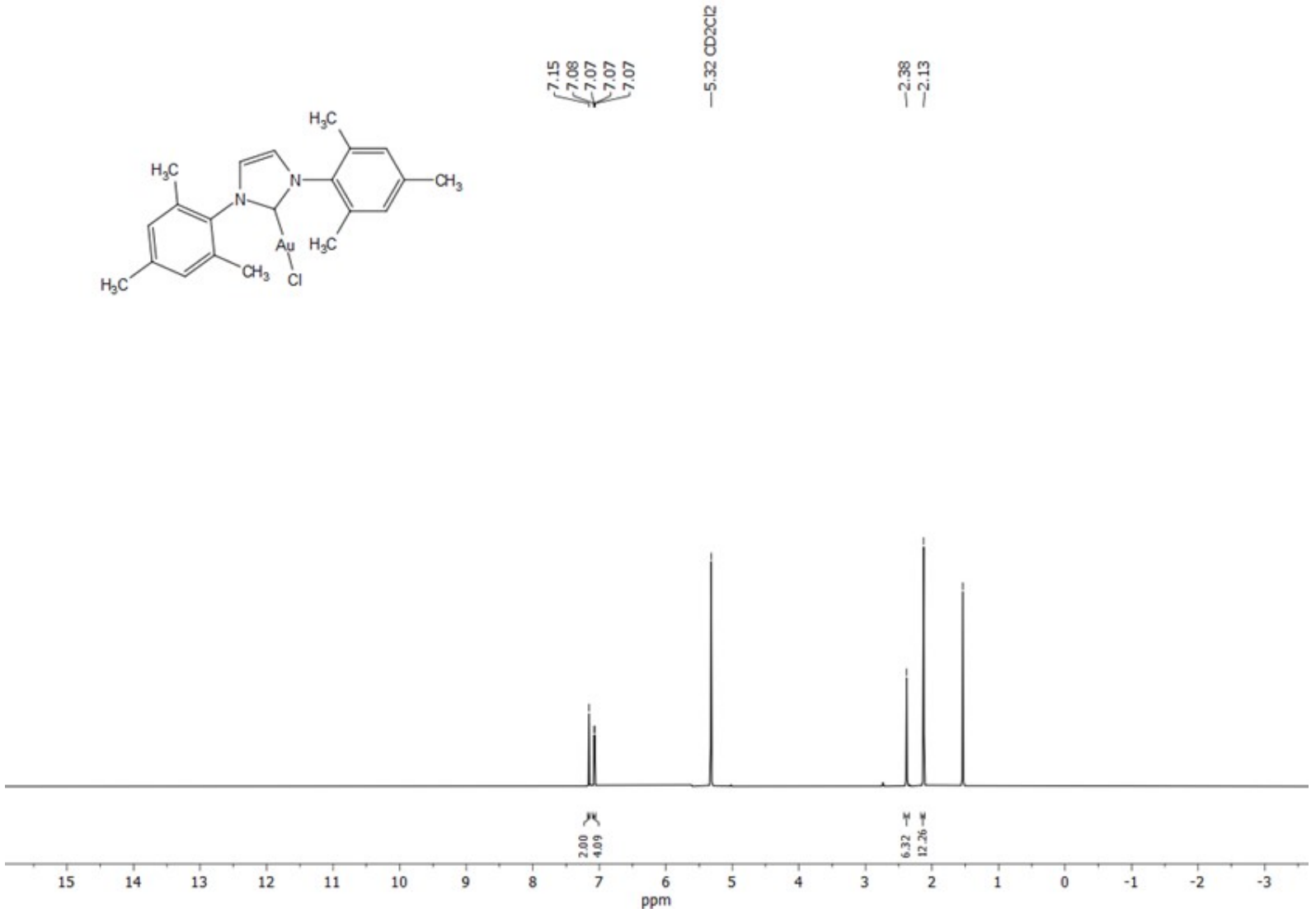

Figure S49. ^{1}H NMR spectrum of **IMesAuCl** (CD_2Cl_2, 300 MHz).

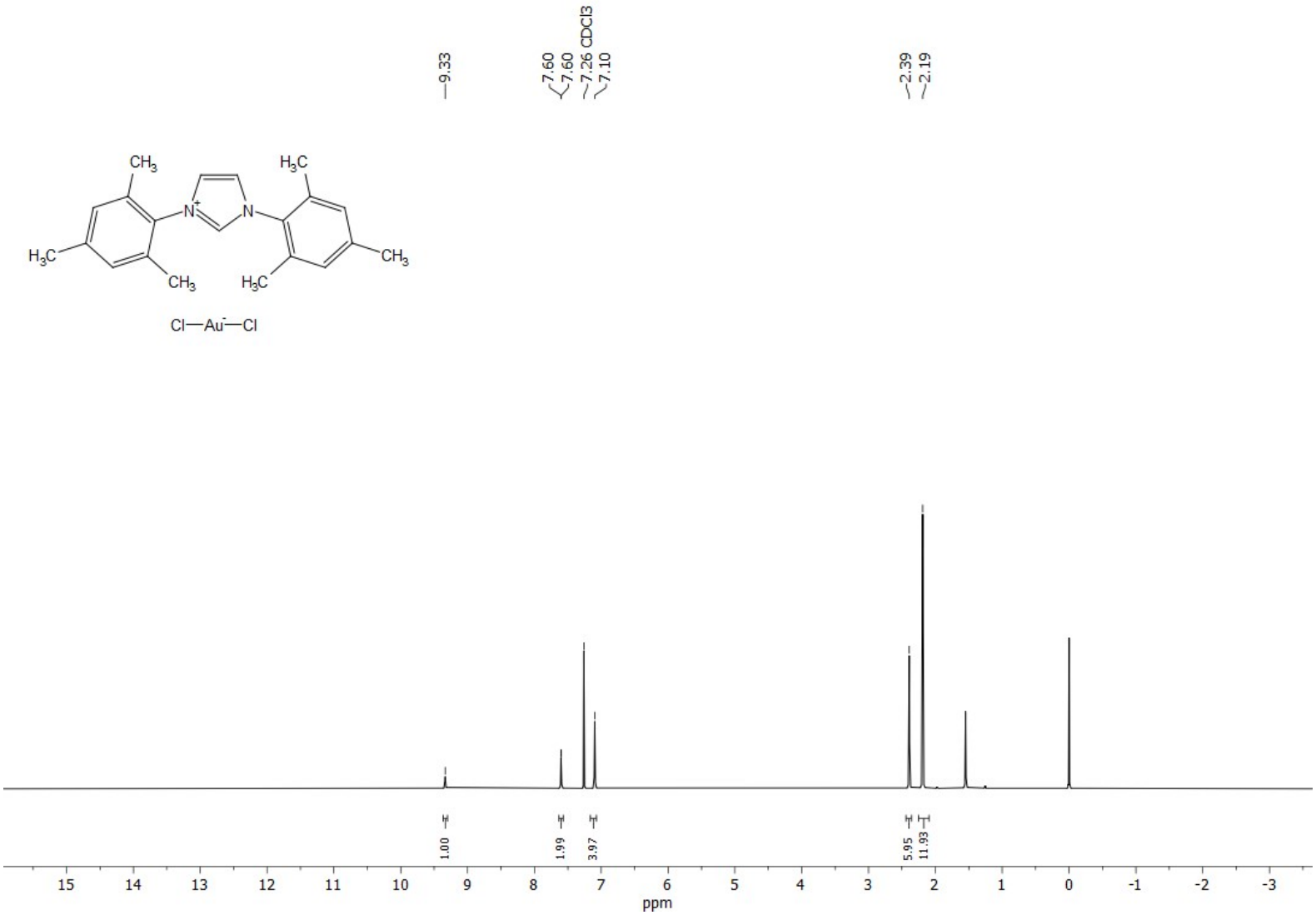

Figure S50. ^{1}H NMR spectrum of [**IMesH][AuCl$_2$]** ($CDCl_3$, 300 MHz).

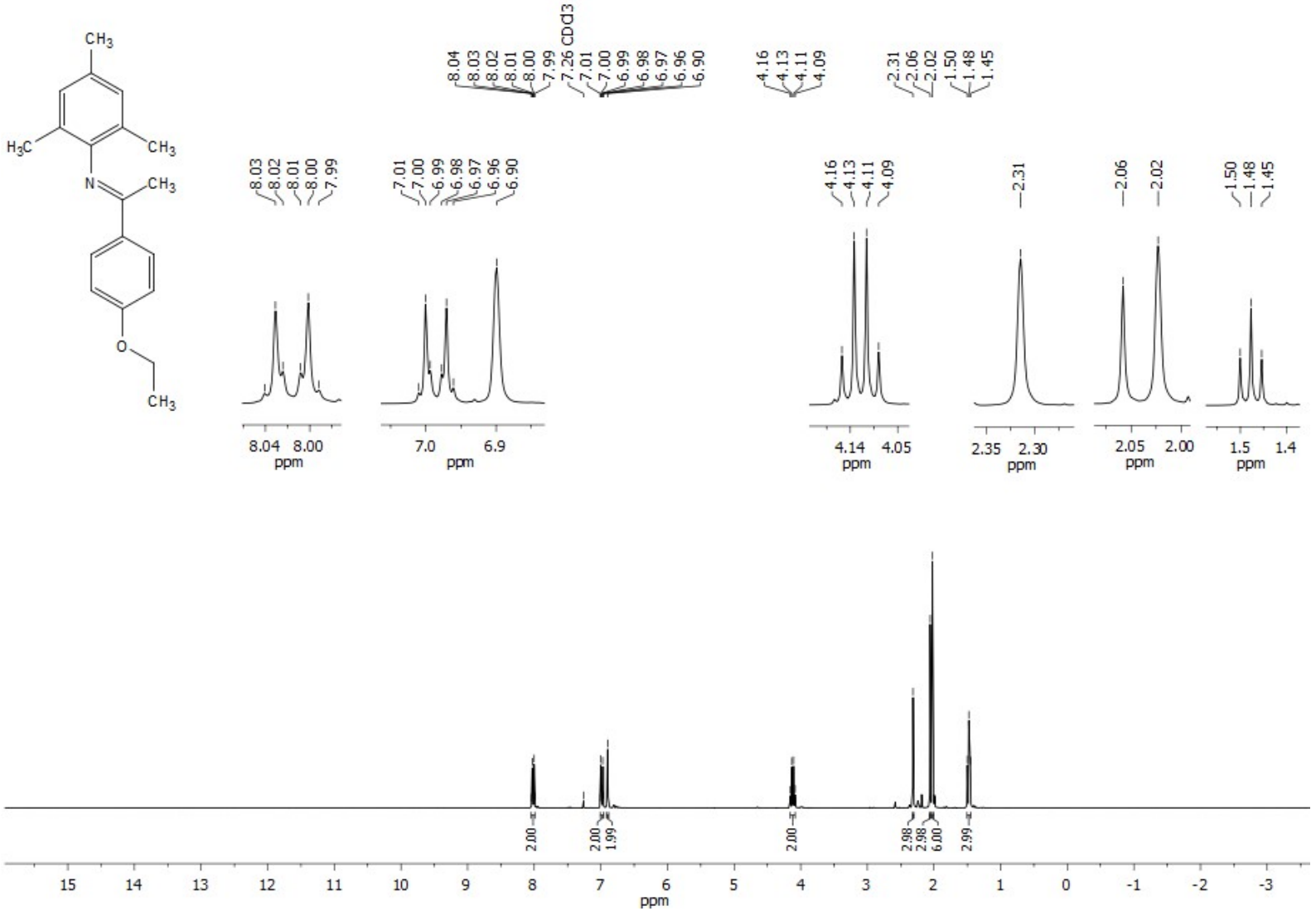

Figure S51. ^{1}H NMR spectrum of compound **6b** ($CDCl_3$, 300 MHz).

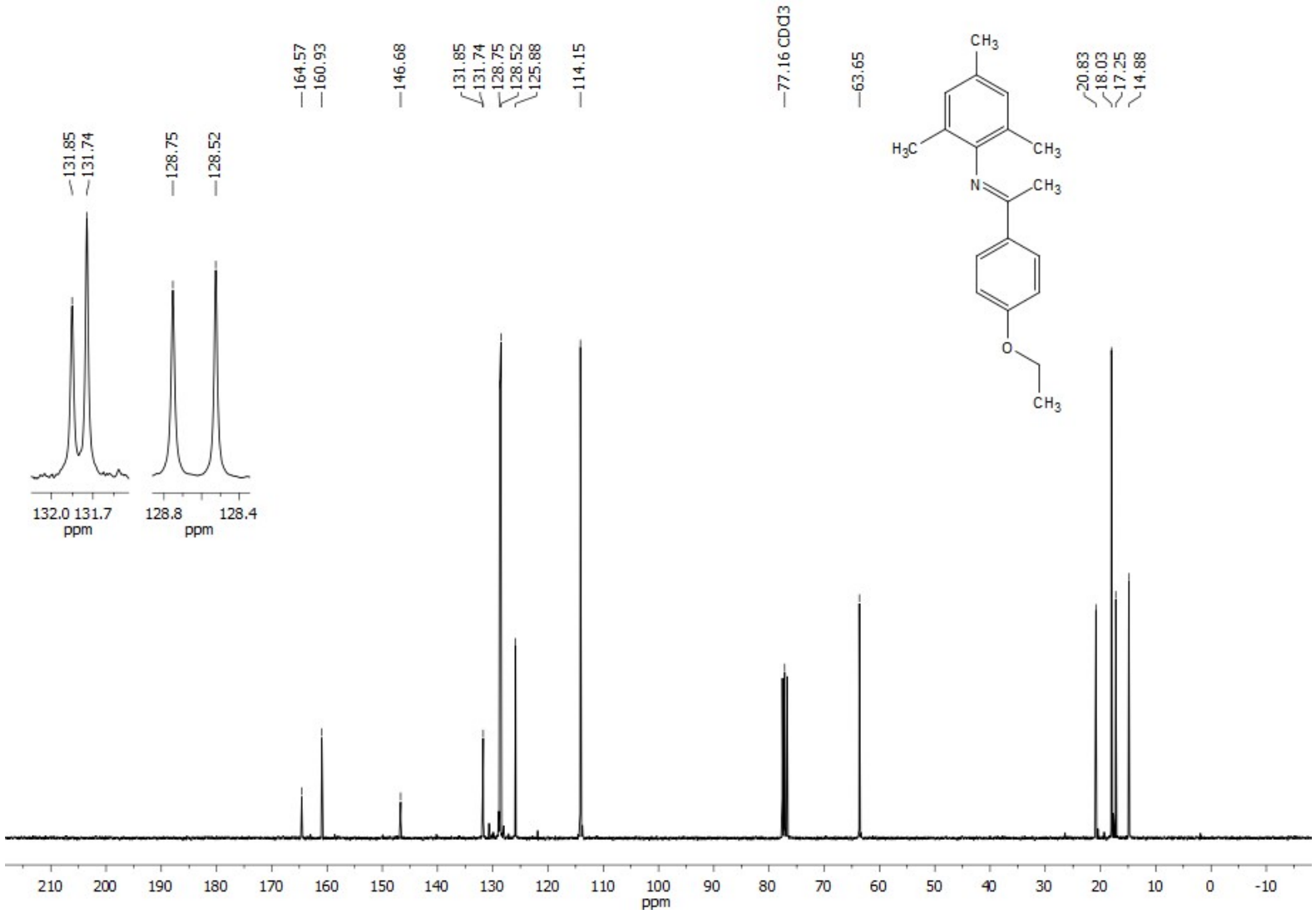

Figure S52. ^{13}C {^{1}H} NMR spectrum of compound **6b** ($CDCl_3$, 76 MHz).

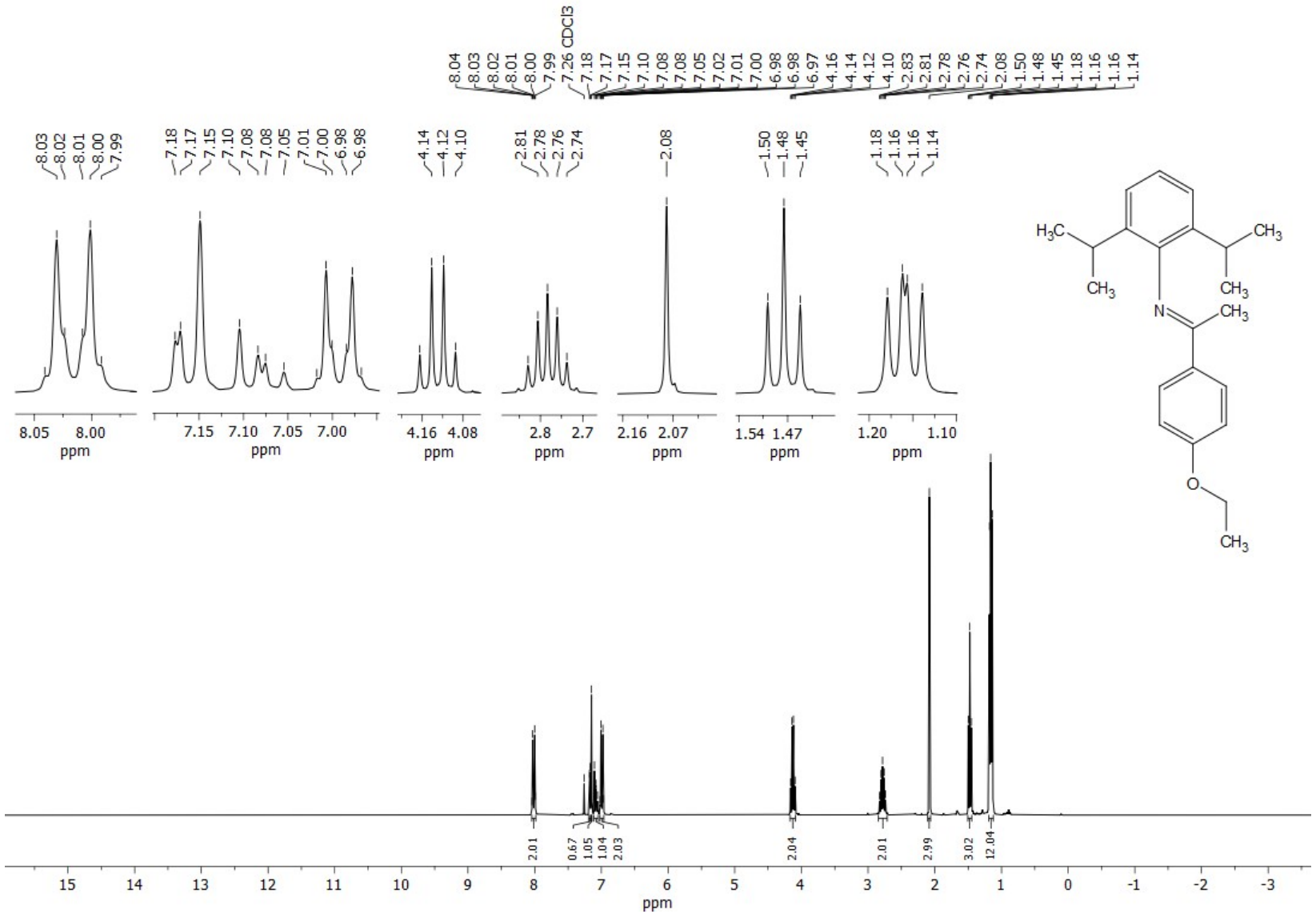

Figure S53. ^{1}H NMR spectrum of compound **6c** ($CDCl_3$, 300 MHz).

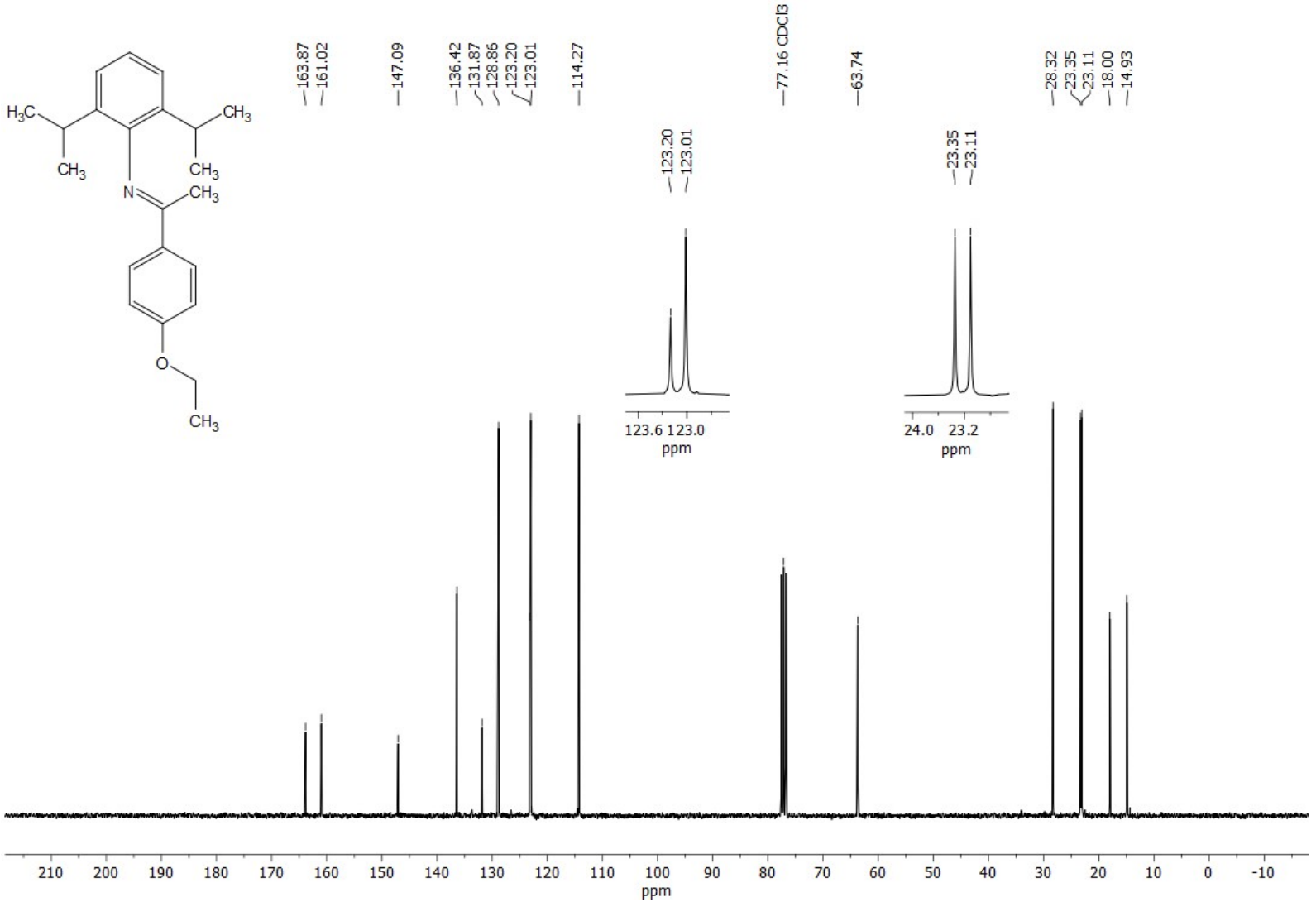

Figure S54. ^{13}C {^{1}H} NMR spectrum of compound **6c** ($CDCl_3$, 76 MHz).

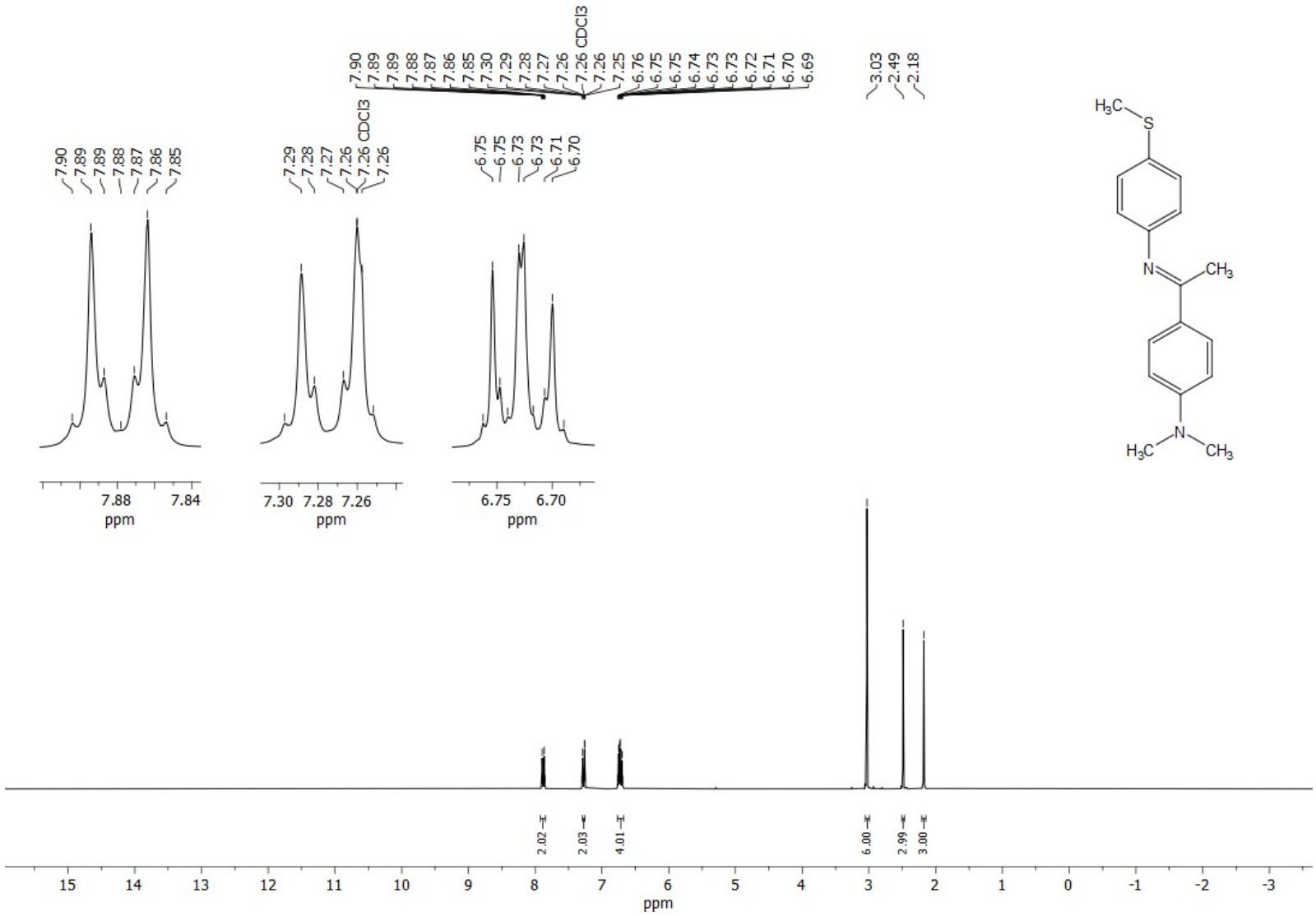

Figure S55. ^{1}H NMR spectrum of compound **6d** ($CDCl_3$, 300 MHz).

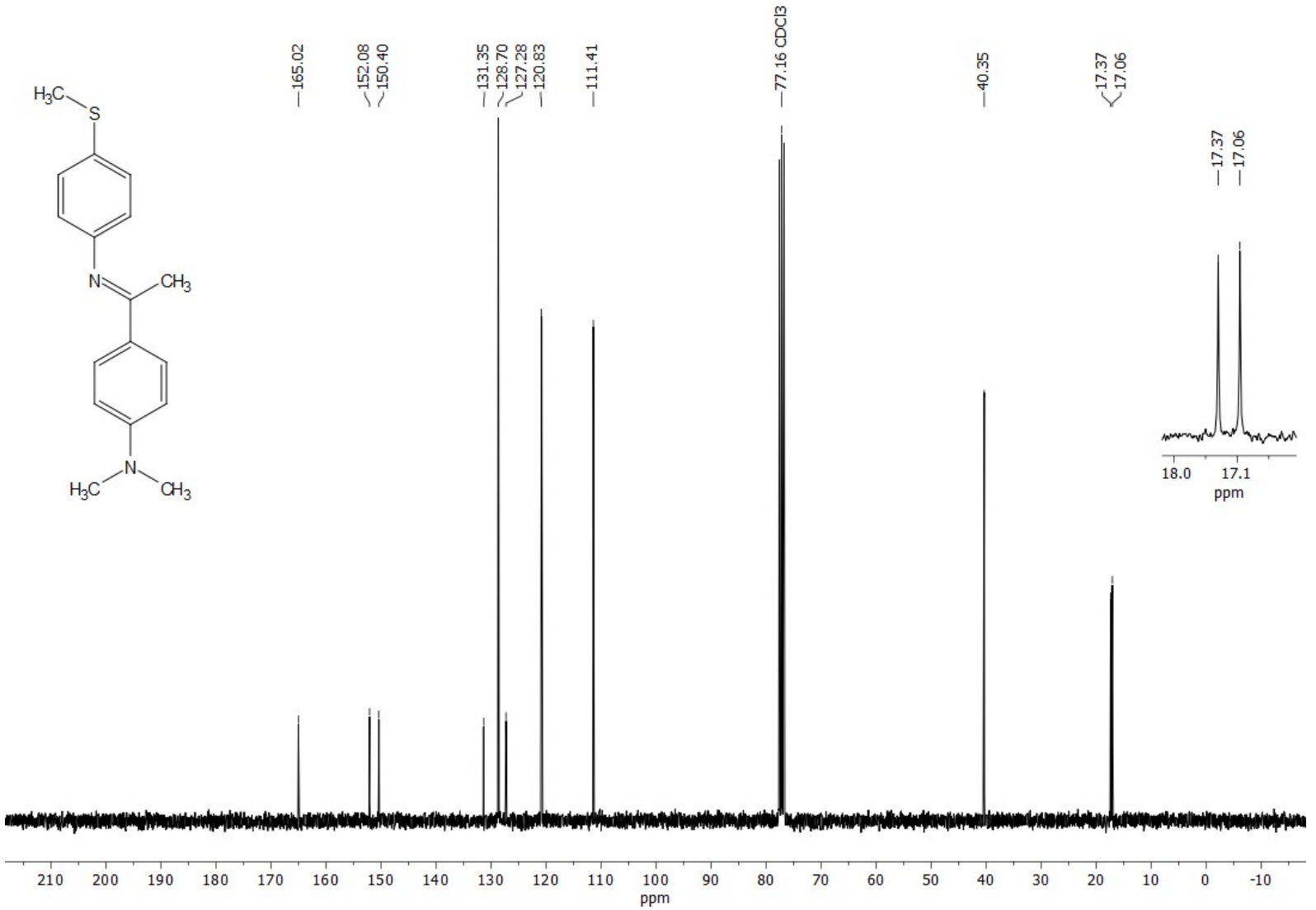

Figure S56. ^{13}C {^{1}H} NMR spectrum of compound **6d** ($CDCl_3$, 76 MHz).

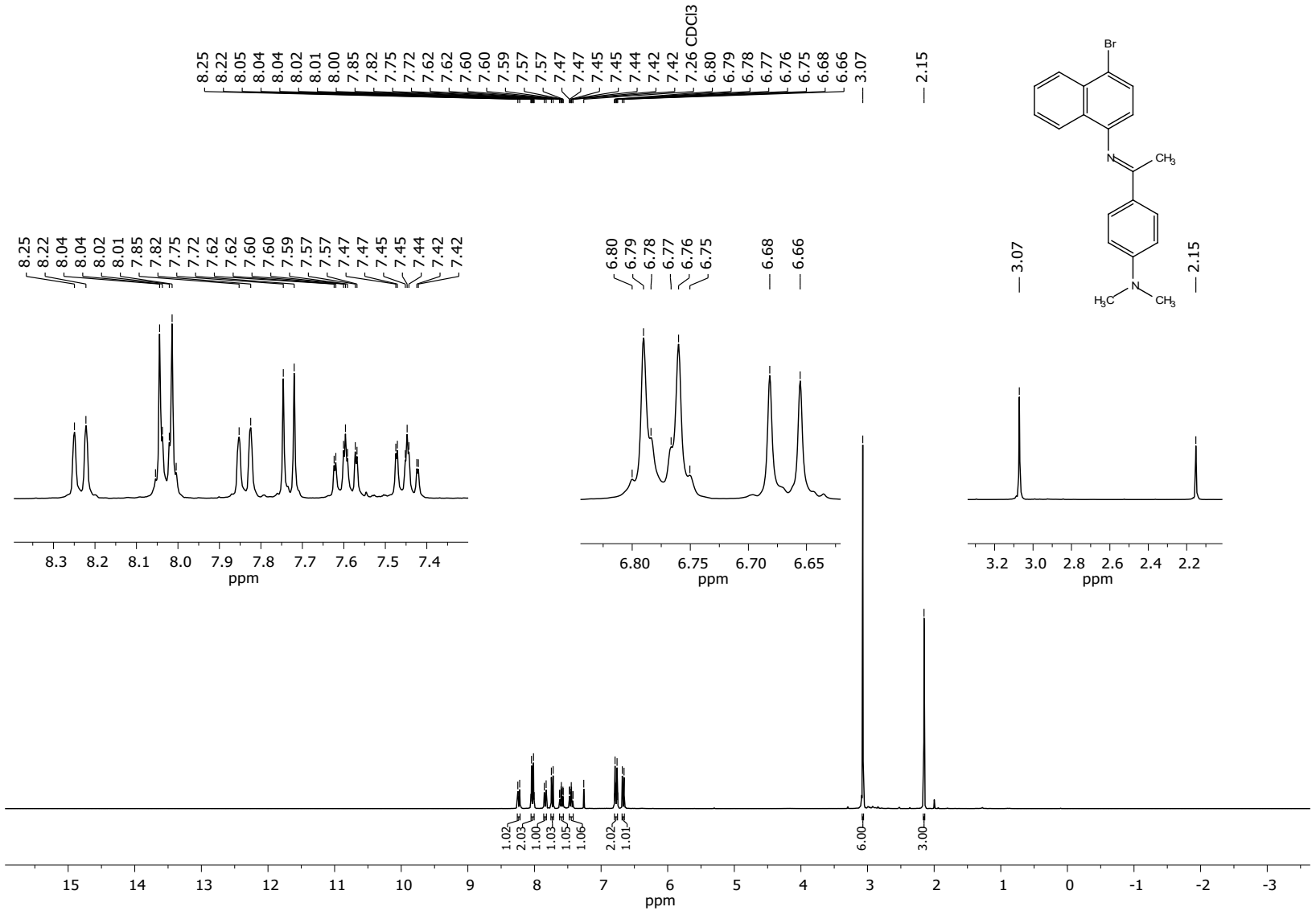

Figure S57. ^{1}H NMR spectrum of compound **6e** ($CDCl_3$, 300 MHz).

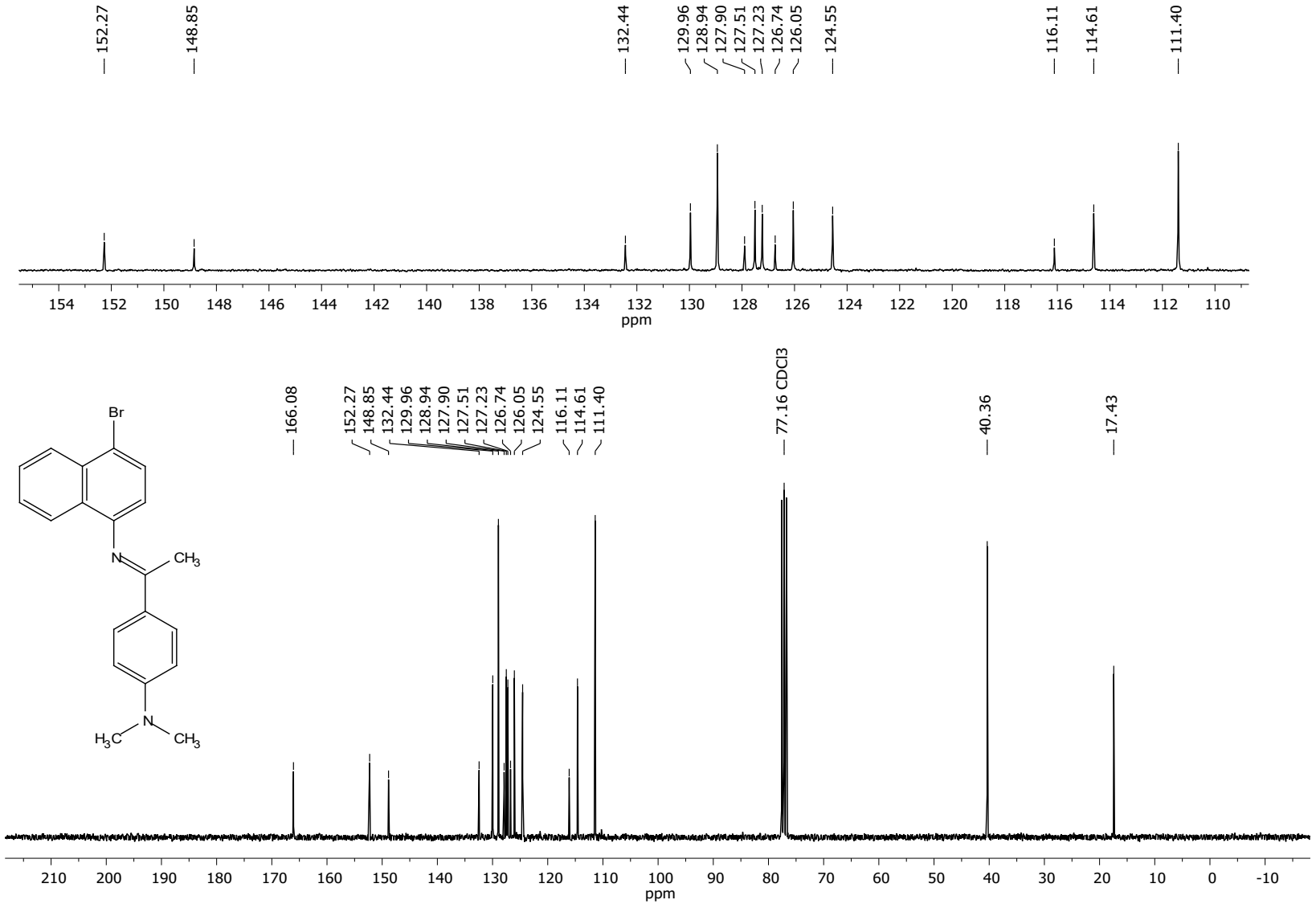

Figure S58. ^{13}C {^{1}H} NMR spectrum of compound **6e** ($CDCl_3$, 76 MHz).

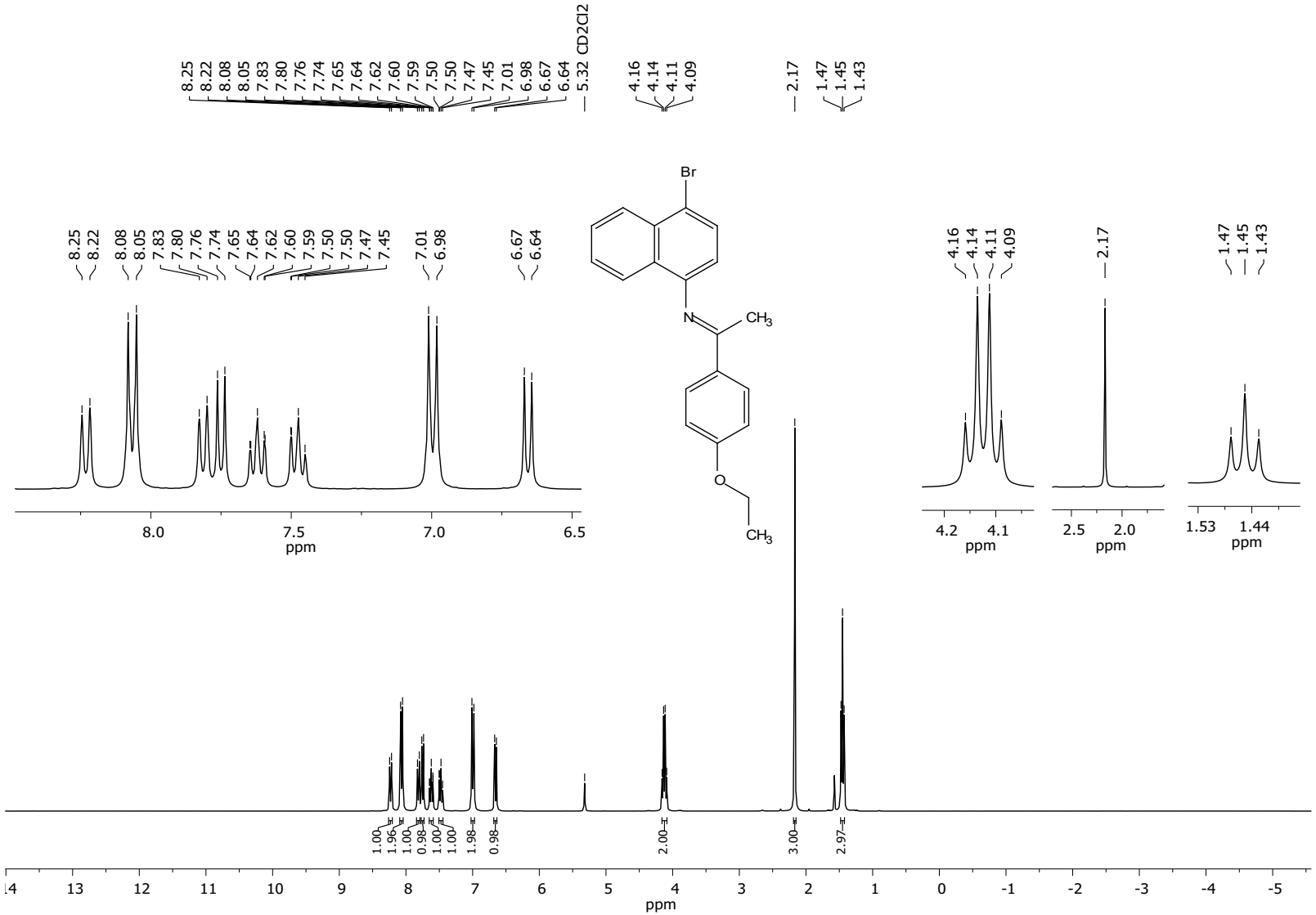

Figure S59. ^{1}H NMR spectrum of compound **6f** (CD_2Cl_2, 300 MHz).

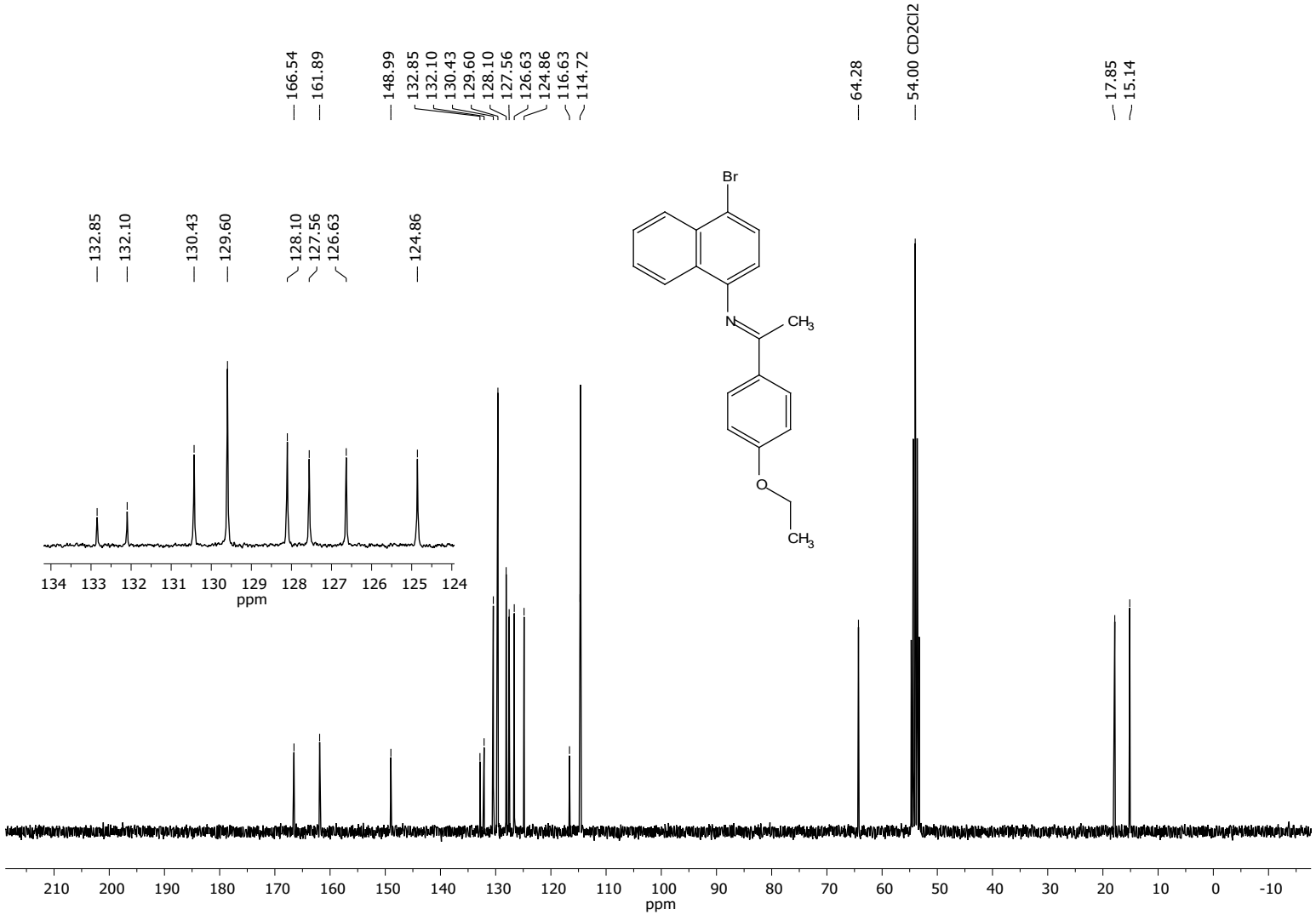

Figure S60. ^{13}C {^{1}H} NMR spectrum of compound **6f** (CD_2Cl_2, 76 MHz).

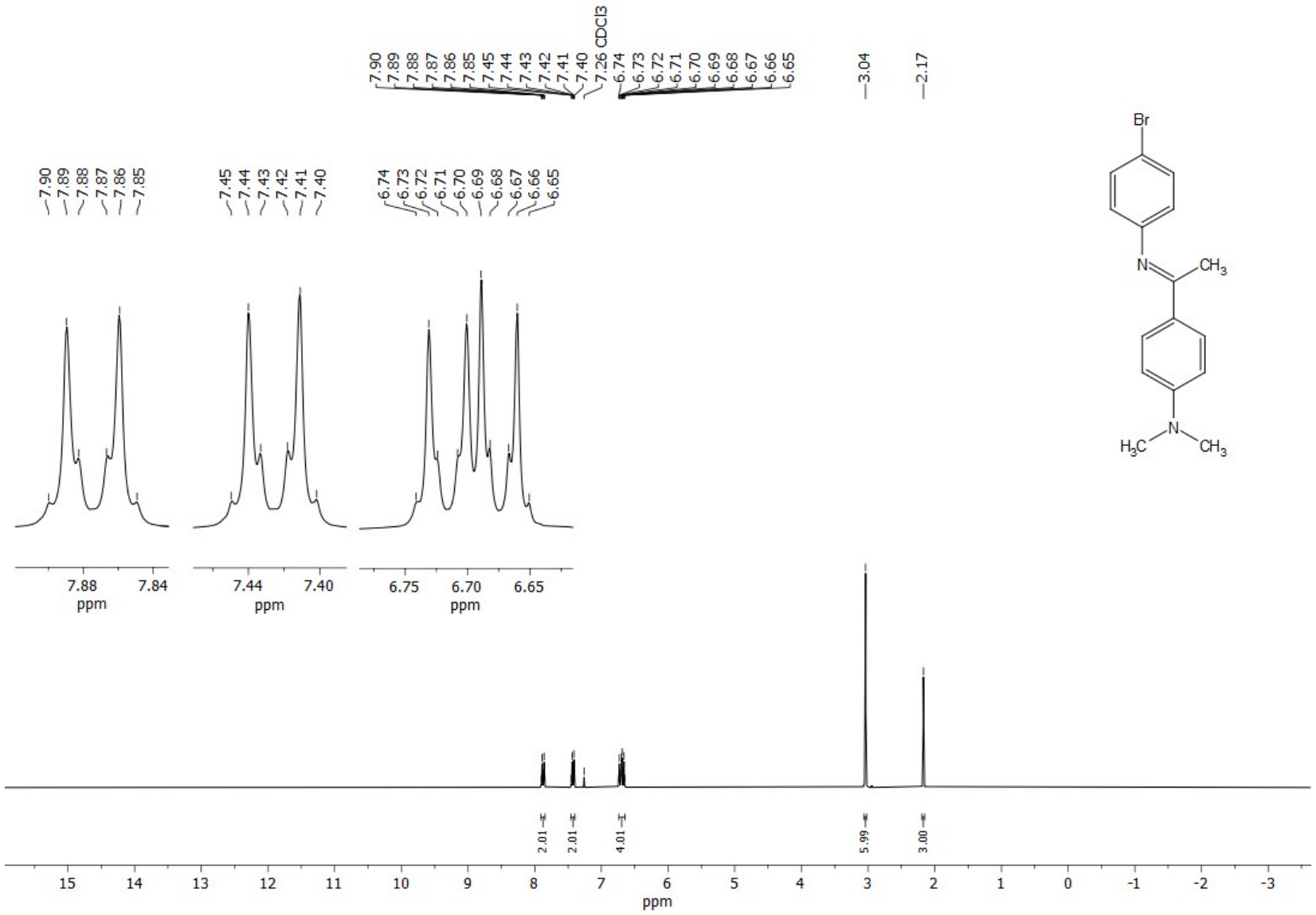

Figure S61. ^{1}H NMR spectrum of compound **6g** ($CDCl_3$, 300 MHz).

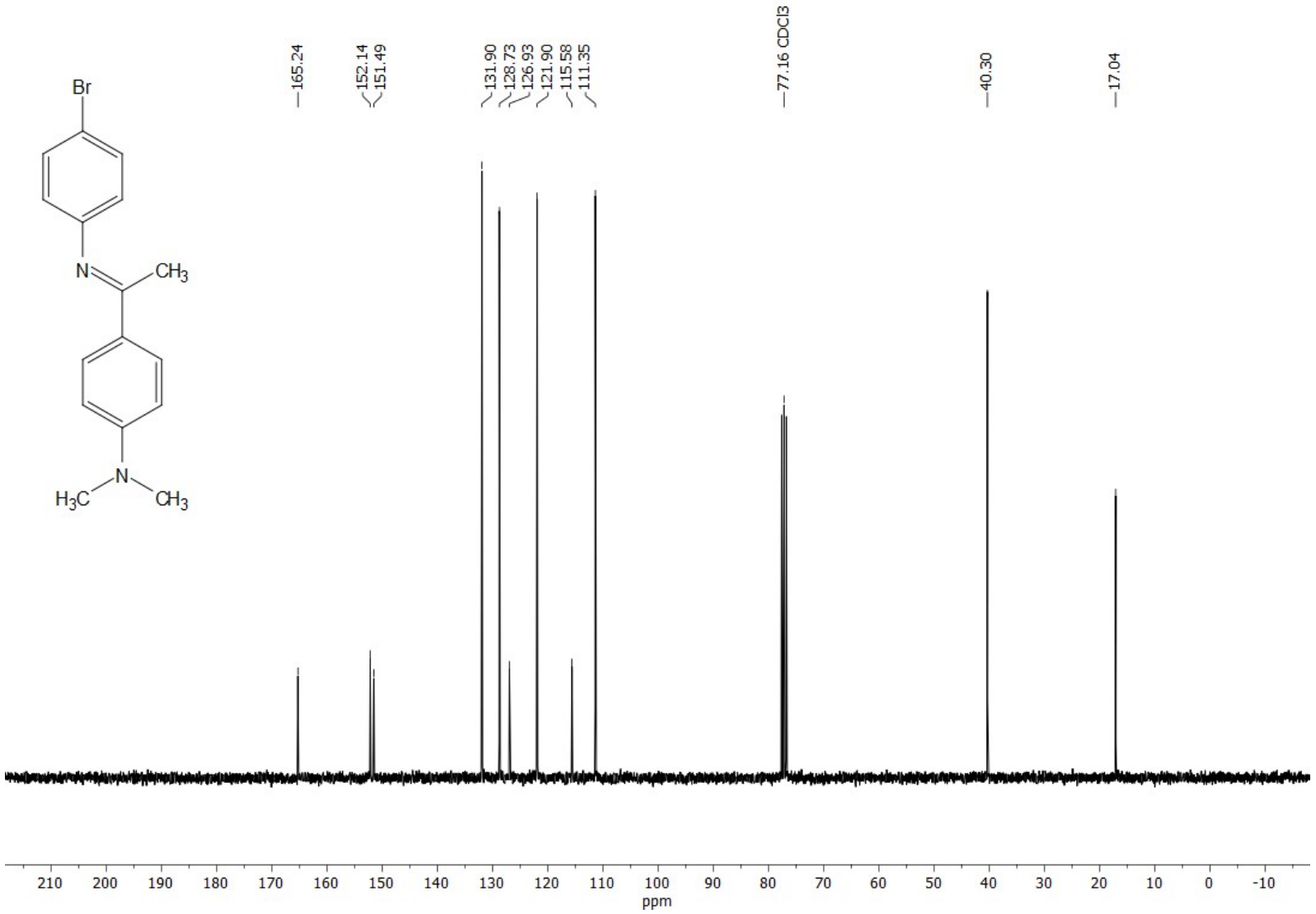

Figure S62. ^{13}C {^{1}H} NMR spectrum of compound **6g** ($CDCl_3$, 76 MHz).

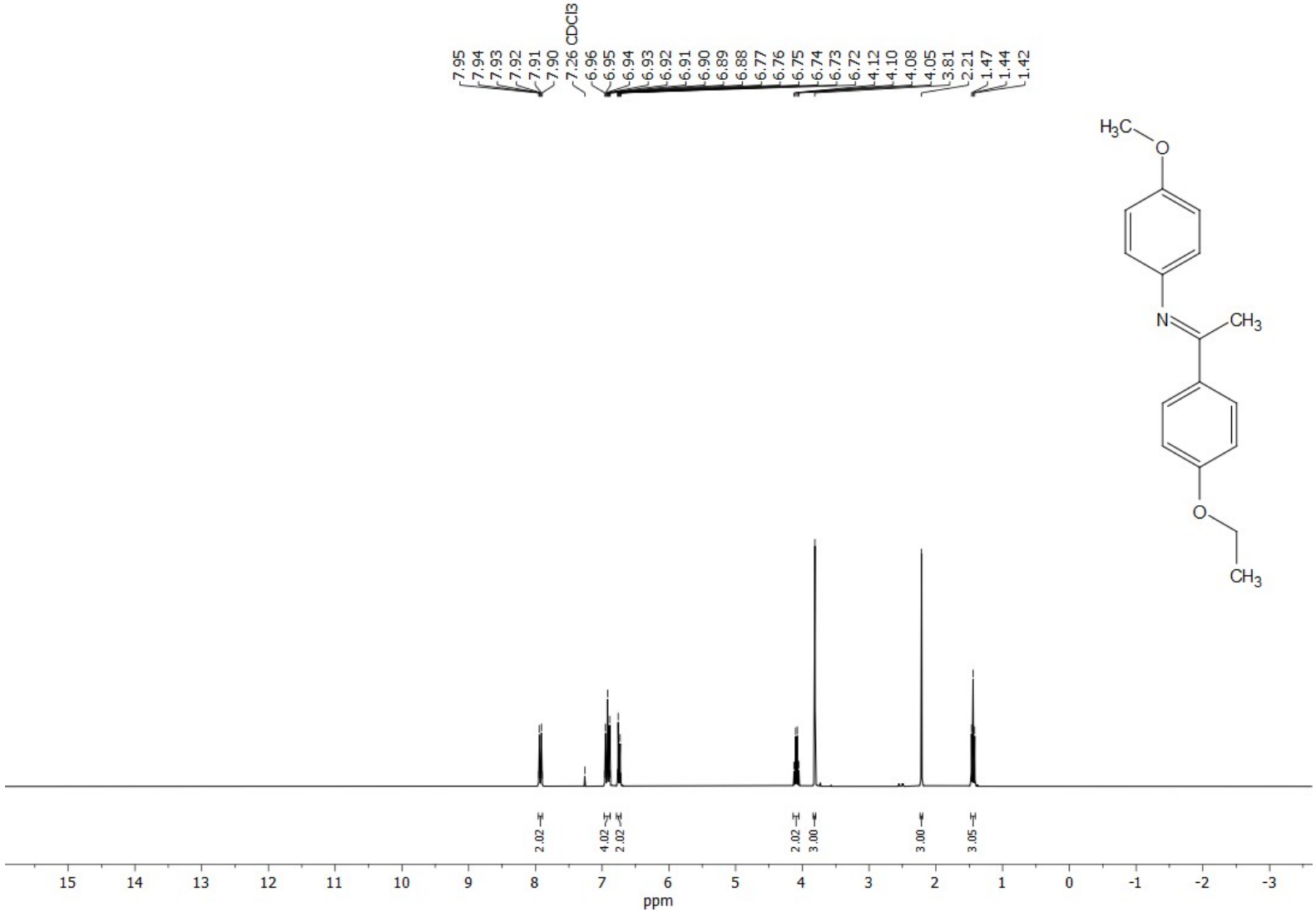

Figure S63. ^{1}H NMR spectrum of compound **6h** ($CDCl_3$, 300 MHz).

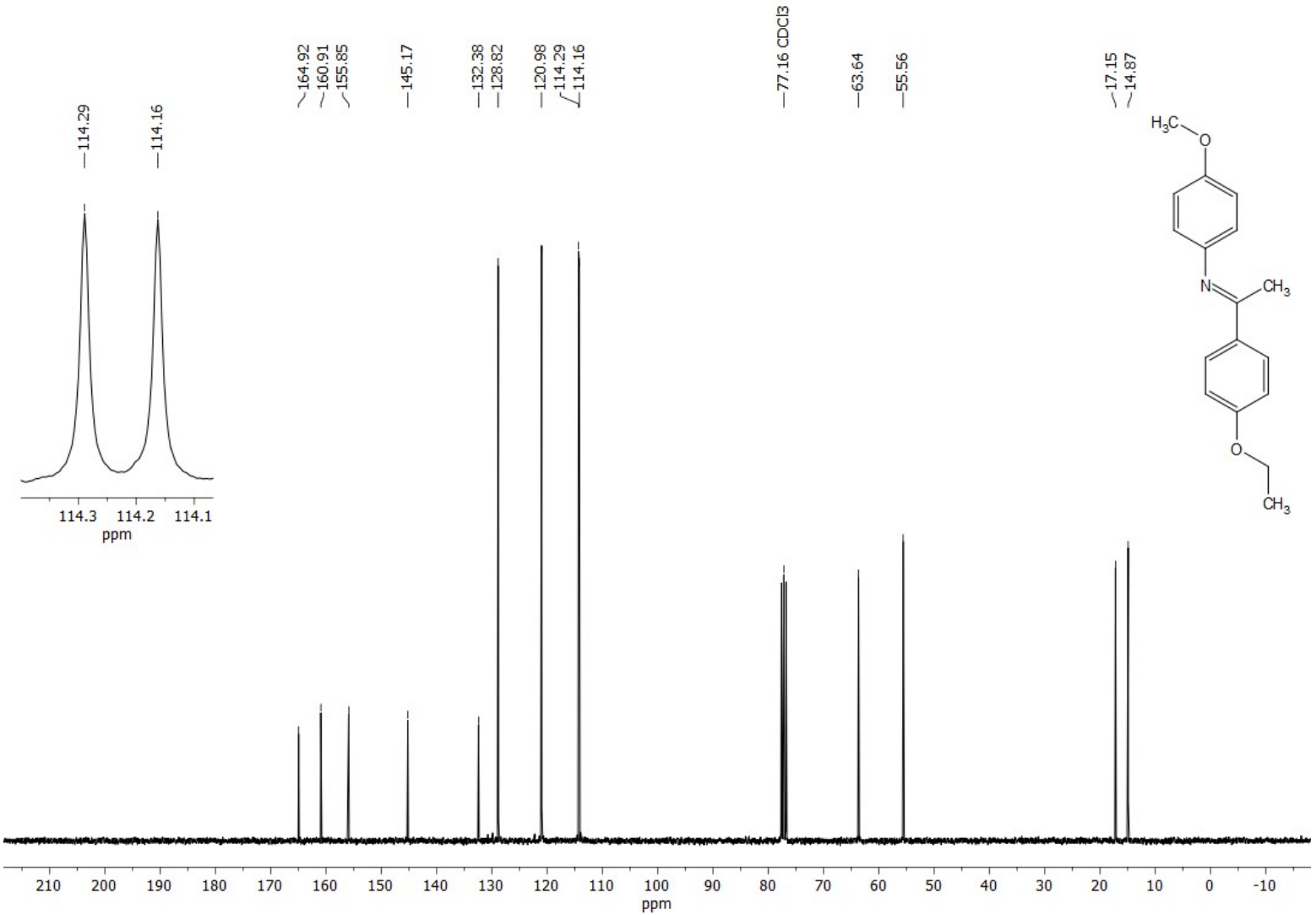

Figure S64. ^{13}C {^{1}H} NMR spectrum of compound **6h** ($CDCl_3$, 76 MHz).

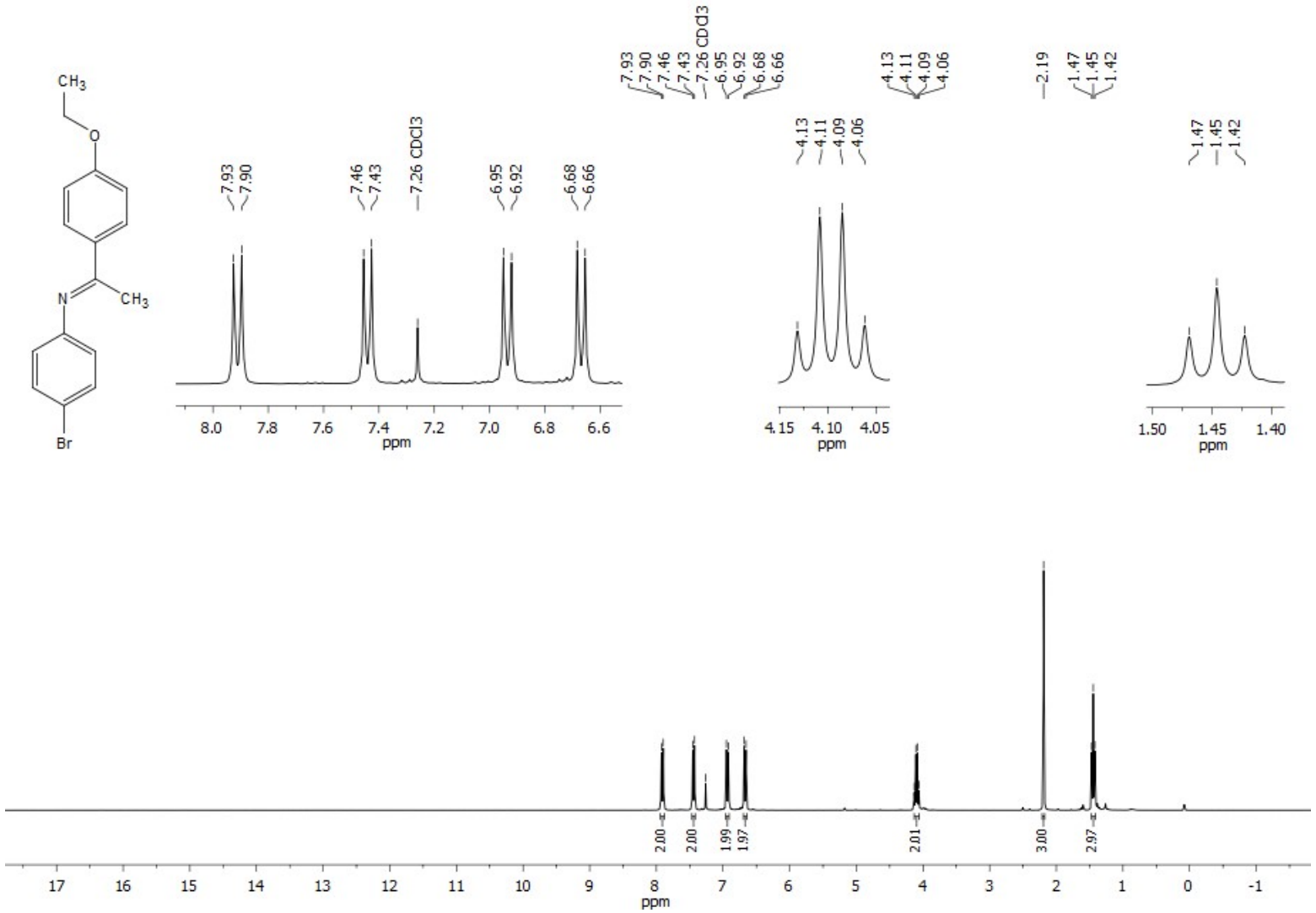

Figure S65. ^{1}H NMR spectrum of compound **6i** ($CDCl_3$, 300 MHz).

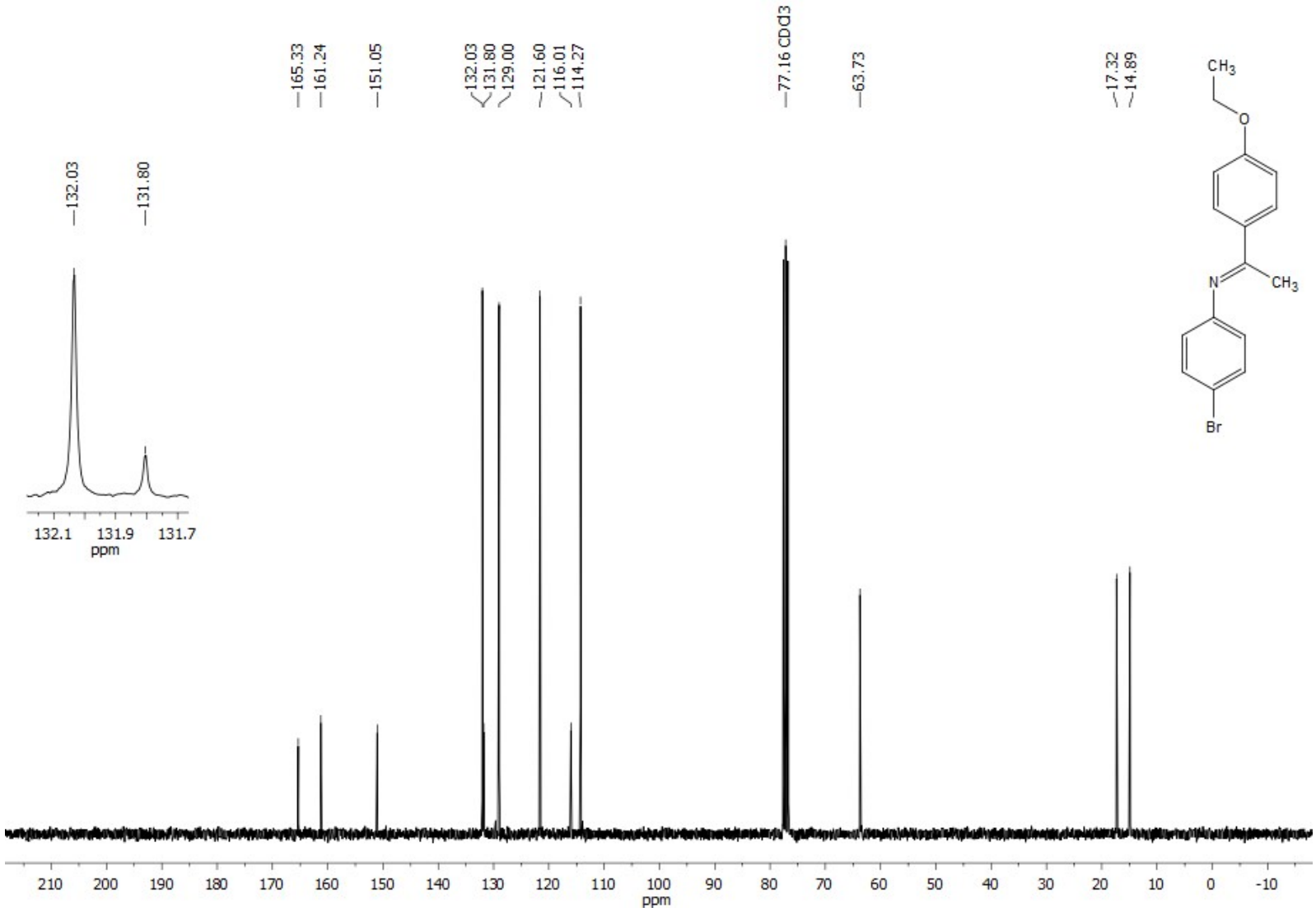

Figure S66. ^{13}C {^{1}H} NMR spectrum of compound **6i** ($CDCl_3$, 76 MHz).

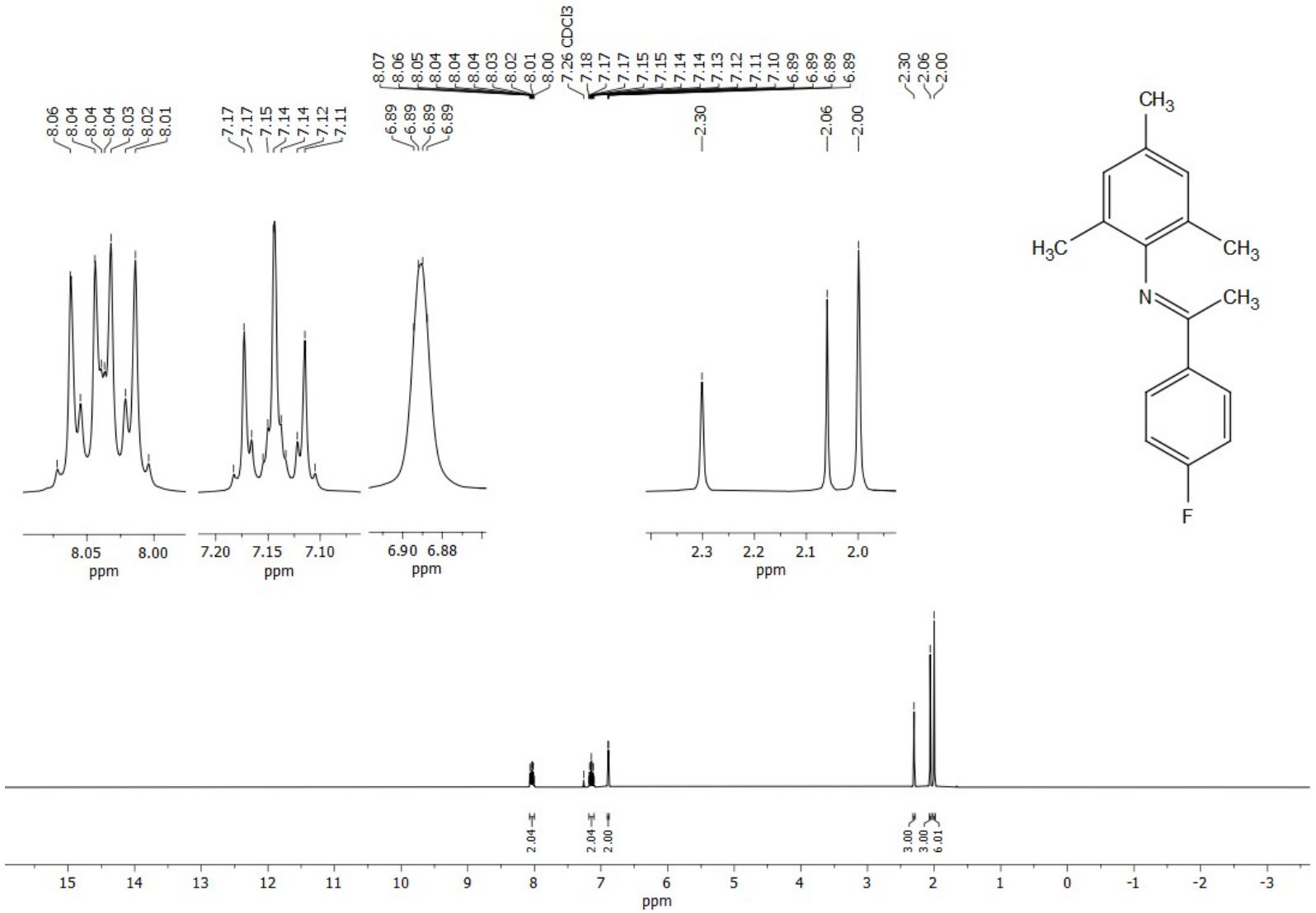

Figure S67. ^{1}H NMR spectrum of compound **6j** ($CDCl_3$, 300 MHz).

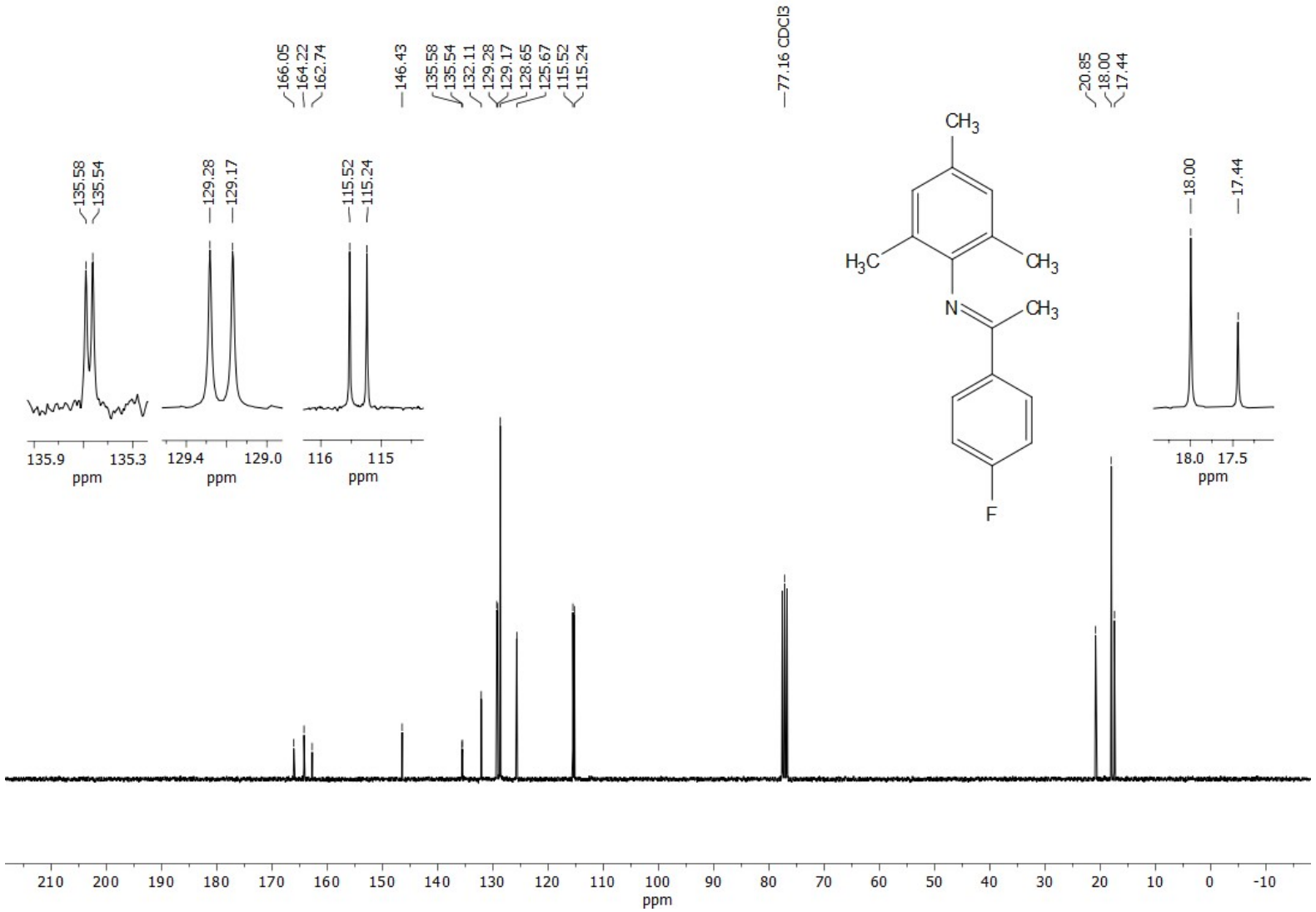

Figure S68. ^{13}C {^{1}H} NMR spectrum of compound **6j** ($CDCl_3$, 76 MHz).

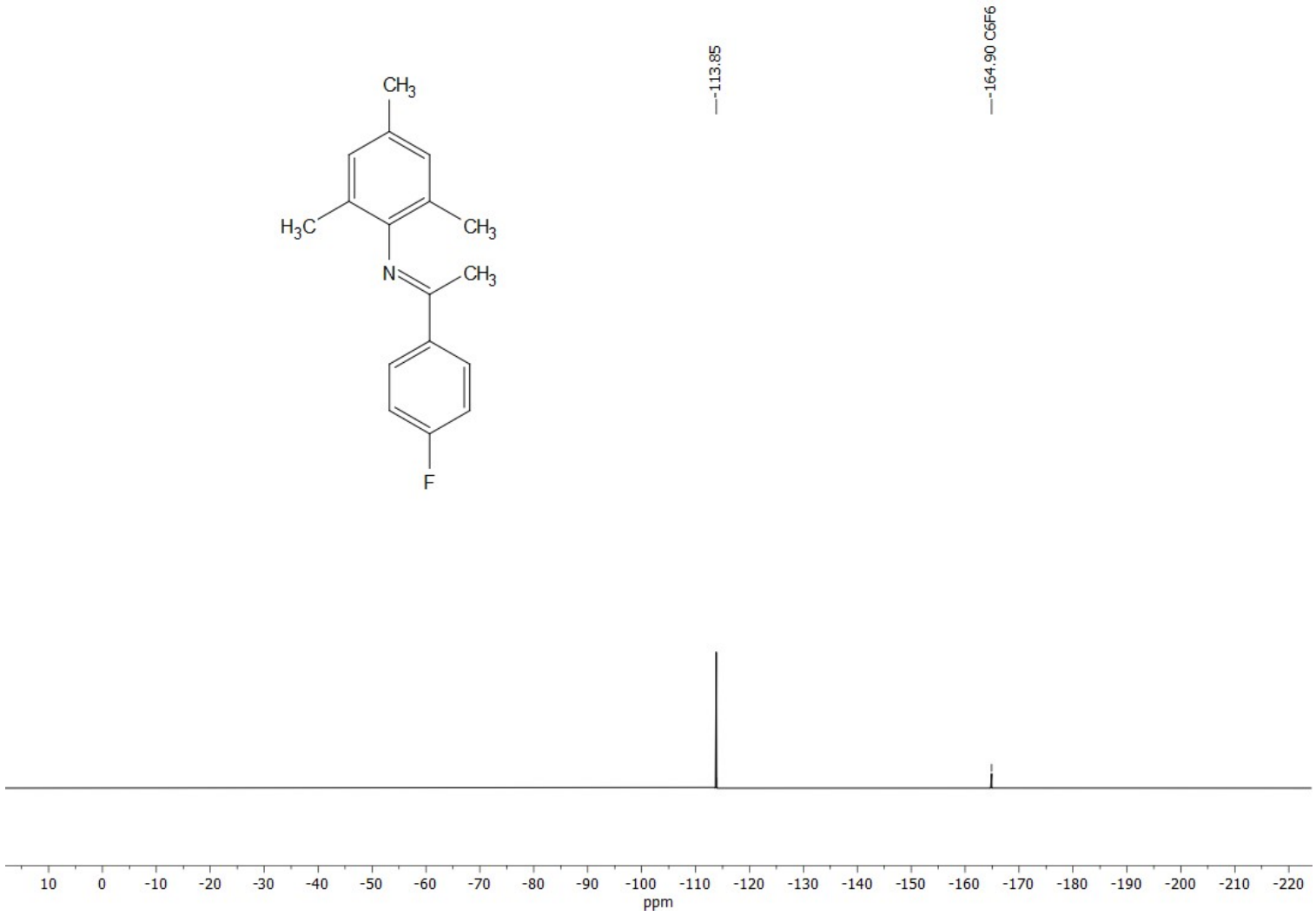

Figure S69. ^{19}F {^{1}H} NMR spectrum of compound **6j** ($CDCl_3$, 282 MHz). Standard C_6F_6 with respect to $CFCl_3$.

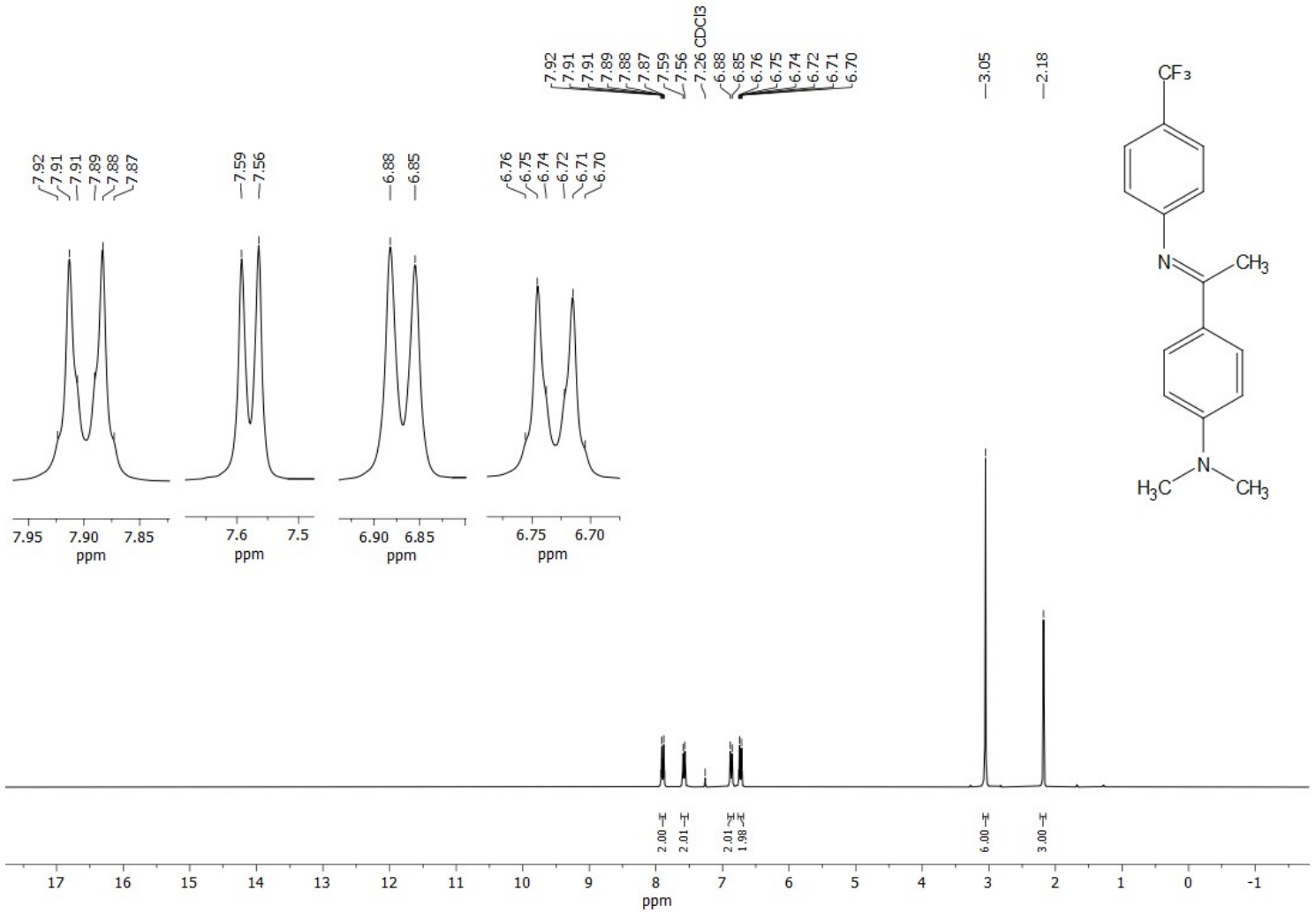

Figure S70. ^{1}H NMR spectrum of compound **6k** ($CDCl_3$, 300 MHz).

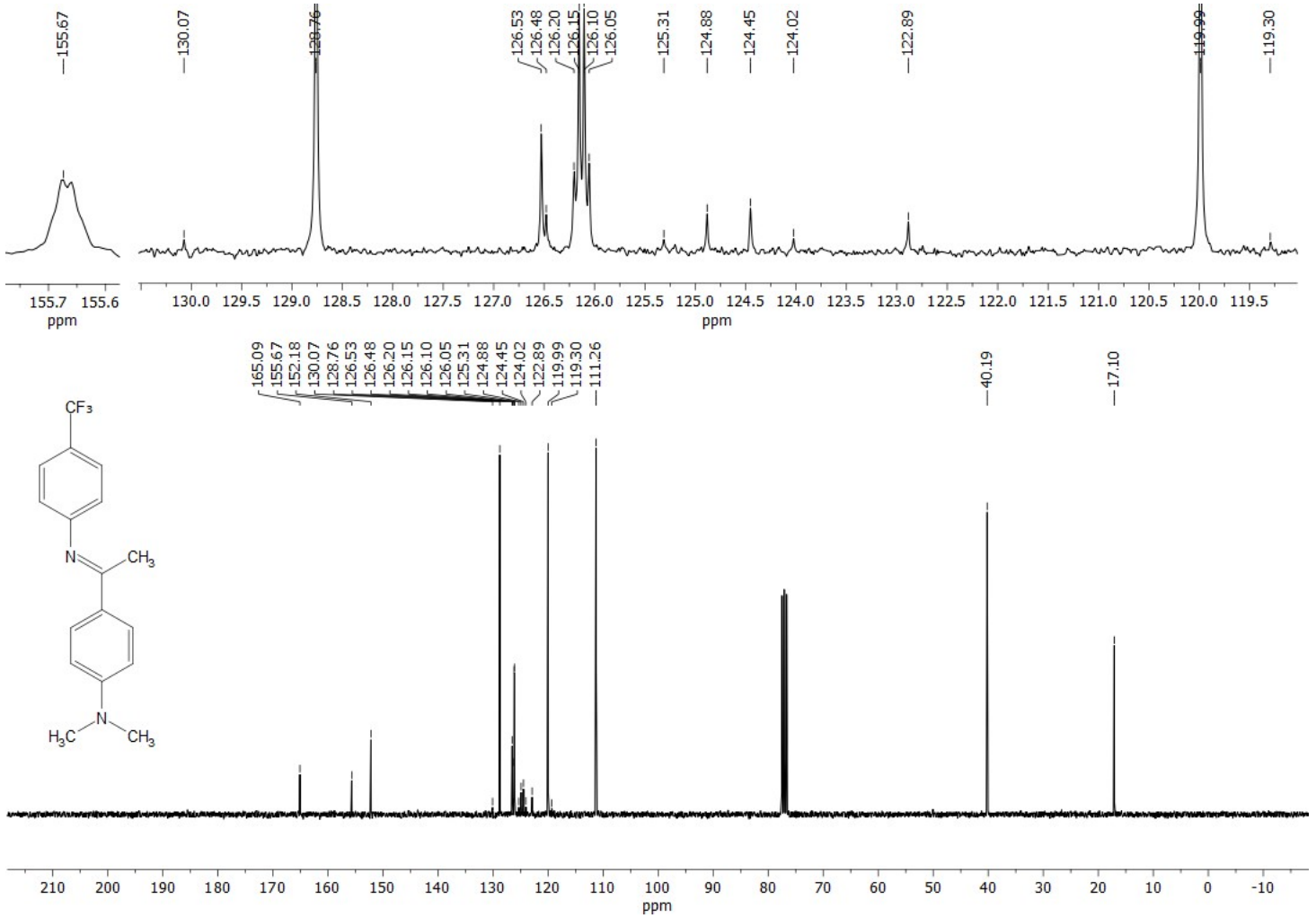

Figure S71. ^{13}C {^{1}H} NMR spectrum of compound **6k** ($CDCl_3$, 76 MHz).

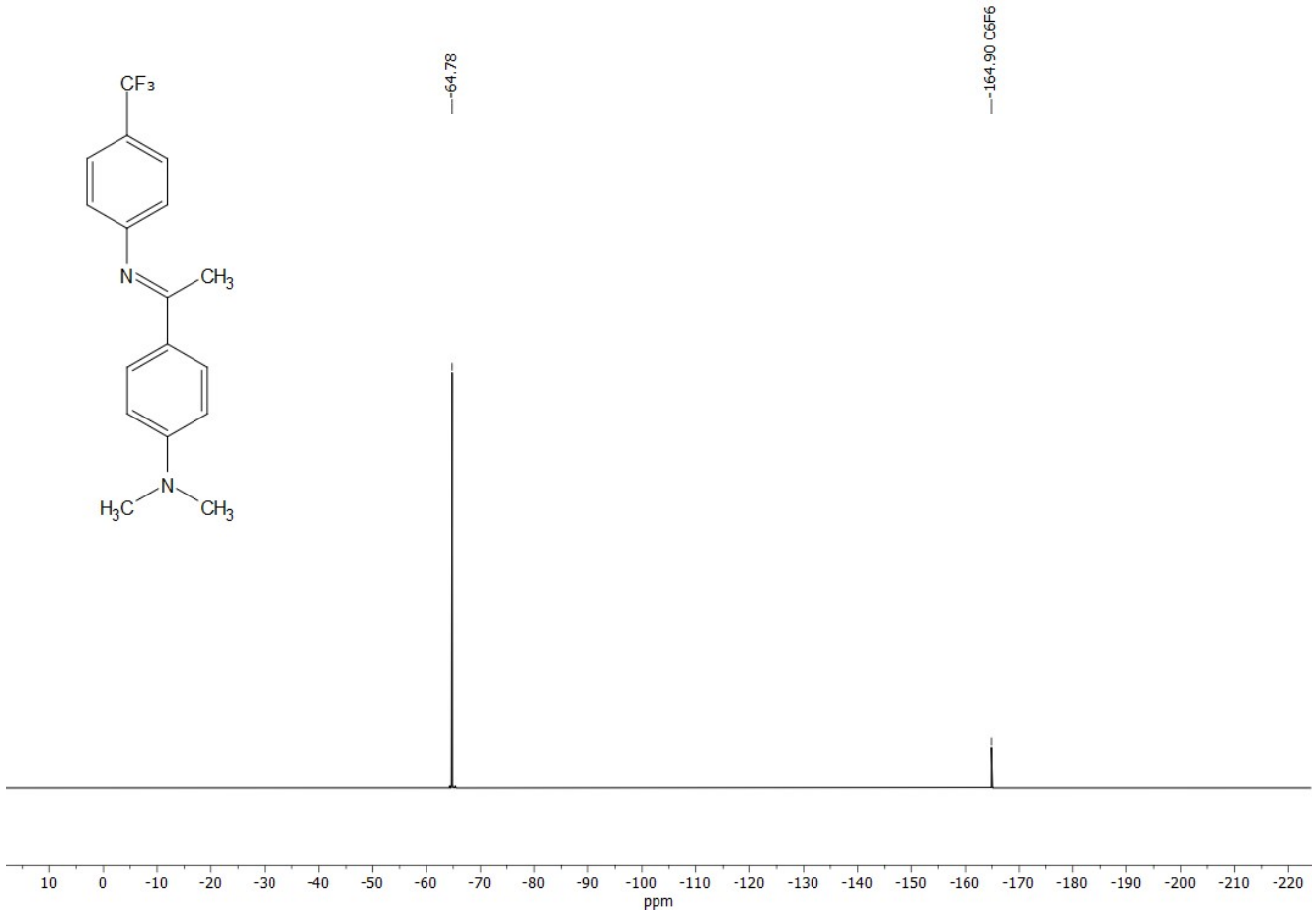

Figure S72. ^{19}F $\{^{1}H\}$ NMR spectrum of compound **6k** ($CDCl_3$, 282 MHz). Standard C_6F_6 with respect to $CFCl_3$.

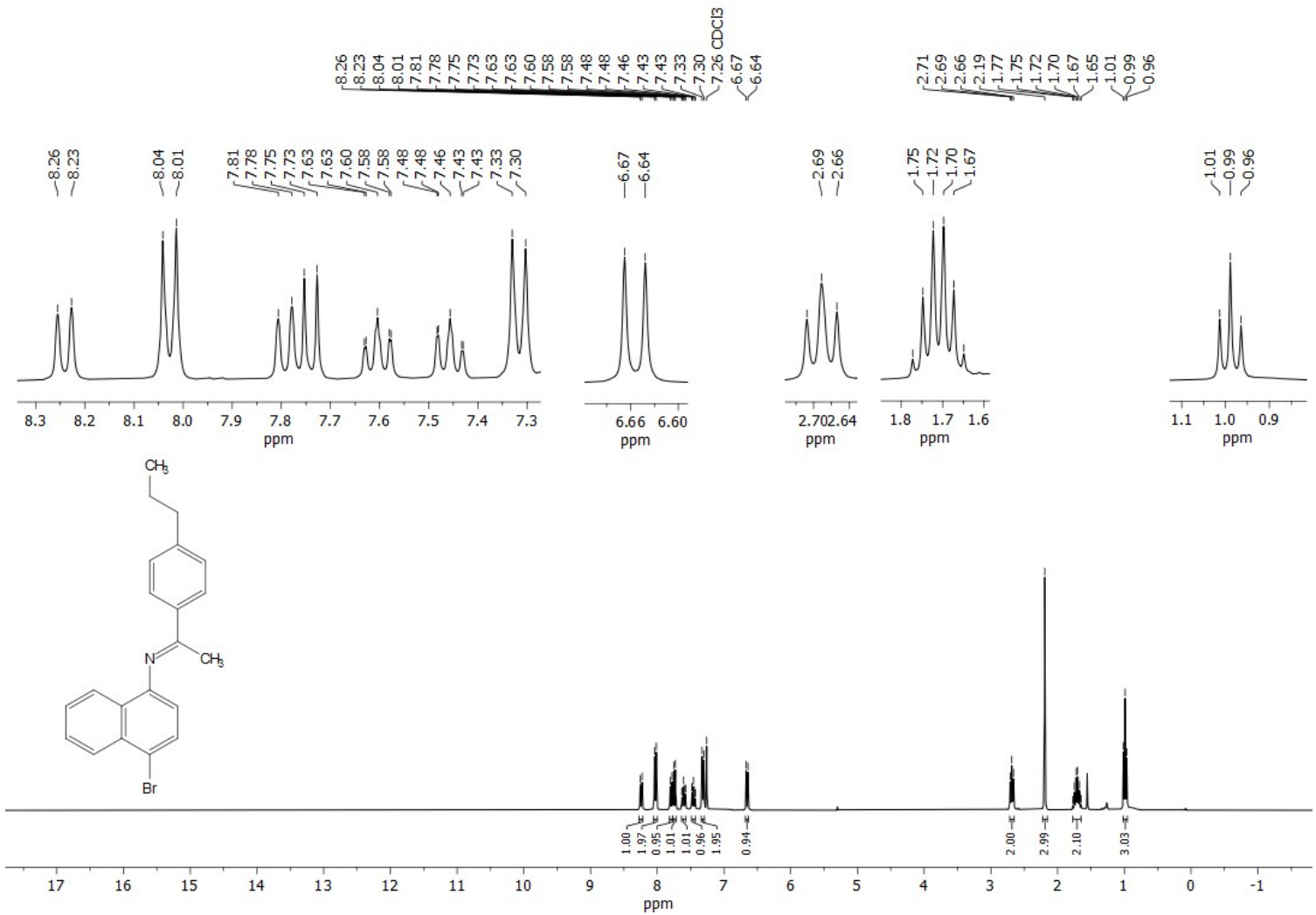

Figure S73. ^{1}H NMR spectrum of compound **6l** ($CDCl_3$, 300 MHz).

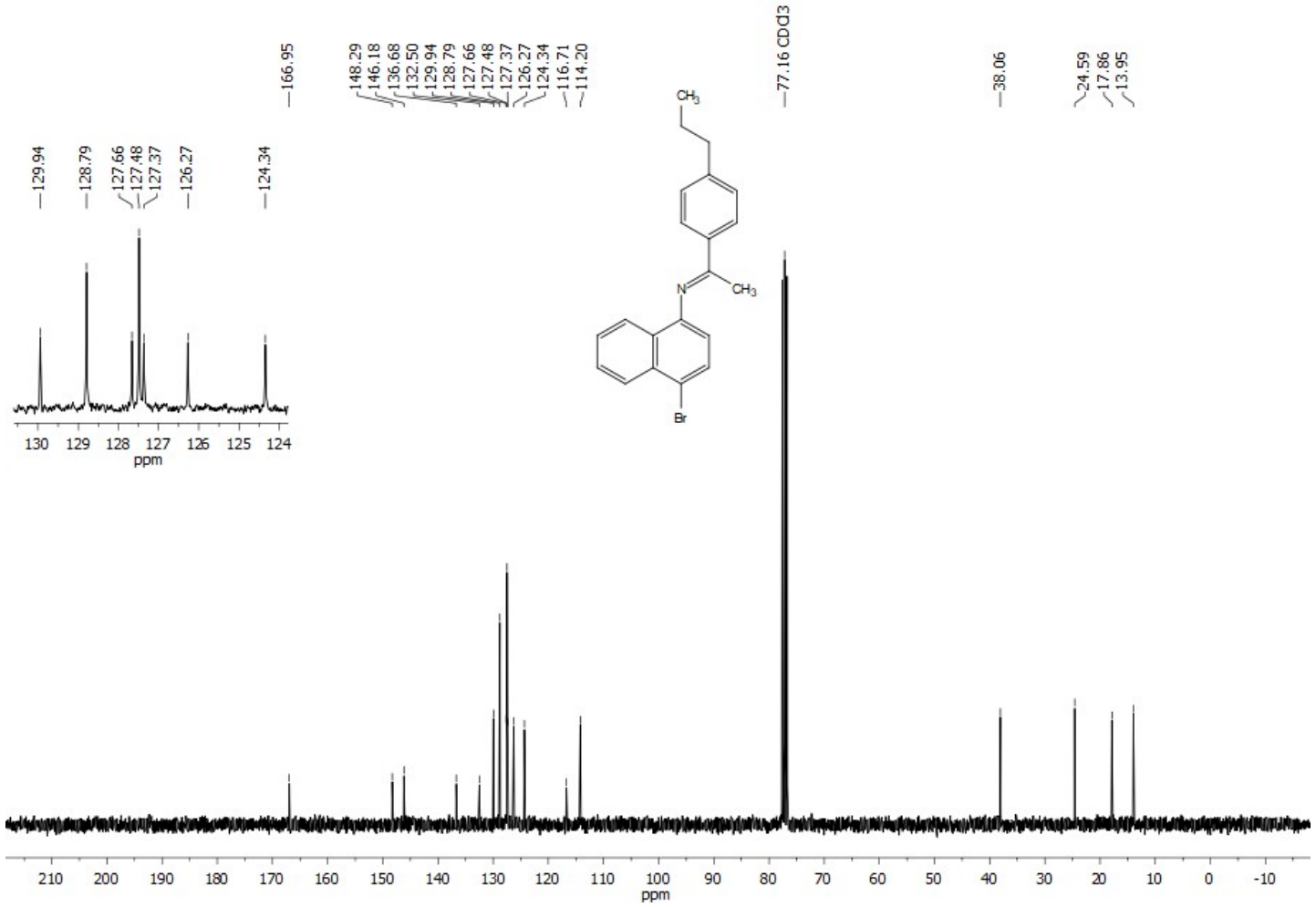

Figure S74. ^{13}C {^{1}H} NMR spectrum of compound **6l** ($CDCl_3$, 76 MHz).

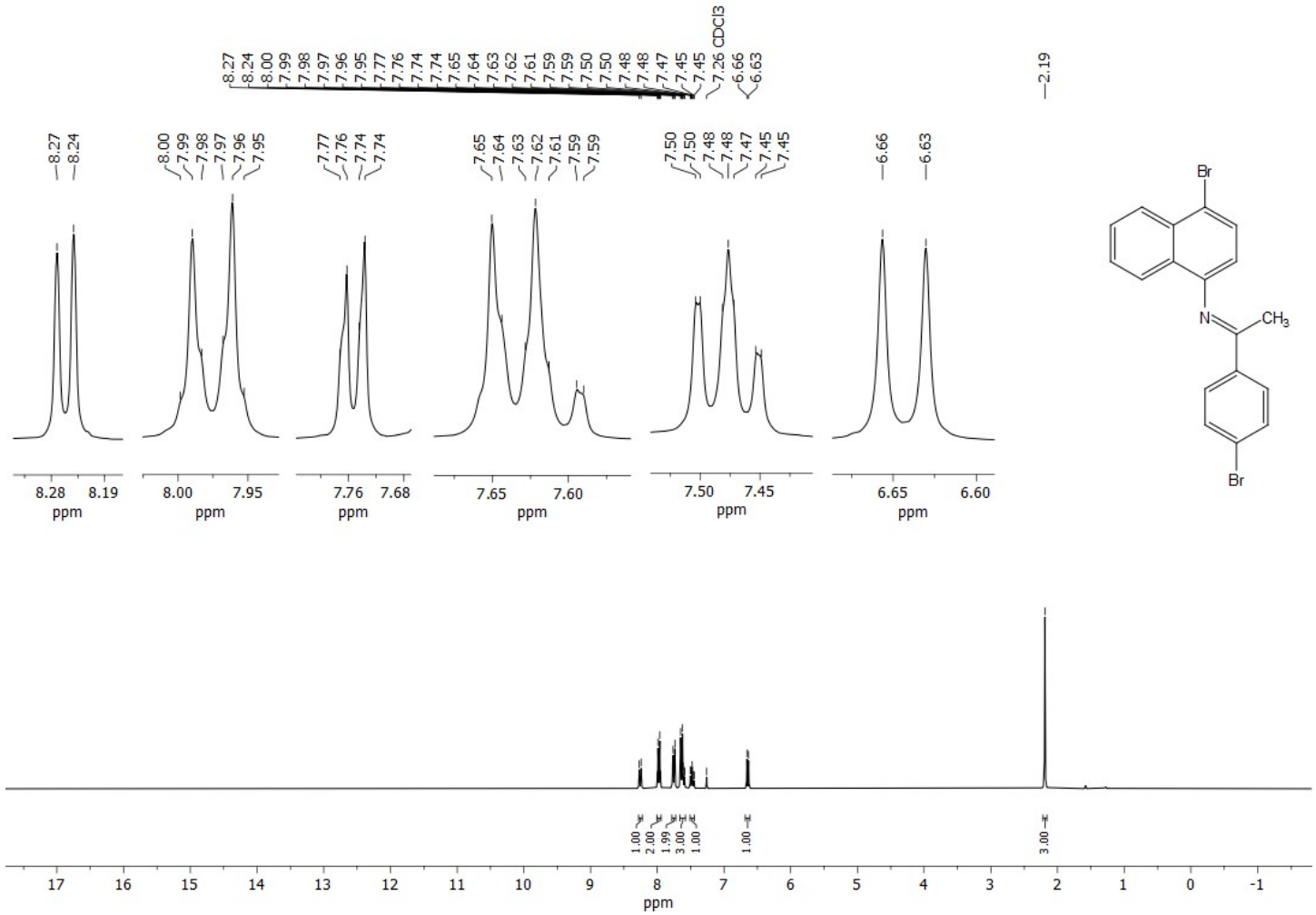

Figure S75. ^{1}H NMR spectrum of compound **6m** ($CDCl_3$, 300 MHz).

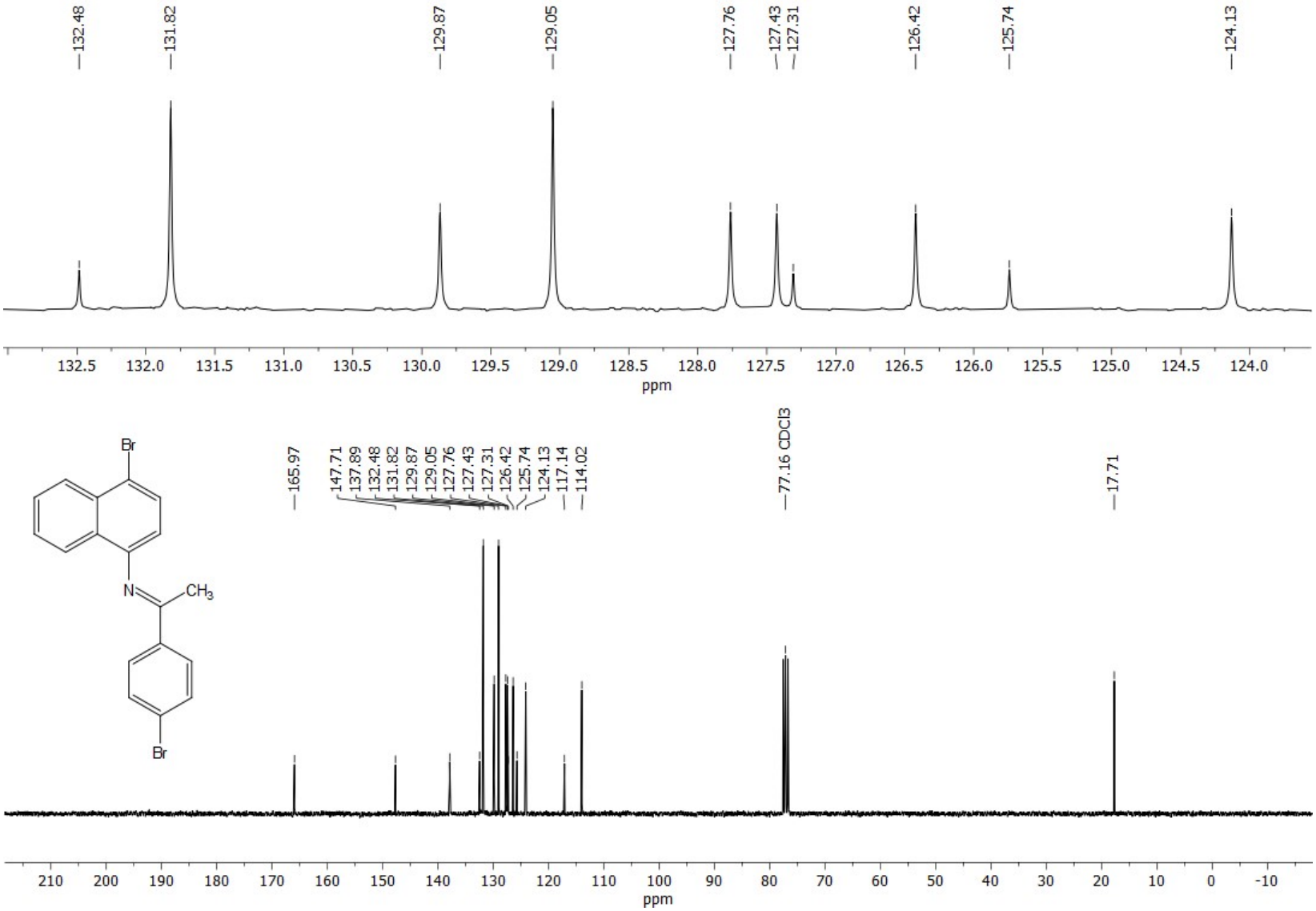

Figure S76. ^{13}C {^{1}H} NMR spectrum of compound **6m** ($CDCl_3$, 76 MHz).

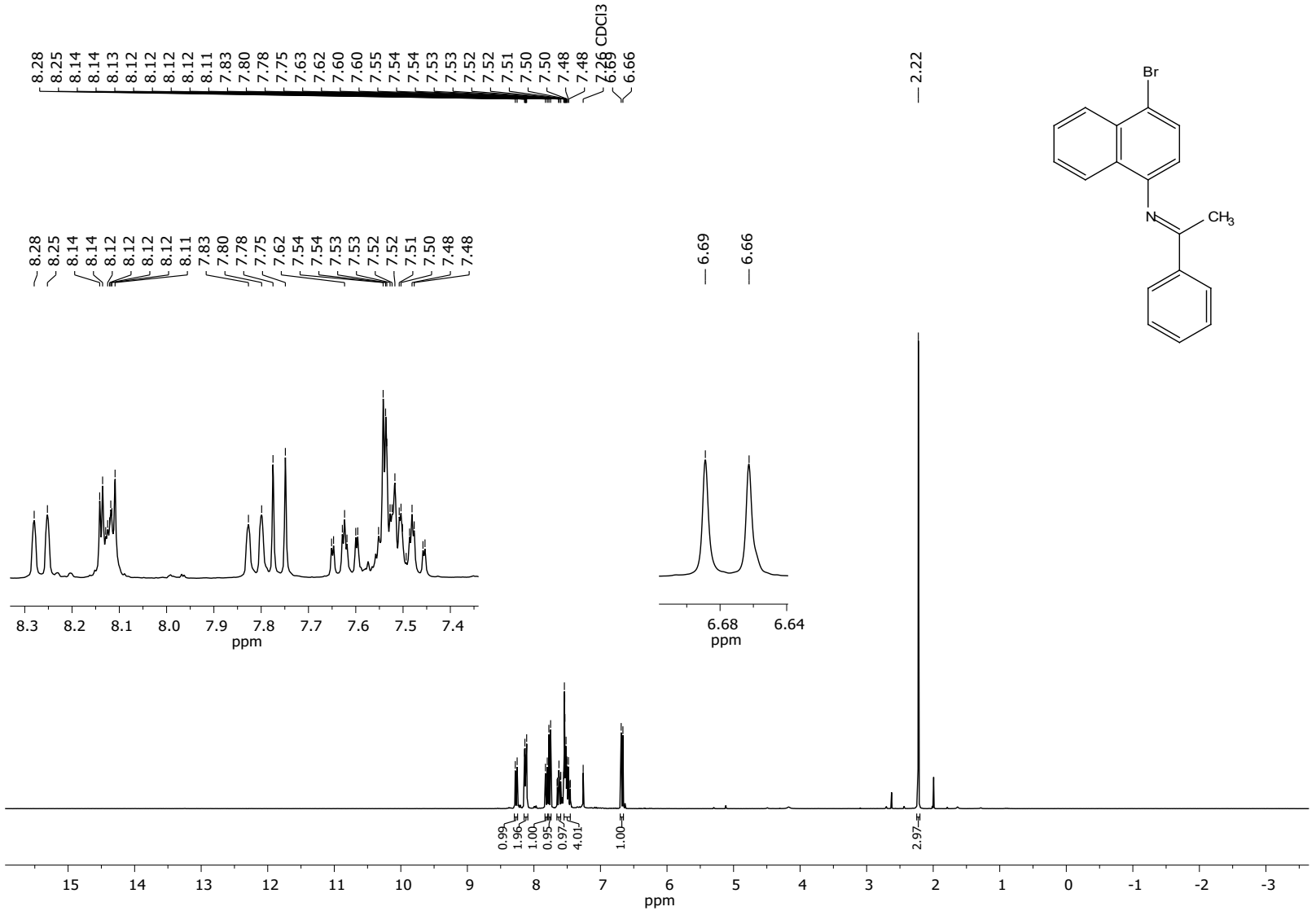

Figure S77. ^{1}H NMR spectrum of compound **6n** ($CDCl_3$, 300 MHz).

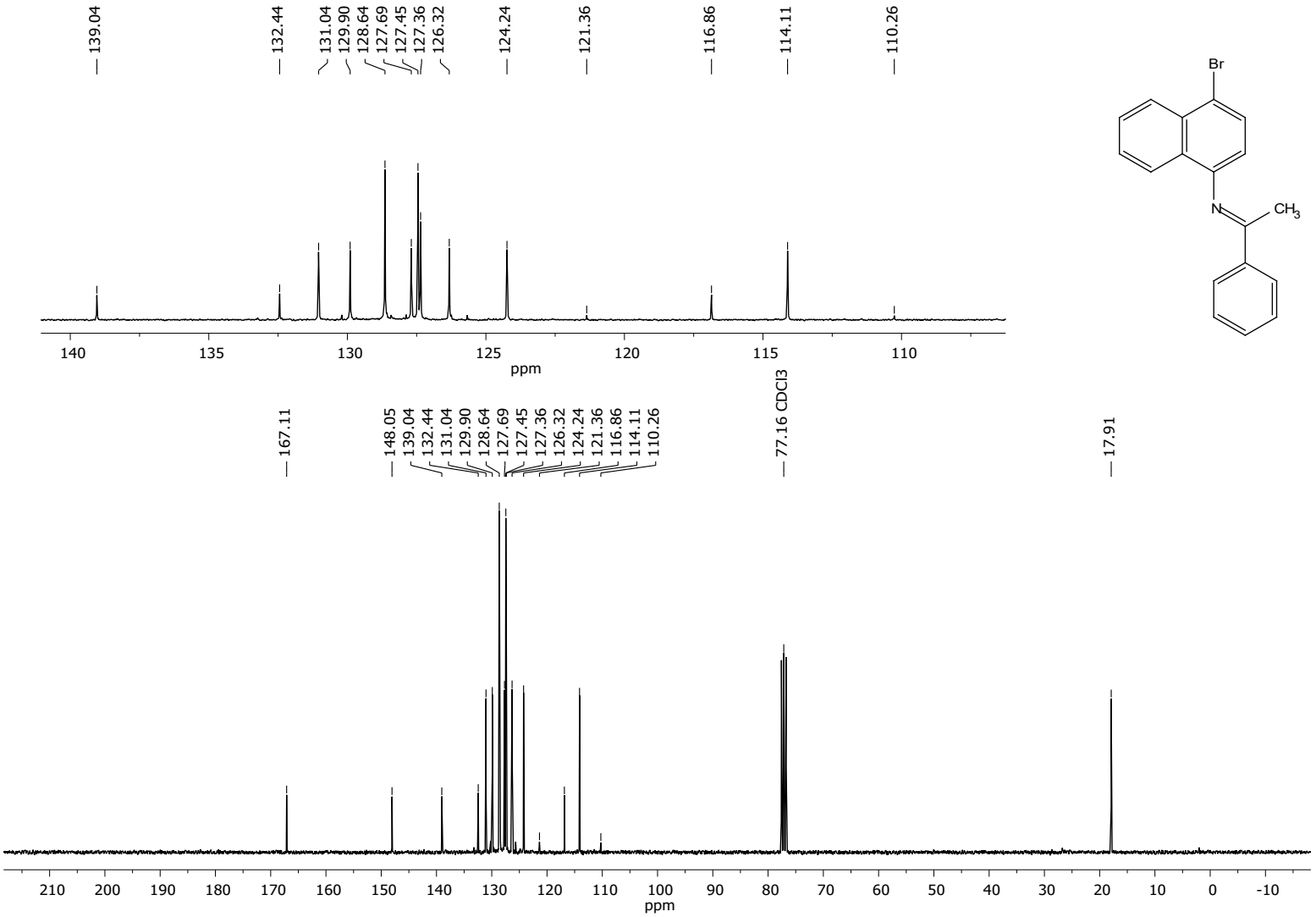

Figure S78. ^{13}C {^{1}H} NMR spectrum of compound **6n** ($CDCl_3$, 76 MHz).

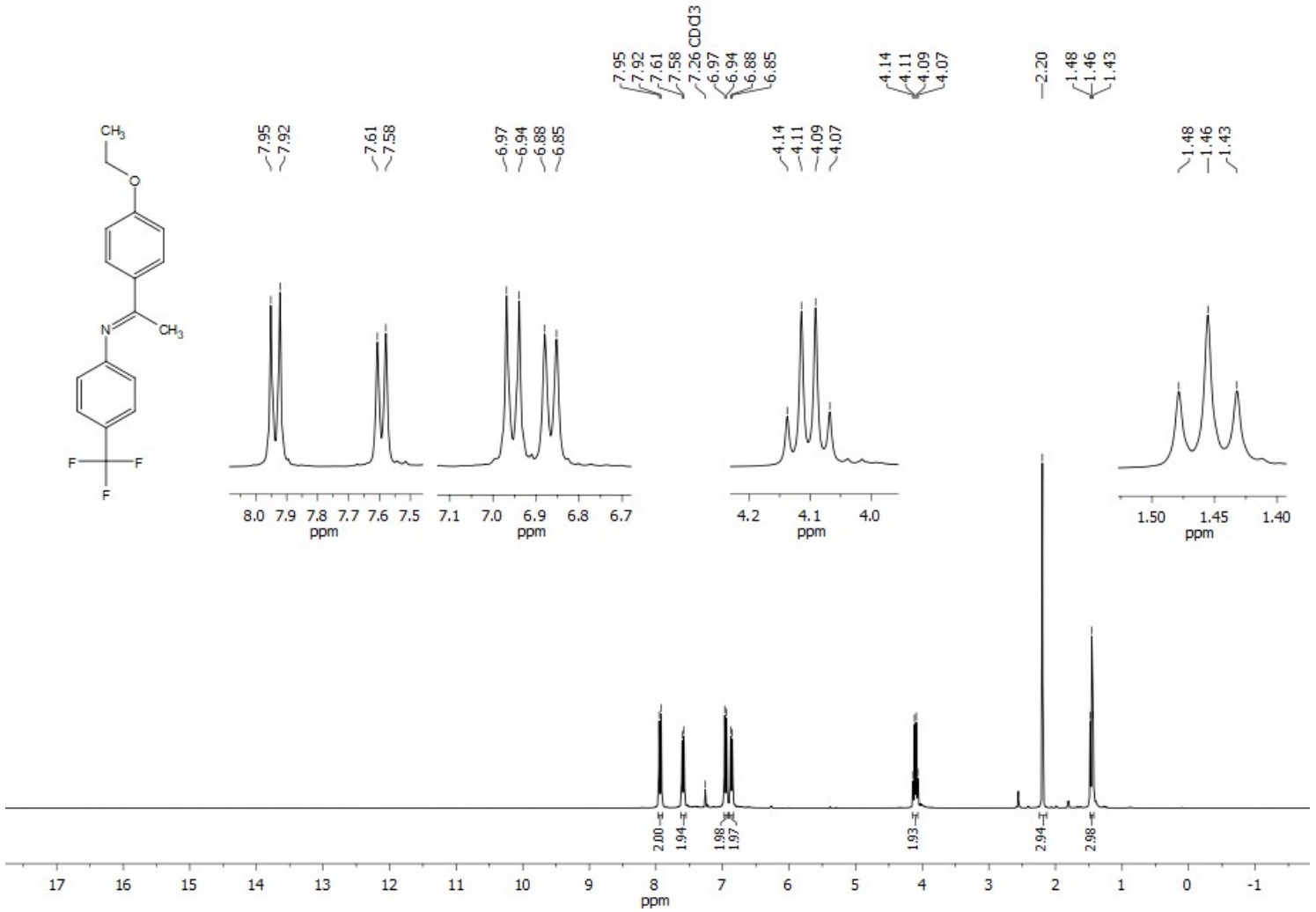

Figure S79. ^{1}H NMR spectrum of compound **6o** ($CDCl_3$, 300 MHz).

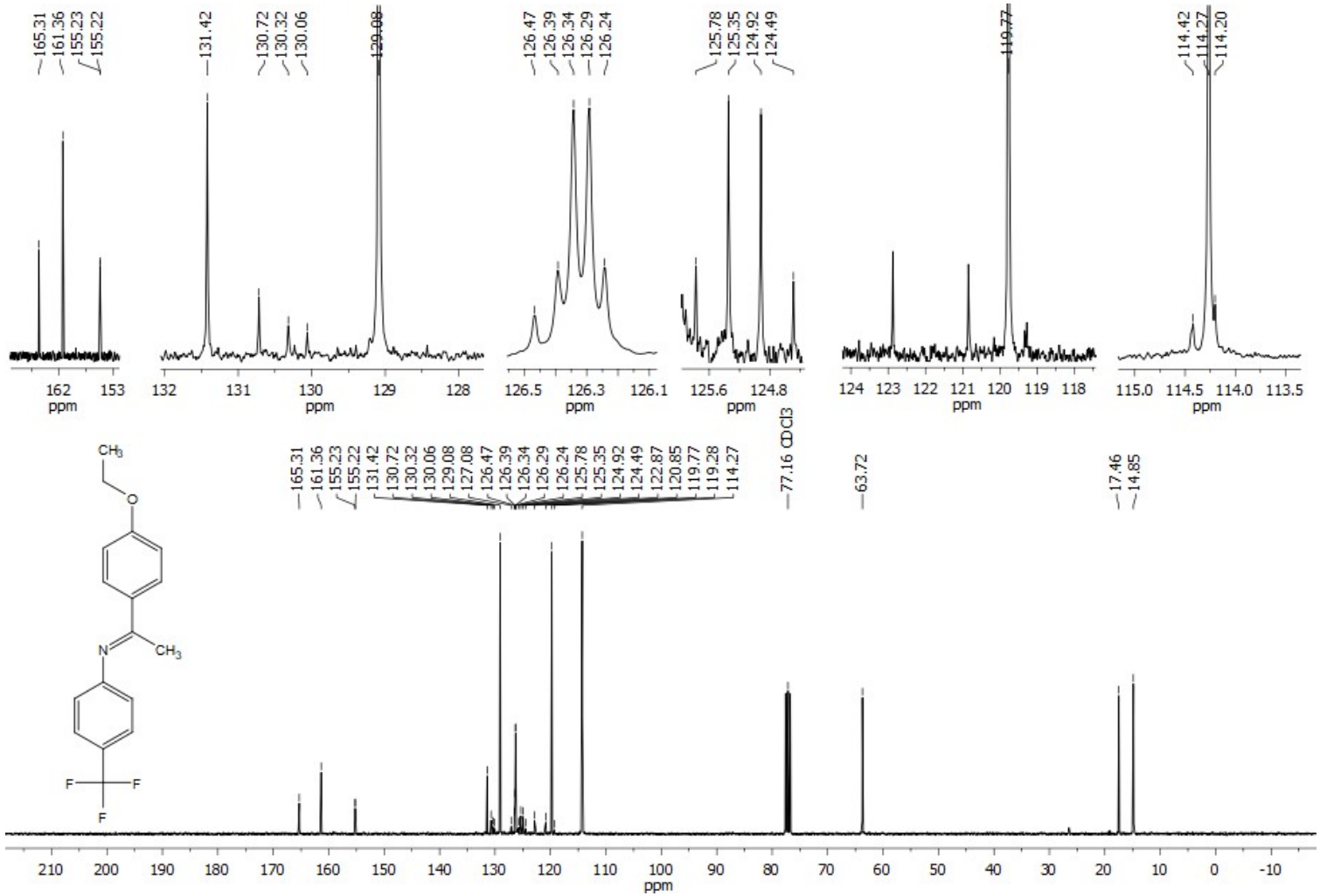

Figure S80. ^{13}C {^{1}H} NMR spectrum of compound **6o** ($CDCl_3$, 76 MHz).

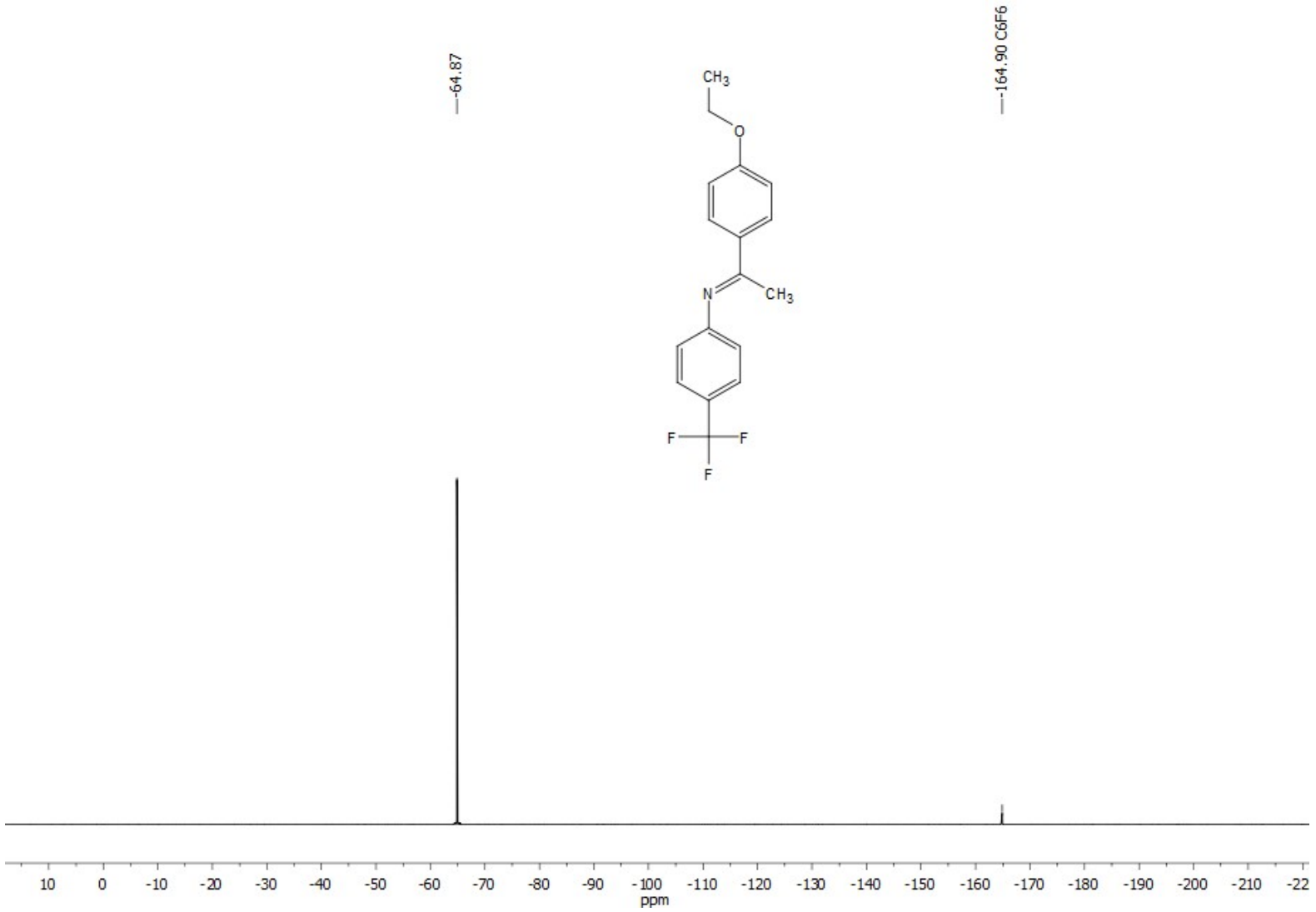

Figure S81. ^{19}F {^{1}H} NMR spectrum of compound **6o** ($CDCl_3$, 282 MHz). Standard C_6F_6 with respect to $CFCl_3$.

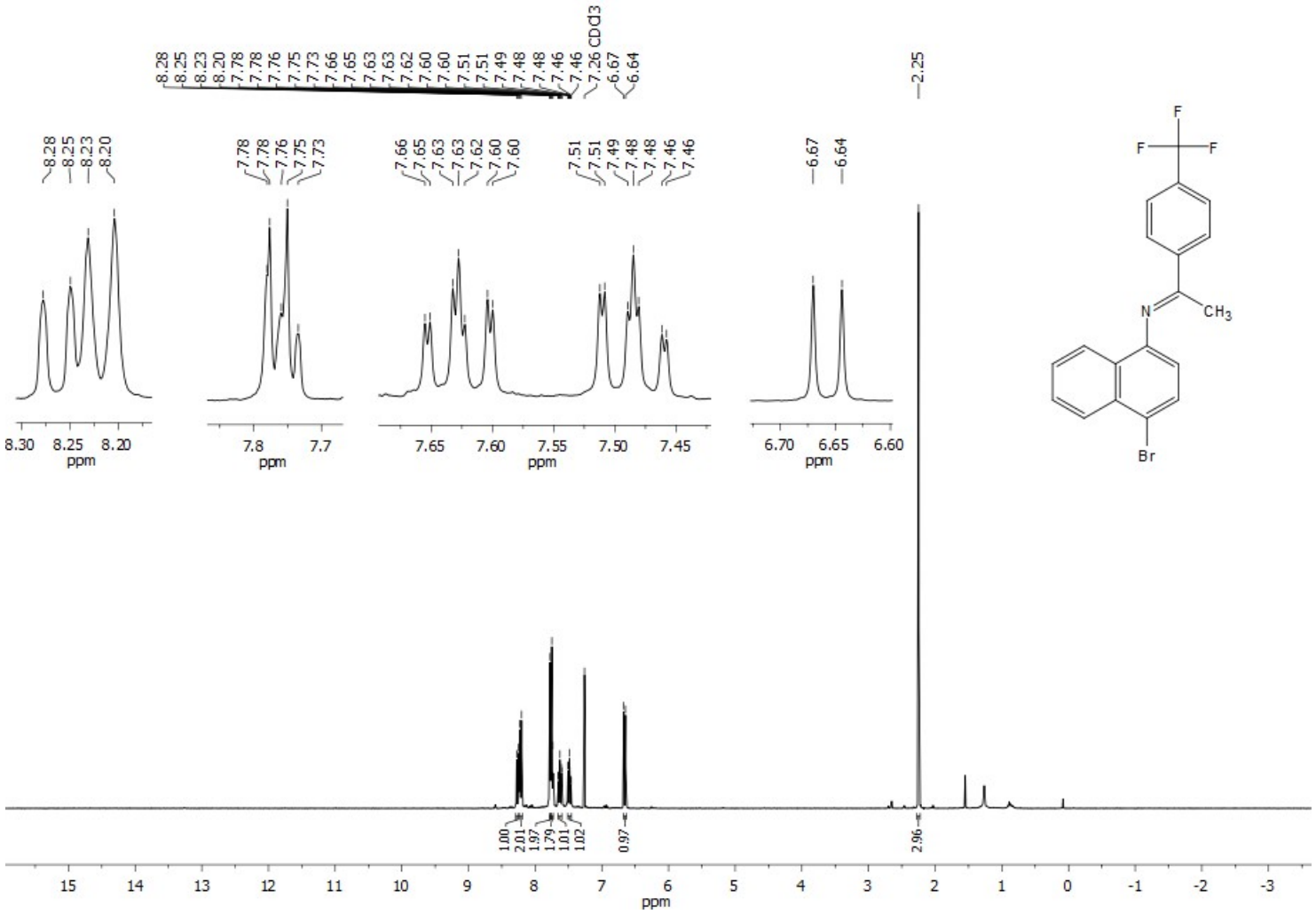

Figure S82. ^{1}H NMR spectrum of compound **6p** ($CDCl_3$, 300 MHz).

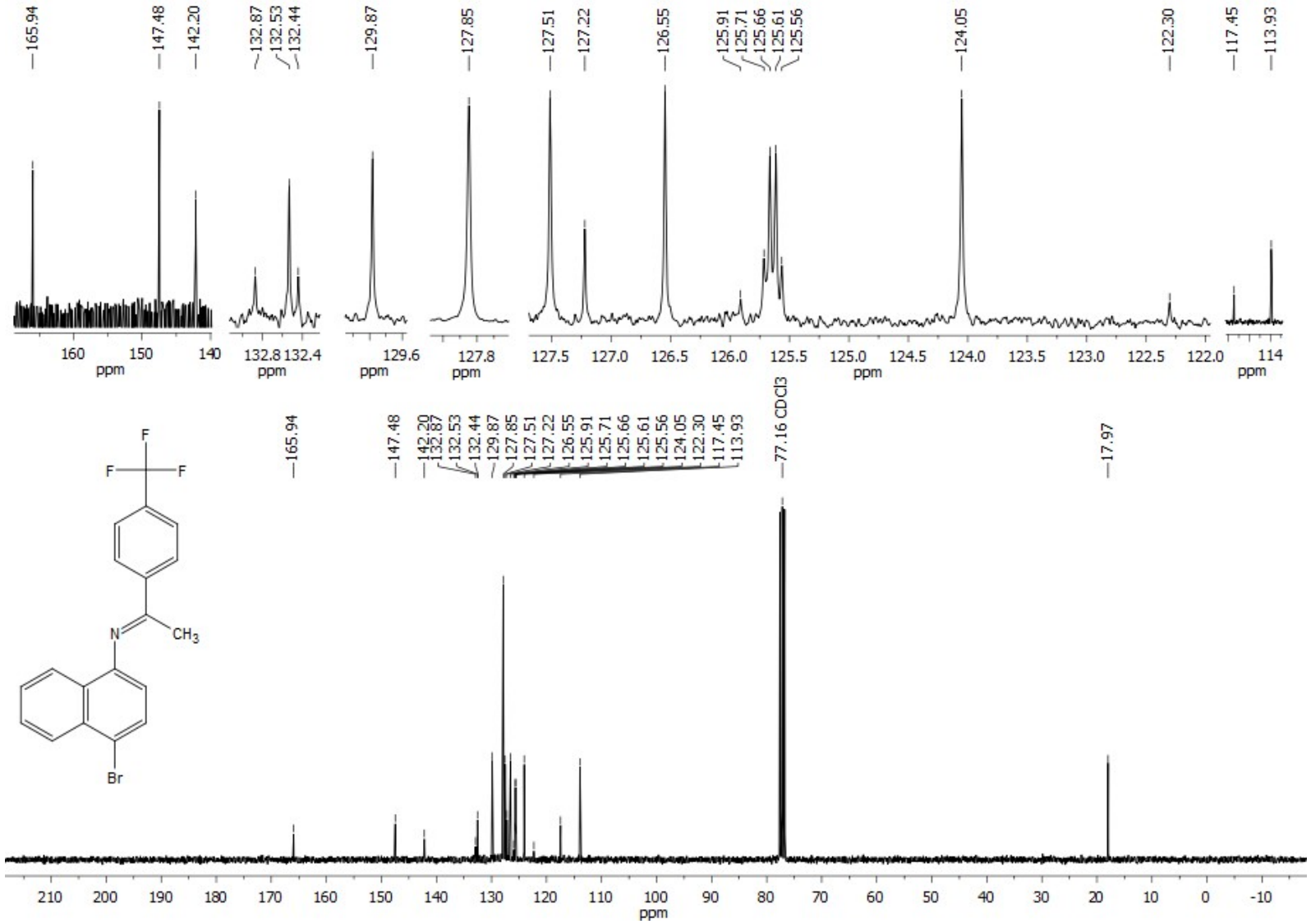

Figure S83. ^{13}C {^{1}H} NMR spectrum of compound **6p** ($CDCl_3$, 76 MHz).

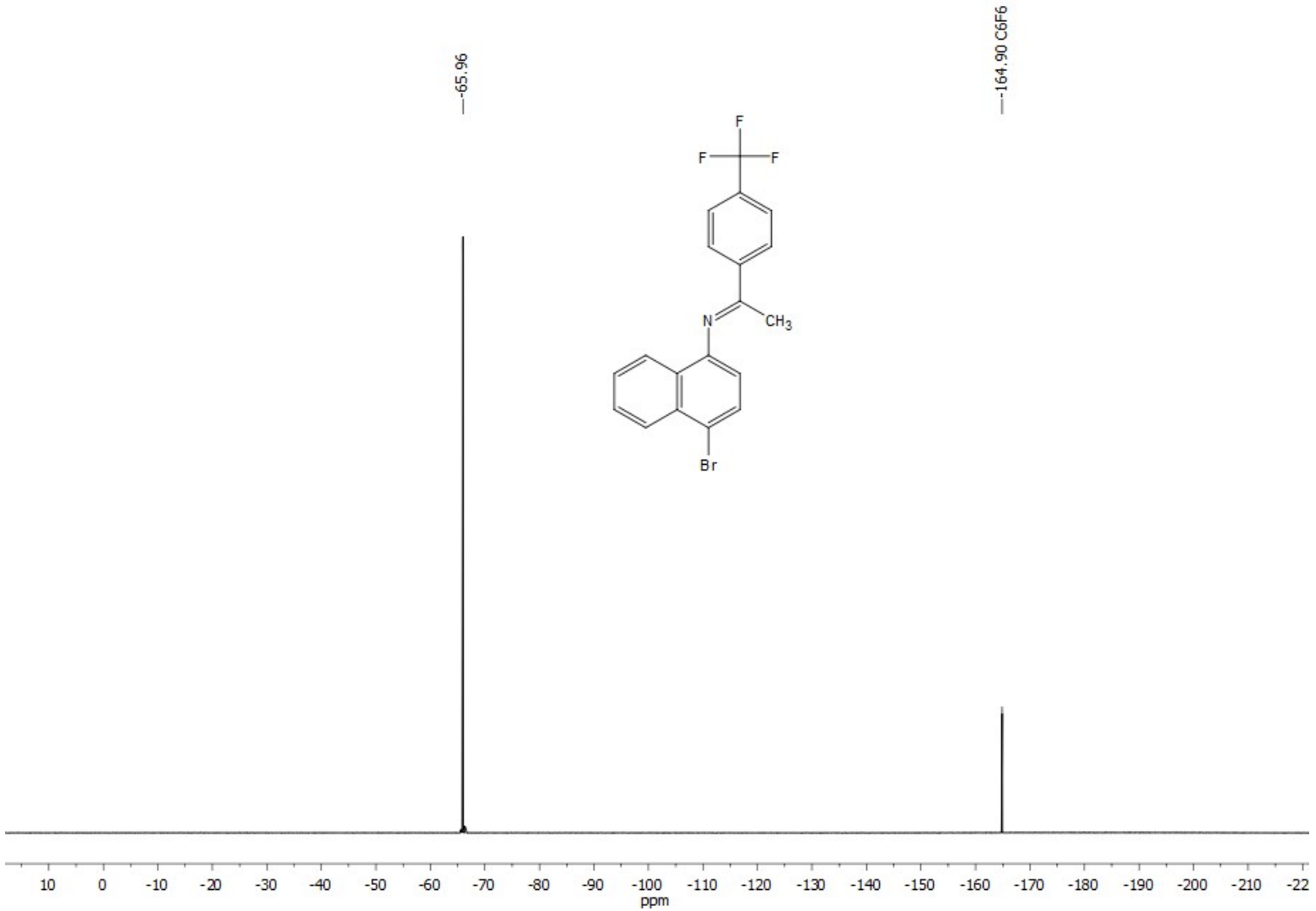

Figure S84. ^{19}F {^{1}H} NMR spectrum of compound **6p** ($CDCl_3$, 282 MHz). Standard C_6F_6 with respect to $CFCl_3$.

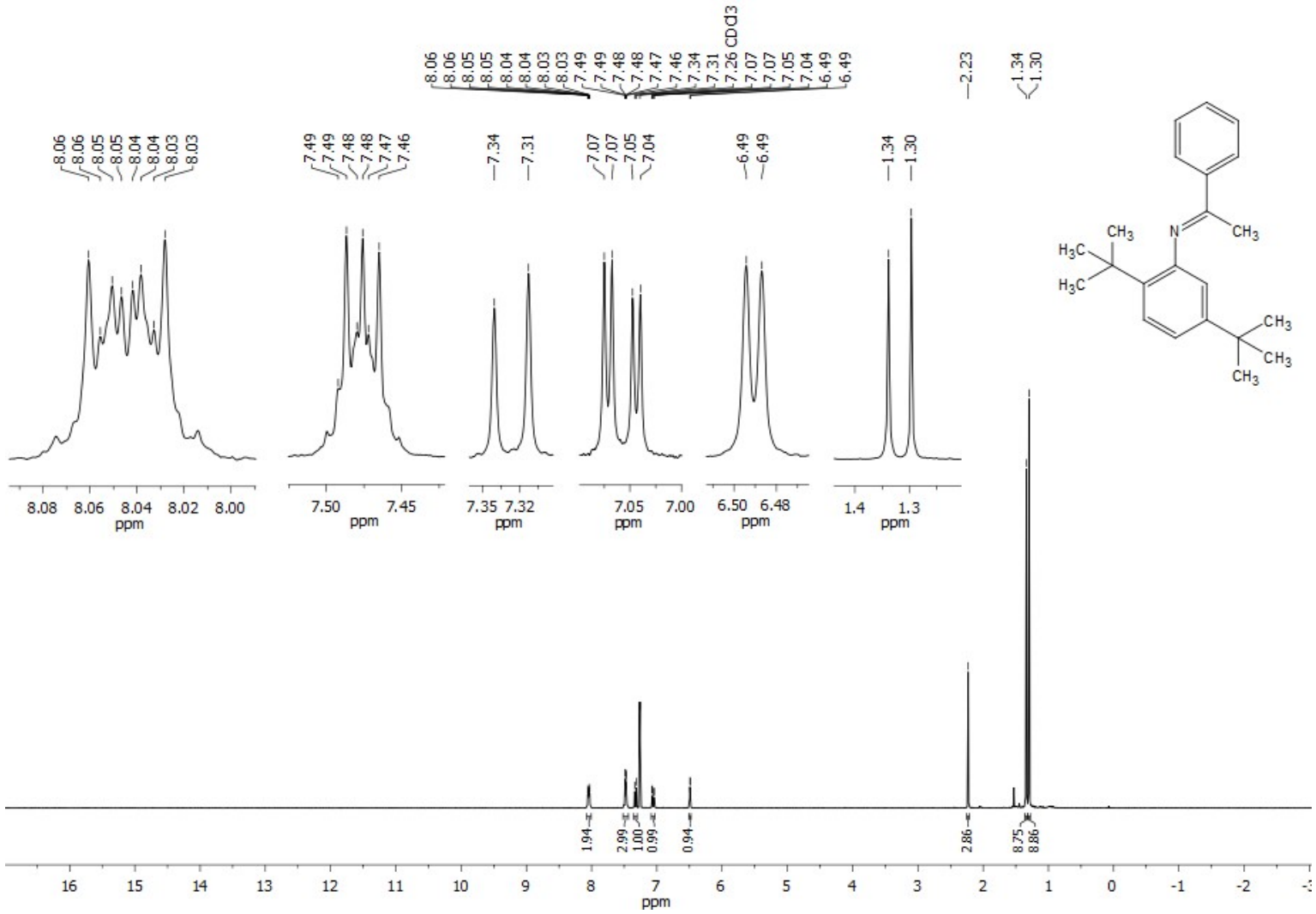

Figure S85. ^{1}H NMR spectrum of compound **6q** ($CDCl_3$, 300 MHz).

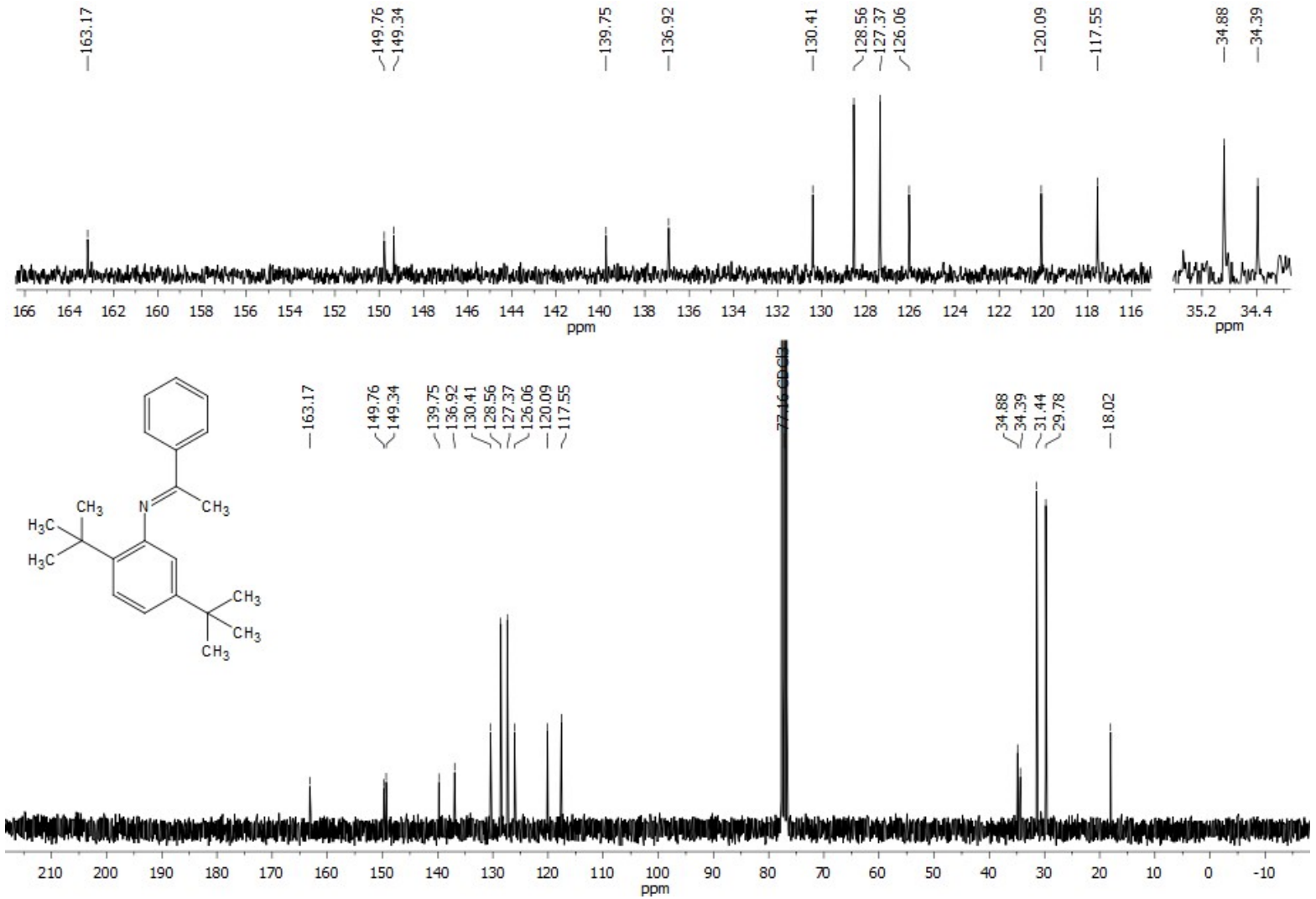

Figure S86. ^{13}C {^{1}H} NMR spectrum of compound **6q** ($CDCl_3$, 76 MHz).

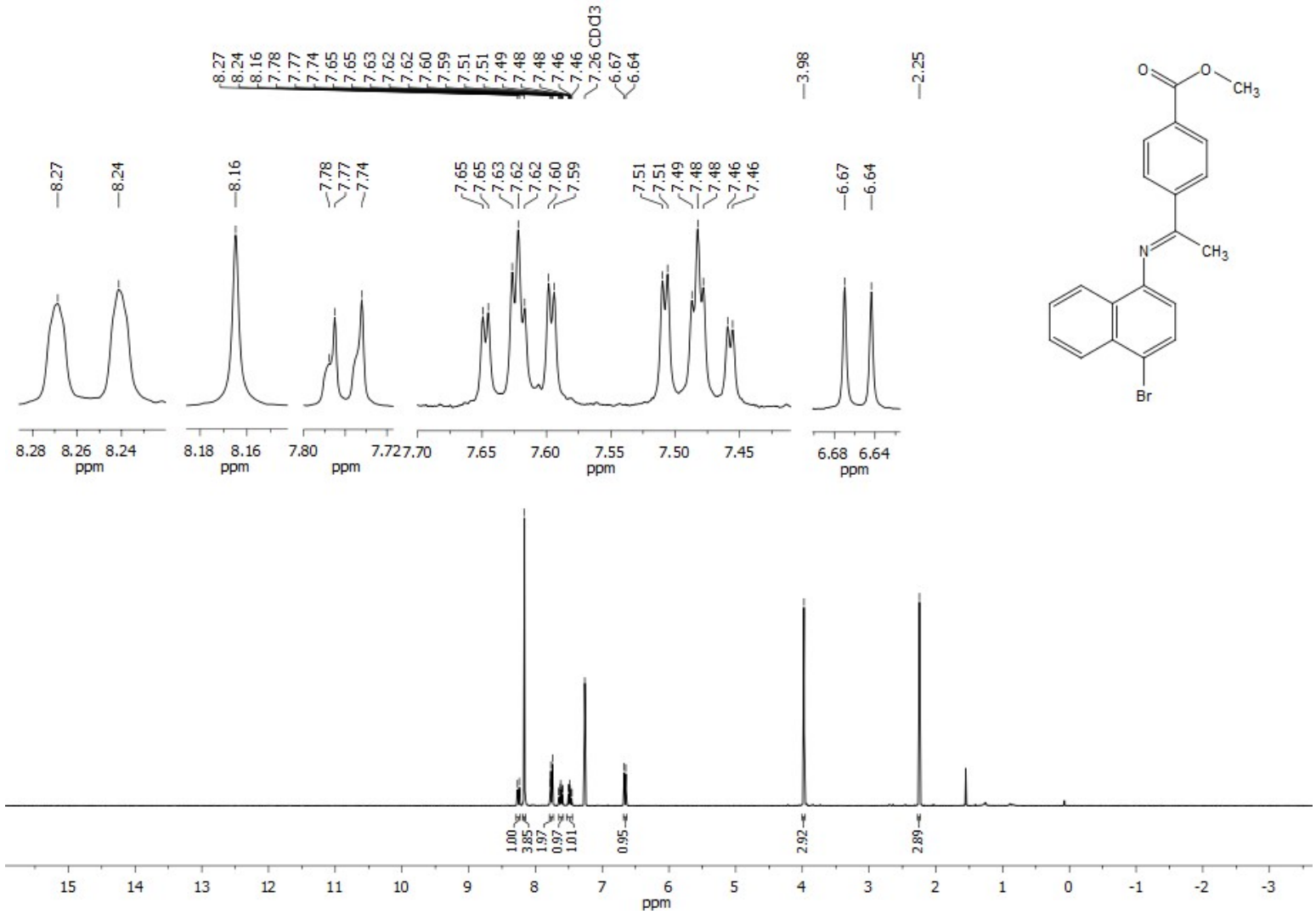

Figure S87. ^{1}H NMR spectrum of compound **6r** ($CDCl_3$, 300 MHz).

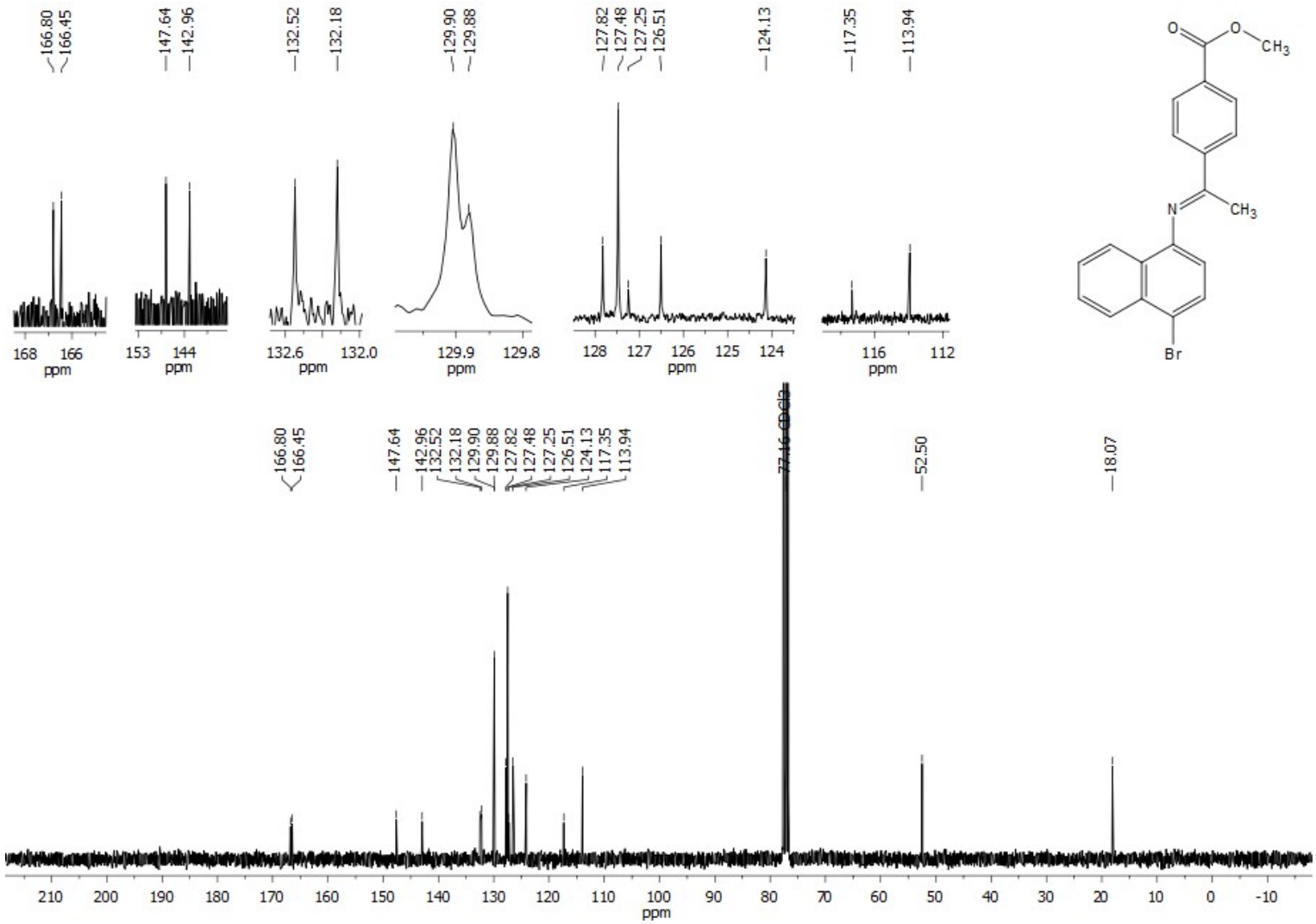

Figure S88. ^{13}C {^{1}H} NMR spectrum of compound **6r** ($CDCl_3$, 76 MHz).

S6. Single crystal X-ray diffraction data

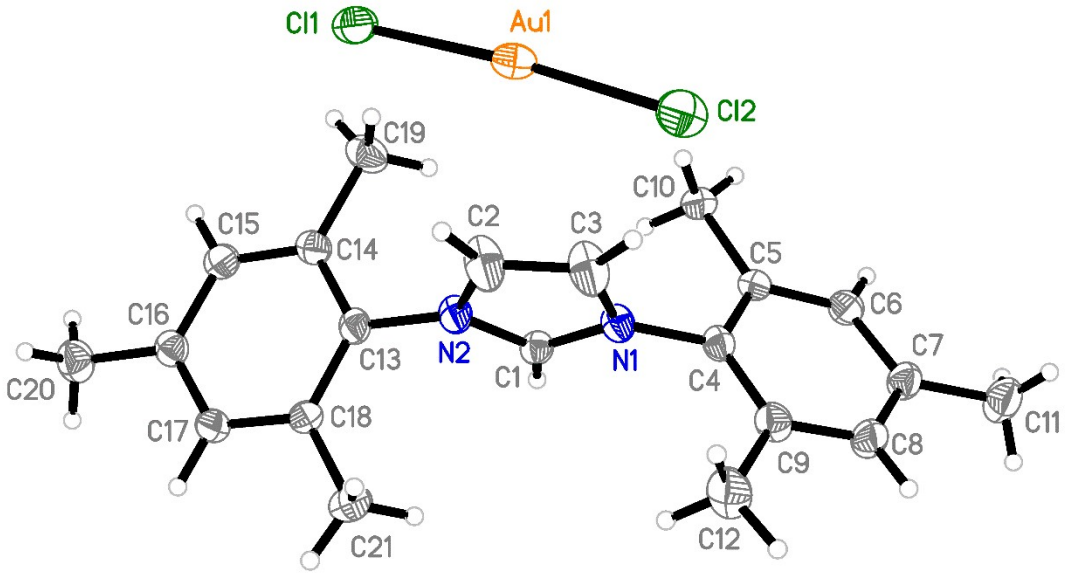

Figure S89. Crystal structures of **[IMesH][AuCl$_2$]**. Thermal ellipsoids are set to a 50% probability level. Disorder is omitted.

Table S1. Crystal data and structure refinement for **[IMesH][AuCl$_2$]**.

Identification code	[IMesH][AuCl$_2$]	
Empirical formula	C21 H25 Au Cl2 N2	
Formula weight	573.29	
Temperature	100(2) K	
Wavelength	0.71073 Å	
Crystal system	Monoclinic	
Space group	P2$_1$/c	
Unit cell dimensions	a = 8.5969(2) Å	α = 90°.
	b = 16.0302(3) Å	β = 98.3750(10)°.
	c = 15.7911(3) Å	γ = 90°.
Volume	2152.97(8) Å^3	
Z	4	
Density (calculated)	1.769 g·cm^{-3}	
Absorption coefficient	7.088 mm^{-1}	
F(000)	1112	
Crystal size	0.177 x 0.174 x 0.145 mm	
Theta range for data collection	2.395 to 33.173°.	
Index ranges	-13 ≤ h ≤ 13, -24 ≤ k ≤ 24, -24 ≤ l ≤ 24	
Reflections collected	115164	
Independent reflections	8228 [R(int) = 0.0404]	
Observed reflections	7232	
Completeness to θ_{full} = 25.242°	99.9 %	
Absorption correction	Semi-empirical from equivalents	
Max. and min. transmission	0.4353 and 0.3490	
Refinement method	Full-matrix least-squares on F^2	
Data / restraints / parameters	8228 / 0 / 255	
Goodness-of-fit on F^2	1.129	
Final R indices [I>2σ(I)]	R$_1$ = 0.0207, wR$_2$ = 0.0405	
R indices (all data)	R$_1$ = 0.0270, wR$_2$ = 0.0425	
Extinction coefficient	0.00031(4)	
Largest diff. peak and hole	0.903 and -1.304 e·Å^{-3}	
CCDC number	2530450	

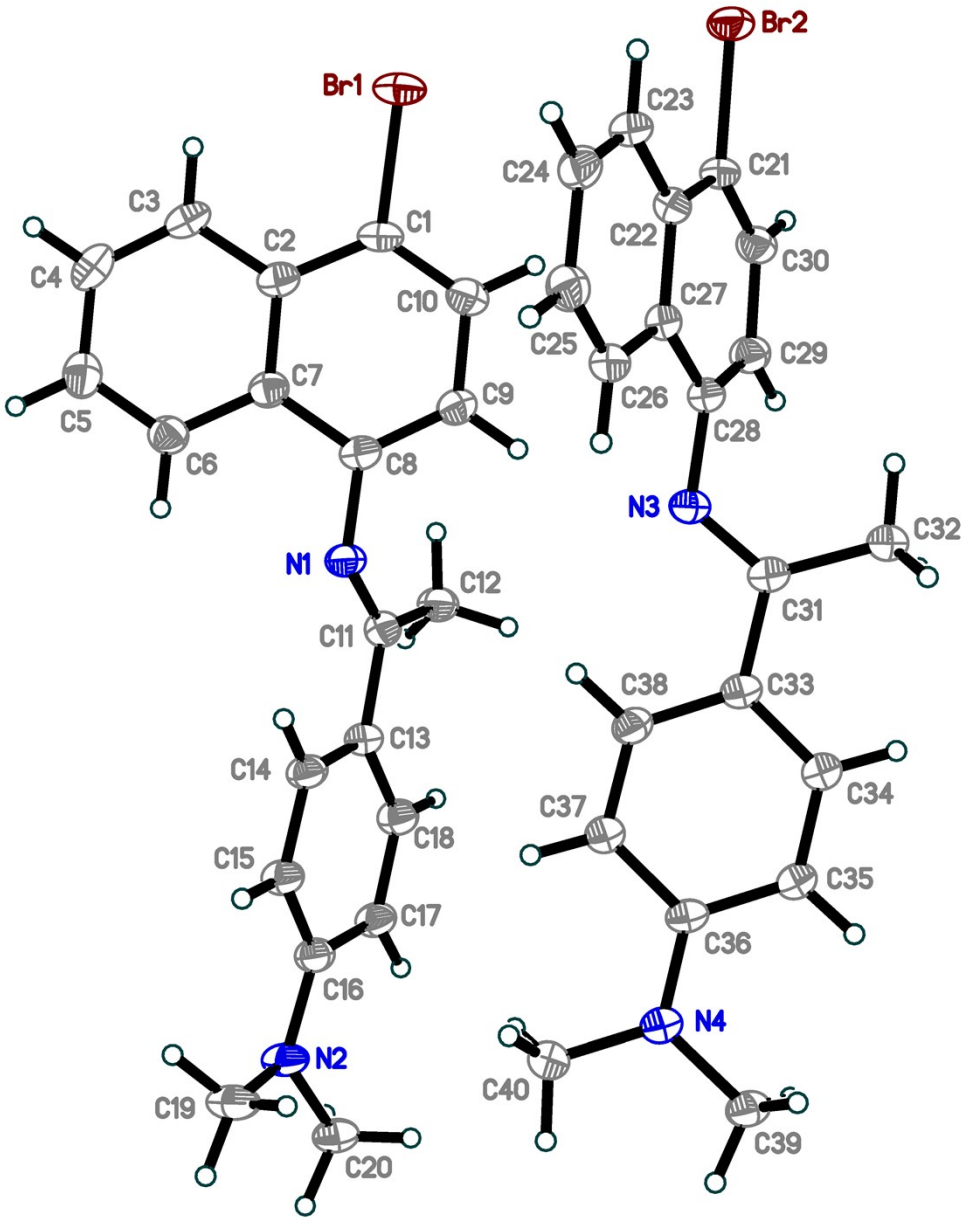

Figure S90. The structure of **6e**. Thermal ellipsoids are shown at a 50% probability level. Hydrogen atoms are drawn as fixed-size spheres. Disorder is omitted.

Table S2. Crystal data and structure refinement for **6e**.

Identification code	mg-479-1	
Empirical formula	C20 H19 Br N2	
Formula weight	367.28	
Temperature	100.00(10) K	
Wavelength	1.54184 Å	
Crystal system	Triclinic	
Space group	P-1	
Unit cell dimensions	a = 6.39790(10) Å	a= 92.979(2)°.
	b = 15.6118(3) Å	b= 92.396(2)°.
	c = 16.6250(4) Å	g = 90.863(2)°.
Volume	1656.61(6) $Å^3$	
Z	4	
Density (calculated)	1.473 Mg/m^3	
Absorption coefficient	3.370 mm^{-1}	
F(000)	752	
Crystal size	0.342 x 0.228 x 0.17 mm^3	
Theta range for data collection	2.664 to 80.214°.	
Index ranges	-8<=h<=8, -19<=k<=19, -21<=l<=20	
Reflections collected	13001	
Independent reflections	13001	
Completeness to theta = 67.684°	99.8 %	
Absorption correction	Gaussian	
Max. and min. transmission	0.981 and 0.964	
Refinement method	Full-matrix least-squares on F^2	
Data / restraints / parameters	13001 / 0 / 422	
Goodness-of-fit on F^2	1.068	
Final R indices [I>2sigma(I)]	R1 = 0.0396, wR2 = 0.1125	
R indices (all data)	R1 = 0.0416, wR2 = 0.1148	
Largest diff. peak and hole	0.923 and -0.483 $e.Å^{-3}$	
CCDC number	2530449	

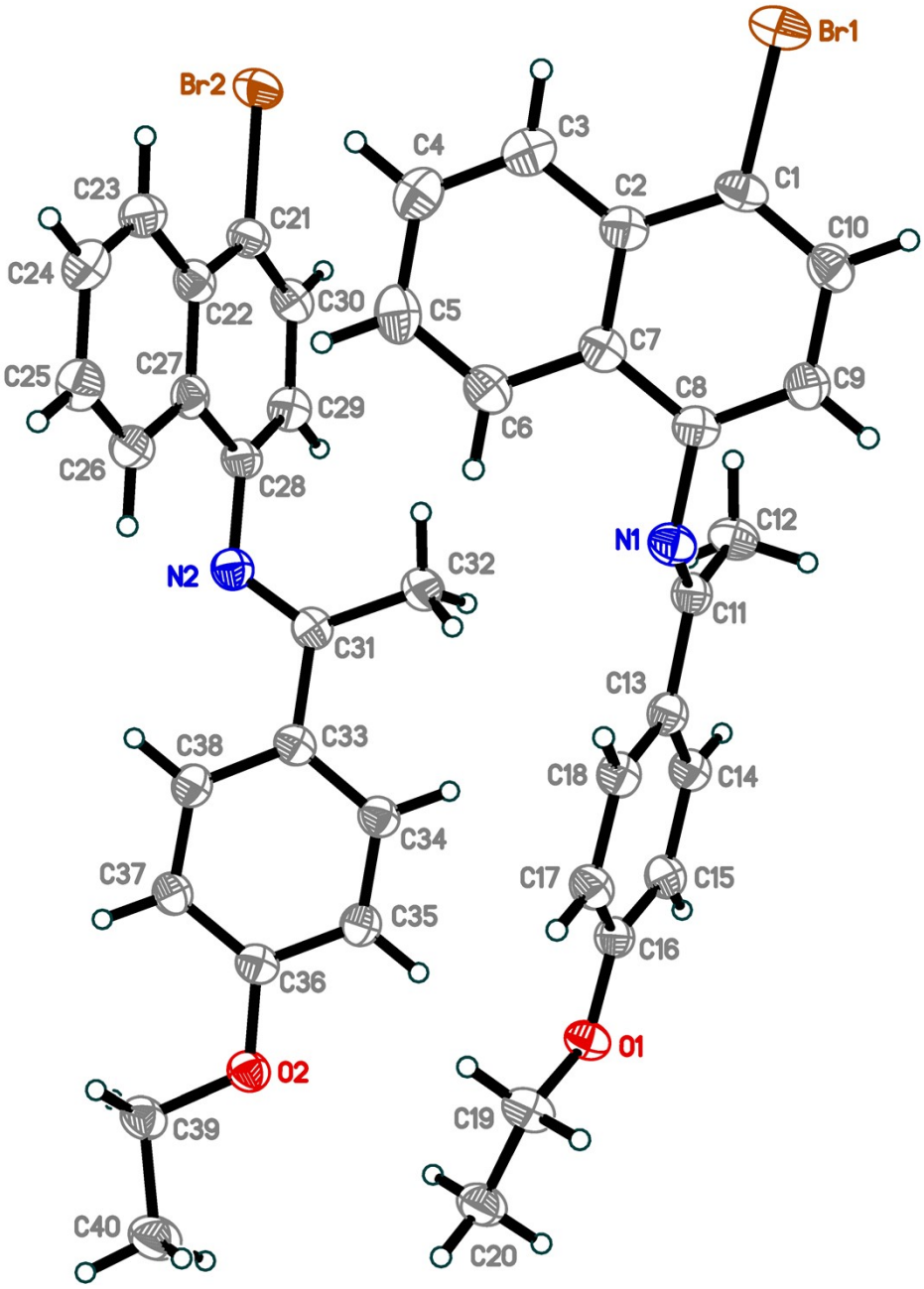

Figure S91. Crystal structures of **6f**. Thermal ellipsoids are set to a 50% probability level. Disorder is omitted.

Table S3. Crystal data and structure refinement for **6f**.

Identification code	**6f**	
Empirical formula	C20 H18 Br N O	
Formula weight	368.26	
Temperature	100.01(10) K	
Wavelength	1.54184 Å	
Crystal system	Triclinic	
Space group	P-1	
Unit cell dimensions	a = 6.38260(10) Å	a= 74.904(2)°.
	b = 16.2140(3) Å	b= 87.595(2)°.
	c = 16.7920(2) Å	g = 87.054(2)°.
Volume	1674.84(5) $Å^3$	
Z	4	
Density (calculated)	1.460 Mg/m^3	
Absorption coefficient	3.364 mm^{-1}	
F(000)	752	
Crystal size	0.48 x 0.28 x 0.12 mm^3	
Theta range for data collection	2.825 to 80.178°.	
Index ranges	-7<=h<=6, -20<=k<=20, -21<=l<=21	
Reflections collected	43252	
Independent reflections	7183 [R(int) = 0.0744]	
Completeness to theta = 67.684°	99.7 %	
Absorption correction	Gaussian	
Max. and min. transmission	1.000 and 0.309	
Refinement method	Full-matrix least-squares on F^2	
Data / restraints / parameters	7183 / 0 / 419	
Goodness-of-fit on F^2	1.074	
Final R indices [I>2sigma(I)]	R1 = 0.0570, wR2 = 0.1663	
R indices (all data)	R1 = 0.0594, wR2 = 0.1688	
Largest diff. peak and hole	0.914 and -1.435 $e.Å^{-3}$	
CCDC number	2530448	

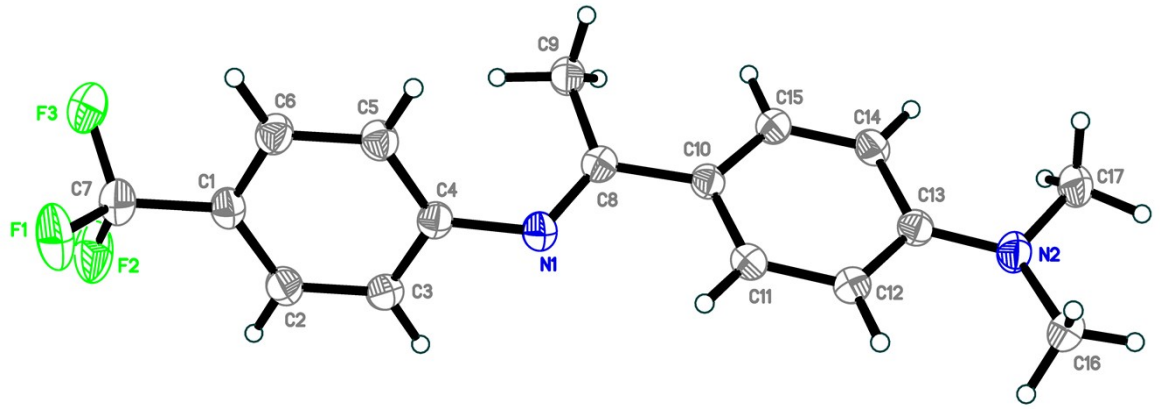

Figure S92. Crystal structures of **6k**. Thermal ellipsoids are set to a 50% probability level. Disorder is omitted.

Table S4. Crystal data and structure refinement for **6k**.

Identification code	mg-566	
Empirical formula	C17 H17 F3 N2	
Formula weight	306.32	
Temperature	99.99(10) K	
Wavelength	1.54184 Å	
Crystal system	Monoclinic	
Space group	Ia	
Unit cell dimensions	a = 5.76250(10) Å	a= 90°.
	b = 7.97390(10) Å	b= 91.769(2)°.
	c = 32.0048(5) Å	g = 90°.
Volume	1469.91(4) $Å^3$	
Z	4	
Density (calculated)	1.384 Mg/m^3	
Absorption coefficient	0.920 mm^{-1}	
F(000)	640	
Crystal size	0.28 x 0.21 x 0.13 mm^3	
Theta range for data collection	2.763 to 80.102°.	
Index ranges	-7<=h<=7, -10<=k<=10, -40<=l<=40	
Reflections collected	9879	
Independent reflections	2543 [R(int) = 0.0329]	
Completeness to theta = 67.684°	99.8 %	
Absorption correction	Gaussian	
Max. and min. transmission	1.000 and 0.531	
Refinement method	Full-matrix least-squares on F^2	
Data / restraints / parameters	2543 / 2 / 202	
Goodness-of-fit on F^2	1.114	
Final R indices [I>2sigma(I)]	R1 = 0.0368, wR2 = 0.1031	
R indices (all data)	R1 = 0.0374, wR2 = 0.1036	
Absolute structure parameter	-0.09(10)	
Largest diff. peak and hole	0.156 and -0.203 $e.Å^{-3}$	
CCDC number	2530447	

S7. References

1. M. H. Voges, C. Rømming and M. Tilset, Synthesis and Characterization of 14-Electron Cyclopentadienyl Chromium(II) Complexes Containing a Heterocyclic Carbene Ligand. *Organometallics*, 1999, **18**, 529-533.
2. D. V. Pasyukov, M. A. Shevchenko, K. E. Shepelenko, O. V. Khazipov, J. V. Burykina, E. G. Gordeev, M. E. Minyaev, V. M. Chernyshev and V. P. Ananikov, One-Step Access to Heteroatom-Functionalized Imidazol(in)ium Salts. *Angew. Chem. Int. Ed.*, 2022, **61**, e202116131.
3. T. N. Hooper, C. P. Butts, M. Green, M. F. Haddow, J. E. McGrady and C. A. Russell, Synthesis, Structure and Reactivity of Stable Homoleptic Gold(I) Alkene Cations. *Chem. Eur. J.*, 2009, **15**, 12196-12200.
4. Z. Yu, L.-S. Tan and E. Fossum, Aryl ether synthesis via low-cost Ullmann coupling systems. *Arkivoc*, 2009, **xiv**, 255-265.
5. S. G. Chalkidis and G. C. Vougioukalakis, KA2 Coupling, Catalyzed by Well-Defined NHC-Coordinated Copper(I): Straightforward and Efficient Construction of α-Tertiary Propargylamines. *Eur. J. Org. Chem.*, 2023, **26**, e202301095.
6. O. Santoro, A. Collado, A. M. Z. Slawin, S. P. Nolan and C. S. J. Cazin, A general synthetic route to [Cu(X)(NHC)] (NHC = N-heterocyclic carbene, X = Cl, Br, I) complexes. *Chem. Commun.*, 2013, **49**, 10483-10485.
7. N. C. Baenziger, W. E. Bennett and D. M. Soborofe, Chloro (triphenylphosphine) gold (I). *Acta Crystallographica B*, 1976, **32**, 962-963.
8. R. Prabhakaran, P. Kalaivani, S. V. Renukadevi, R. Huang, K. Senthilkumar, R. Karvembu and K. Natarajan, Copper Ion Mediated Selective Cleavage of C–S Bond in Ferrocenylthiosemicarbazone Forming Mixed Geometrical [(PPh3)Cu(μ-S)2Cu(PPh3)2] Having Cu2S2 Core: Toward a New Avenue in Copper–Sulfur Chemistry. *Inorg. Chem.*, 2012, **51**, 3525-3532.
9. F. Han, J. Li, H. Zhang, T. Wang, Z. Lin and H. Xia, Reactions of Osmabenzene with Silver/Copper Acetylides: From Metallabenzene to Benzene. *Chem. Eur. J.*, 2015, **21**, 565-567.
10. P. de Frémont, N. M. Scott, E. D. Stevens and S. P. Nolan, Synthesis and Structural Characterization of N-Heterocyclic Carbene Gold(I) Complexes. *Organometallics*, 2005, **24**, 2411-2418.
11. S. Díez-González, E. C. Escudero-Adán, J. Benet-Buchholz, E. D. Stevens, A. M. Z. Slawin and S. P. Nolan, [(NHC)CuX] complexes: Synthesis, characterization and catalytic activities in reduction reactions and Click Chemistry. On the advantage of using well-defined catalytic systems. *Dalton Trans.*, 2010, **39**, 7595-7606.
12. G. Sheldrick, SHELXT - Integrated space-group and crystal-structure determination. *Acta Crystallographica Section A*, 2015, **71**, 3-8.
13. G. Sheldrick, Crystal structure refinement with SHELXL. *Acta Crystallographica Section C*, 2015, **71**, 3-8.
14. O. V. Dolomanov, L. J. Bourhis, R. J. Gildea, J. A. K. Howard and H. Puschmann, OLEX2: a complete structure solution, refinement and analysis program. *Journal of Applied Crystallography*, 2009, **42**, 339-341.
15. S. S. Zalesskiy, A. E. Sedykh, A. S. Kashin and V. P. Ananikov, Efficient General Procedure To Access a Diversity of Gold(0) Particles and Gold(I) Phosphine Complexes from a Simple HAuCl4 Source. Localization of Homogeneous/Heterogeneous System's Interface and Field-Emission Scanning Electron Microscopy Study. *J. Am. Chem. Soc.*, 2013, **135**, 3550-3559.
16. G. Ciancaleoni, L. Biasiolo, G. Bistoni, A. Macchioni, F. Tarantelli, D. Zuccaccia and L. Belpassi, NHC-Gold-Alkyne Complexes: Influence of the Carbene Backbone on the Ion Pair Structure. *Organometallics*, 2013, **32**, 4444-4447.
17. X. Ma, N. V. Tzouras, M. Peng, K. Van Hecke and S. P. Nolan, Azolium Aurates as Pre-Catalysts for the Oxidative Coupling of Terminal Alkynes under Mild Conditions. *J. Org. Chem.*, 2022, **87**, 4883-4893.
18. T. Nagata, Y. Adachi and Y. Obora, Thiolate-Protected $Au_{25}(SC_2H_4Ph)_{18}$ Nanoclusters as a Catalyst for Intermolecular Hydroamination of Terminal Alkynes. *Synlett*, 2018, **29**, 2655-2659.